The Journal of Chemical Physics

RESEARCH ARTICLE | SEPTEMBER 02 2025

Exact lattice summations for Lennard-Jones potentials coupled to a three-body Axilrod–Teller–Muto term applied to cuboidal phase transitions

Special Collection: Michele Parrinello Festschrift

Andres Robles-Navarro ; Shaun Cooper ; Andreas A. Buchheit ; Jonathan K. Busse ; Antony Burrows ; Odile Smits ; Peter Schwerdtfeger

J. Chem. Phys. 163, 094104 (2025)
https://doi.org/10.1063/5.0276677

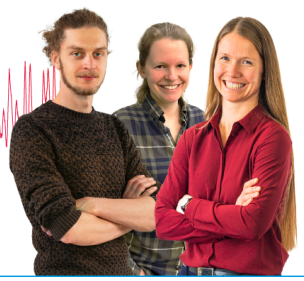

The Journal of Chemical Physics ARTICLE pubs.aip.org/aip/jcp

Exact lattice summations for Lennard-Jones potentials coupled to a three-body Axilrod–Teller–Muto term applied to cuboidal phase transitions

Cite as: J. Chem. Phys. 163, 094104 (2025); doi: 10.1063/5.0276677
Submitted: 19 April 2025 • Accepted: 7 August 2025 •
Published Online: 2 September 2025

Andres Robles-Navarro,[1,a] Shaun Cooper,[2,b] Andreas A. Buchheit,[3,b] Jonathan K. Busse,[3,4,c] Antony Burrows,[1,d] Odile Smits,[5,e] and Peter Schwerdtfeger[1,b]

AFFILIATIONS

[1] Centre for Theoretical Chemistry and Physics, The New Zealand Institute for Advanced Study, Massey University Auckland, Private Bag 102904, 0745 Auckland, New Zealand
[2] School of Natural and Computational Sciences, Massey University Albany, Private Bag 102904, Auckland 0745, New Zealand
[3] Saarland University, Department of Mathematics, P.O. Box 15 11 50, D-66041 Saarbrücken, Germany
[4] German Aerospace Center (DLR), Institute of Software Technology, High-Performance Computing Department, Linder Höhe, Cologne 51147, Germany
[5] The School of Mathematics and Physics, University of Queensland, Brisbane QLD 4072, Australia

Note: This paper is part of the JCP Special Topic, Michele Parrinello Festschrift.
[a] **Electronic mail:** andres.robles.n@gmail.com
[b] **Authors to whom correspondence should be addressed:** s.cooper@massey.ac.nz; andreas.buchheit@uni-saarland.de; and peter.schwerdtfeger@gmail.com
[c] **Electronic mail:** jonathan@jbusse.de
[d] **Electronic mail:** antony@yottabyte27.com
[e] **Electronic mail:** smits.odile.rosette@gmail.com

ABSTRACT

Three-body interactions have long been conjectured to play a crucial role in the stability of matter. However, rigorous studies have been scarce due to the computational challenge of evaluating small energy differences in high-dimensional lattice sums. This work provides a rigorous analysis of Bain-type cuboidal lattice transformations, which connect the face-centered cubic (fcc), mean-centered cubic (mcc), body-centered cubic (bcc), and axially centered cubic (acc) lattices. Our study incorporates a general (n, m) Lennard-Jones (LJ) two-body potential and a long-range repulsive Axilrod–Teller–Muto (ATM) three-body potential. The two-body lattice sums and their meromorphic continuations are evaluated to full precision using super-exponentially convergent series expansions. Furthermore, we introduce a novel approach to computing three-body lattice sums by converting the multi-dimensional sum into an integral involving products of Epstein zeta functions. This enables us to evaluate three-body lattice sums and their meromorphic continuations to machine precision within minutes on a standard laptop. Using our computational framework, we analyze the stability of cuboidal lattice phases relative to the close-packed fcc structure along a Bain transformation path for varying ATM coupling strengths. We analytically demonstrate that the ATM cohesive energy exhibits an extremum at the bcc phase and show numerically that it corresponds to a minimum for repulsive three-body forces along the Bain path. Our results indicate that strong repulsive three-body interactions can destabilize the fcc phase and render bcc energetically favorable for soft LJ potentials. However, even in this scenario, the bcc phase remains susceptible to further cuboidal distortions. These results suggest that the stability of the bcc phase is, besides vibrational, temperature, and pressure effects, strongly influenced by higher than two-body forces. Because of the wrong short-range behavior of the triple–dipole ATM model, the LJ

potential is limited to exponents $n > 9$ for the repulsive wall, otherwise one observes distortion into a set of linear chains collapsing to the origin.

 https://doi.org/10.1063/5.0276677

I. INTRODUCTION

Crystalline solid-to-solid phase transitions are induced by temperature or pressure change and often involve symmetry breaking away from the original space group of the starting phase along the minimum energy transition path toward the final crystal phase.[1] The special class of martensitic phase transformations is described by diffusionless transitions induced by lattice strain and a collective movement of the atoms in the lattice.[2–6] Such martensitic transitions are found not only in many important materials such as steel or oxide ceramics[7] but also for some elements in the Periodic Table such as lithium.[8,9] The body-centered cubic (bcc) to face-centered cubic (fcc) phase transition belongs to the class of martensitic transformations.[10] Both the bcc lattice ($c/a = 1$) and the face-centered cubic (fcc) lattice ($c/a = \sqrt{2}$) have the body-centered tetragonal (bct) lattice (crystallographic group #139 or $I4/mmm$) in common defined by the lattice constants ($a_1 = a_2 = a$ and $a_3 = c$ and right angles $\alpha_1 = \alpha_2 = \alpha_3 = 90^\circ$), as shown in Fig. 1.

Concerning the interactions between the atoms or molecules in a lattice, the associated infinite lattice sums describing such interactions have a long history in solid-state physics and discrete mathematics.[11] They connect lattices to observables such as the equation of state for a bulk system with inverse power potentials $V(r) = r^{-k}$ acting between lattice points.[12–15] Most notable cases for such interaction potentials are the Lennard-Jones (LJ) potential[16] (see Ref. 17 for a historical account), which in its most general case is given by

$$E_{\mathrm{LJ}}(r) = \varepsilon \frac{\mathrm{nm}}{n-m}\left[\frac{1}{n}\left(\frac{r_e}{r}\right)^n - \frac{1}{m}\left(\frac{r_e}{r}\right)^m\right], \tag{1}$$

and the Coulomb potential, leading to the famous Madelung constant being derived as early as 1918 by Madelung.[18] In Eq. (1), r_e is the equilibrium distance for a diatomic molecule, ε the corresponding dissociation energy, and we have the condition $n > m > d$ with d the dimension of the lattice. The application of the Lennard-Jones and other empirical potentials has been invaluable to gain deeper insight into bulk phases and their phase transitions.[17,19–25]

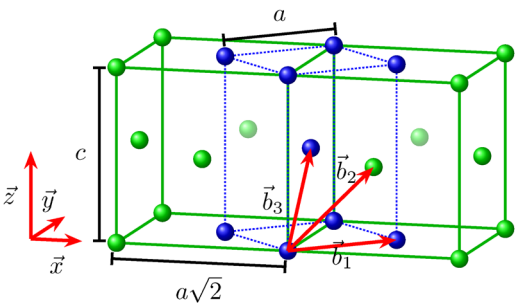

FIG. 1. Body-centered tetragonal lattice shown in blue with lattice constants a and c. For $a = c$, we have the bcc lattice. The usual fcc unit cell with additional green atoms is also shown with lattice constants $a' = a\sqrt{2} = c$.

In the following, we consider d-dimensional Bravais lattices $\Lambda = B^{\mathsf{T}}\mathbb{Z}^d = \{B^{\mathsf{T}}\vec{i} \mid \vec{i} \in \mathbb{Z}^d\}$, with $d = 1, 2, 3$, where the generator matrix $B^{\mathsf{T}} = (\vec{b}_1, \ldots, \vec{b}_d)$ contains the lattice basis vectors.[26] When evaluating energies or forces in such long-range interacting lattices, we encounter lattice sums of the form

$$L = \sum_{\vec{x}\in\Lambda} f(\vec{x}) = \sum_{\vec{i}\in\mathbb{Z}^d} f\left(B^{\mathsf{T}}\vec{i}\right), \tag{2}$$

where f is a scalar or vector-valued function that decreases sufficiently fast such that the sum is absolutely convergent. An important special case is given by an inverse power-law potential $f(\vec{x}) = |\vec{x}|^{-\nu}$, where the resulting lattice sum is a special case of the Epstein zeta function, a generalization of the Riemann zeta function to multidimensional lattice sums[27] with many applications in physics.[16,28–30] These lattice sums are often slowly convergent and their efficient and precise computation poses significant challenges. Moreover, meaning can be given to conditionally convergent or even divergent series through techniques such as meromorphic continuation.[31] The theory of converting lattice sums, including their meromorphic continuations, into fast converging series has become a research field on its own.[11]

The dominant long-range three-body interaction contribution comes from the triple–dipole interaction and is described approximately by the Axilrod–Teller–Muto (ATM) potential.[32,33] For a trimer of atoms at positions $\vec{r}_1, \vec{r}_2, \vec{r}_3$, the ATM potential reads[34]

$$E^{(3)}_{\mathrm{ATM}} = \lambda \frac{r_{12}^2 r_{13}^2 r_{23}^2 + 3(\vec{r}_{12}\cdot\vec{r}_{13})(\vec{r}_{21}\cdot\vec{r}_{23})(\vec{r}_{31}\cdot\vec{r}_{32})}{(r_{12}r_{13}r_{23})^5}. \tag{3}$$

Here, $\lambda > 0$ represents the ATM coupling constant, while $\vec{r}_{ij} = \vec{r}_i - \vec{r}_j$ denotes the relative position vector between distinct atoms i and j with norm $r_{ij} = |\vec{r}_{ij}|$. The coupling strength λ depends on the polarizabilities of the interacting atoms, where three-body interactions can become highly relevant, among others, for the heavier and more polarizable noble gases. Notably, for solid argon at 0 K, three-body forces have been shown to contribute ~8.9% of the total cohesive energy.[35] We should mention, however, that the expansion of the total interaction energy in terms of many-body interaction contributions in a cluster or bulk system can become problematic when atoms start to interact strongly.[36]

The precise simulation of solid–solid phase transitions can be highly challenging due to the movement of many atoms within

the simulation cell.[7,37] Martensitic transformations are less complex in nature but are nevertheless difficult to predict theoretically and to measure experimentally.[6,38,39] For a general (n,m) LJ two-body potential, we recently showed by exact lattice summations that the bcc phase is at an extremum along the cuboidal distortion path and becomes either energetically unstable or metastable. In addition, one requires rather soft Lennard-Jones potentials to stabilize the bcc phase against rhombohedral distortion.[19,20,40] This bcc instability persists into the high-pressure regime for a LJ solid.[41] This result can most likely be generalized to all physically relevant two-body interactions. Thus, the existence of the bcc phase, known for a number of elements in the periodic table, likely results from vibrational and temperature effects and/or from dominant higher than two-body forces. We note that Landau theory predicts that the bcc phase becomes dominant near the melting line for metals[42] and for other solids.[43,44]

In this work, we analyze a smooth connection between the cuboidal body-centered tetragonal (bct) lattices through a martensitic Bain transformation including both general two-body LJ interactions and a three-body ATM potential.[45–47] We first write the lattice Λ along the transition path as a function of a single parameter A[48,49] and collect the basic properties of the resulting lattice. We then present efficient methods to evaluate both the arising two-body and three-body lattice sums to full precision. For the two-body potential, we re-express the algebraically decaying sum in terms of a series of super-exponentially decaying sums, which can be efficiently evaluated. We then present a novel efficient method for computing general three-body lattice sums, based on integrals involving zeta functions on multidimensional lattices. Using these advanced numerical techniques, we offer a rigorous study of the stability of the bcc phase relative to the fcc phase as a function of the ATM coupling constant λ. Here, we neglect possible rhombohedral distortions[19,20,50] along the Bain path, which has not been investigated in detail yet beside the work by Ono and Ito,[40] as it requires a different treatment of our lattice sums.

This work is structured as follows: in Sec. II A, we provide basic definitions for general Bravais lattices; subsequently, we discuss cuboidal lattices in Sec. II B; we then introduce the Bain transformation in Sec. II C and discuss the resulting lattice sums for the cohesive energy, including both two- and three-body contributions in Sec. II D; we present our novel method for precisely evaluating three-body lattice sums in Sec. II E; after discussing the optimization of the nearest neighbor distance in Sec. II F, we apply our methods first to a one-dimensional chain in Sec. III A, and subsequently to two-dimensional square (SL) and hexagonal lattices (HL) in Sec. III B; we study three-dimensional lattices along the Bain path in Sec. III C and discuss qualitatively new physical behavior caused by the inclusion of the three-body ATM potential; and finally, we draw our conclusions and provide an outlook in Sec. IV.

II. THEORY

A. General lattice properties

We begin our treatment by defining lattices and important associated quantities. We call a point set $\Lambda \subseteq \mathbb{R}^d$ a (Bravais) lattice, if $\Lambda = B^\top \mathbb{Z}^d = \{\vec{i}^\top B = B^\top \vec{i} \mid \vec{i} \in \mathbb{Z}^d\}$ for some nonsingular matrix $B \in \mathbb{R}^{d\times d}$. The matrix $B = (\vec{b}_1, \ldots, \vec{b}_d)^\top$, called the generator matrix, contains the set of linearly independent lattice basis vectors $\vec{b}_i^\top$ as its rows. Lattices exhibit discrete translational invariance, meaning that $\Lambda + \vec{x} = \Lambda$ for any $\vec{x} \in \Lambda$. The Gram matrix G is defined in terms of the generator matrix as $G = BB^\top$ and appears in the computation of lattice vector norms. We further define the elementary lattice cell $B^\top(-\frac{1}{2}, \frac{1}{2})^d$. The lattice volume is defined by $V_\Lambda = |\det B| = \sqrt{\det G}$. An important lattice quantity is the minimum or nearest-neighbor distance R_Λ with

$$R_\Lambda = \min\{|\vec{x}-\vec{y}| \mid \vec{x},\vec{y} \in \Lambda,\ \vec{x} \neq \vec{y}\} = \min_{\vec{x}\in\Lambda\setminus\{0\}} |\vec{x}| \tag{4}$$

due to translational invariance of the lattice, where $|\vec{x}|$ denotes the Euclidean distance. In terms of the Gram matrix this is equivalent to

$$R_\Lambda = \min_{\vec{i}\in\mathbb{Z}^d\setminus\{0\}} \sqrt{\vec{i}^\top G \vec{i}}. \tag{5}$$

The packing density Δ_Λ describes the ratio between the volume of particles with radius ρ and the volume of the elementary lattice cell,

$$\Delta_\Lambda = \frac{\pi^{d/2}}{\Gamma(d/2+1)} \frac{\rho^d}{V_\Lambda}, \tag{6}$$

with the gamma function Γ. For dense hard sphere packings, we have $\rho = R_\Lambda/2$. Finally, the kissing number for dense hard sphere packings is defined as the number of nearest neighbors of an arbitrary lattice point,

$$\mathrm{kiss}(\Lambda) = \#\{\vec{v} \in \Lambda \mid |\vec{v}| = R_\Lambda\}. \tag{7}$$

B. Properties of cuboidal lattices

In case of the three-dimensional cuboidal lattices, we start from the work of Conway and Sloane (Ref. 51, Sec. 3) and consider the lattice generated by the vectors $(\pm u, \pm v, 0)^\top$ and $(0, \pm v, \pm v)^\top$, where u and v are non-zero real numbers. We now use the lattice basis vectors $\vec{b}_1^\top = (u,v,0)$, $\vec{b}_2^\top = (u,0,v)$, $\vec{b}_3^\top = (0,v,v)$, where u and v are non-zero real numbers. Let $A = u^2/v^2$. The generator matrix $B^\top$ and the Gram matrix G are

$$\begin{aligned} B^\top &= \begin{pmatrix} \vec{b}_1 & \vec{b}_2 & \vec{b}_3 \end{pmatrix} = v \begin{pmatrix} \sqrt{A} & \sqrt{A} & 0 \\ 1 & 0 & 1 \\ 0 & 1 & 1 \end{pmatrix}, \\ G &= BB^\top = v^2 \begin{pmatrix} A+1 & A & 1 \\ A & A+1 & 1 \\ 1 & 1 & 2 \end{pmatrix}. \end{aligned} \tag{8}$$

The determinant of the generator matrix reads $\det B = -2v^3\sqrt{A}$ and thus $V_\Lambda = 2|v^3|\sqrt{A}$.

Different lattice phases are obtained depending on the choice of the argument A. These are, in decreasing numerical order, as follows.

(i) $A = 1$: the face-centered cubic (fcc) lattice,
(ii) $A = 1/\sqrt{2}$: the mean centered-cuboidal (mcc) lattice,
(iii) $A = 1/2$: the body-centered cubic (bcc) lattice, and
(iv) $A = 1/3$: the axial centered-cuboidal (acc) lattice.

The resulting Gram matrices for the fcc and bcc lattices are identical to the ones shown in our previous work on lattice sums,[26] whereas the mcc and acc lattices occur in Refs. 51 and 52. A more detailed description of these cubic lattices and their transformations can be found in Refs. 48 and 49. The mcc lattice is the densest isodual lattice in three-dimensional space, but in addition to being of theoretical interest, has not been observed in nature so far. However, this lattice is expected to play a role in the dynamics of the cuboidal fcc to bcc transition, as we investigate in detail in this work.

Inserting either the generator matrix or the Gram matrix in Eq. (5) yields the nearest neighbor distance as a function of A,

$$R_\Lambda = \begin{cases} 2v\sqrt{A}, & 0 < A < 1/3, \\ v\sqrt{A+1}, & 1/3 \le A \le 1, \\ v\sqrt{2}, & A > 1. \end{cases} \tag{9}$$

From Eq. (6) then follows the packing density Δ_Λ for dense sphere packings,

$$\Delta_\Lambda = \begin{cases} (2\pi/3)A, & 0 < A < 1/3, \\ (\pi/12)\sqrt{(A+1)^3/A}, & 1/3 \le A \le 1, \\ (\pi/6)\sqrt{2/A}, & A > 1, \end{cases} \tag{10}$$

which is displayed in Fig. 2. On the interval $1/3 \le A \le 1$, which includes the acc, bcc, mcc, and fcc phases, the packing density has a maximum of $\pi\sqrt{2}/6 \approx 0.74$ at $A = 1$ corresponding to fcc and a minimum of $\pi\sqrt{3}/8 \approx 0.68$ at $A = 1/2$ corresponding to bcc. The acc lattice has a rather large packing density of $\Delta_{\text{acc}} = \frac{2\pi}{9} \approx 0.698$, but is the least dense packing with kissing number 10.[53,54] However, it is most likely strictly jammed according to the definition by Torquato and Stillinger.[55] It consists of linear chains of touching spheres surrounded by four neighboring linear chain arranged within a bct cell. It is the starting point of separated linear chain formation within region I ($A \le \frac{1}{3}$).

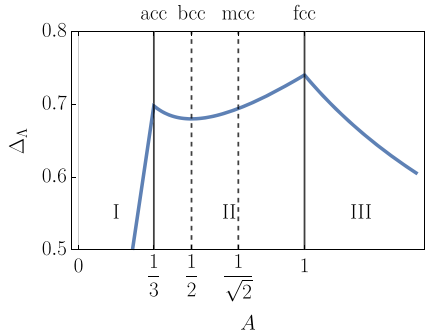

FIG. 2. Graph of the packing density Δ_Λ vs A. The regions I, II, and III, divided by the solid black lines, correspond to the different kissing numbers. Explicit formulas are given in Table I. The location of the fcc, mcc, bcc, and acc lattices are indicated by the black solid and dashed lines.

Finally, Eq. (7) yields the kissing number for dense sphere packings,

$$\text{kiss}(\Lambda) = \#\{\vec{v} \in \Lambda \mid |\vec{v}| = R_\Lambda\} = \begin{cases} 2, & A < 1/3, \\ 10, & A = 1/3 \text{ (acc)}, \\ 8, & 1/3 < A < 1, \\ 12 & A = 1 \text{ (fcc)}, \\ 4, & A > 1. \end{cases} \tag{11}$$

The limiting case $A \to \infty$ corresponds to infinitely separated two-dimensional square lattice layers with kissing number 4, while in the other extreme case, the limit $A \to 0$, we obtain infinitely dense 1D chains with kissing number 2 repeated on a two-dimensional grid, e.g., see Ref. 56.

Figure 2 shows a graph of the packing density as a function of the parameter A. Further information is recorded in Table I.

The cuboidal lattices belong to the body-centered tetragonal lattices (bct) usually defined by the two lattice constants a and c, as shown in Fig. 1. We can easily transform our two parameter space (u, v) used by Conway in terms of (R_Λ, A) used here and (a, c) used for bct lattices in the interval $1/3 \le A \le 1$ by

$$(u, v) = \left(R_\Lambda\sqrt{\frac{A}{A+1}}, \frac{R_\Lambda}{\sqrt{A+1}}\right)$$

and

$$(R_\Lambda, A) = \left(\frac{a}{2}\sqrt{2+\gamma^2}, \frac{1}{2}\gamma^2\right) \tag{12}$$

for the range $1/3 \le A \le 1$ (region II) and $\gamma = c/a$. For example, if we use for the bct lattice shown in Fig. 1 the lattice constants a and $\gamma = \sqrt{2}$, we get $A = 1$ (fcc) and $R_\Lambda = a$, which is the distance from the origin of the lattice to the nearest face-centered point, while for $\gamma = 1$, we get $A = \frac{1}{2}$ (bcc) and $R_\Lambda = a\frac{\sqrt{3}}{2}$, which is the distance from the origin to the nearest body-centered (bc) point, i.e., $R_\Lambda = R_{\text{bc}}$. From Eq. (12), we see that for $A < \frac{1}{2}$, we have $\gamma < 1$, which implies $c < a$. For $A \ge 1$ (region III), we have $R_\Lambda = a$, the distance between nearest neighbors in the base layer. For $A < \frac{1}{3}$, we enter region I for which we get $\gamma < \sqrt{\frac{2}{3}}$ and, therefore, $c < R_{\text{bc}}$. Using the two lattice parameters (R_Λ, A) has the advantage that $R_\Lambda \in a[\frac{\sqrt{3}}{2}, 1]$ in region II varies only slowly, and the Bain transformation introduced in Subsection II C is mostly described by one single dimensionless lattice parameter A.

TABLE I. Kissing number $\text{kiss}(\Lambda)$ and packing density Δ_Λ for the lattice defined in Eq. (8). The values in the table depend only on A and are independent of v.

Region	A	$\text{kiss}(\Lambda)$	Δ_Λ
I	$(0, \frac{1}{3})$	2	$\frac{2\pi A}{3}$
acc	$\frac{1}{3}$	10	$\frac{2\pi}{9}$
II	$(\frac{1}{3}, 1)$	8	$\frac{\pi}{12}\sqrt{\frac{(A+1)^3}{A}}$
fcc	1	12	$\frac{\pi\sqrt{2}}{6}$
III	$(1, \infty)$	4	$\frac{\pi}{6}\sqrt{\frac{2}{A}}$

C. The Bain transformation

The Bain transformation is a diffusionless smooth transformation from bcc to fcc and vice versa. If we start conveniently from the fcc generator matrix, we find a smooth transformation in terms of a diagonal matrix,

$$\tilde{B}^{\top}(A) = c(A)\,T_{\mathrm{Bain}}(A)\,\tilde{B}_{\mathrm{fcc}}^{\top} = c(A)\,\frac{1}{\sqrt{2}}\begin{pmatrix}\sqrt{A} & \sqrt{A} & 0\\ 1 & 0 & 1\\ 0 & 1 & 1\end{pmatrix}, \tag{13}$$

with $\tilde{B}(A) = B(A)/R(A)$ and $\tilde{B}_{\mathrm{fcc}} = \tilde{B}(1)$. The diagonal Bain matrix reads

$$T_{\mathrm{Bain}}(A) = \begin{pmatrix}\sqrt{A} & 0 & 0\\ 0 & 1 & 0\\ 0 & 0 & 1\end{pmatrix}, \tag{14}$$

and the prefactor $c(A)$ is given by

$$c(A) = \begin{cases} 1/\sqrt{2A}, & 0 < A < 1/3,\\ \sqrt{2/(A+1)}, & 1/3 \le A \le 1,\\ 1, & A > 1. \end{cases} \tag{15}$$

In the particularly relevant range $1/3 \le A \le 1$, the rescaled generator matrix takes the form

$$\tilde{B}^{\top}(A) = \frac{1}{\sqrt{A+1}}\begin{pmatrix}\sqrt{A} & \sqrt{A} & 0\\ 1 & 0 & 1\\ 0 & 1 & 1\end{pmatrix}. \tag{16}$$

In later sections, we will extend the above-mentioned definition of $\tilde{B}^{\top}(A)$ in Eq. (16) to the whole range $0 < A \le 1$, where the nearest-neighbor distance for $A \ge 1/3$ is given by the lattice constant a (see Fig. 1) and to the distance between the origin and the body-centered atom for $0 < A < \frac{1}{3}$. As always, the Bain transformation matrix depends on the particular choice of lattice basis vectors.

D. Cohesive energies from a Lennard-Jones potential coupled to a three-body Axilrod–Teller–Muto term

Using translational invariance of the lattice, the static cohesive energy for a lattice can be expressed in terms of a many-body perturbative expansion of the interaction energy from a chosen atom at the origin,

$$E_{\mathrm{coh}} = \sum_{k=2}^{\infty} E_{\mathrm{coh}}^{(k)} = \frac{1}{2}\sum_{i\in\mathbb{N}} E^{(2)}(\vec{r}_{0i}) + \frac{1}{3}\sum_{\substack{i,j\in\mathbb{N}\\ j>i}} E^{(3)}(\vec{r}_{0i},\vec{r}_{0j},\vec{r}_{ij}) + \text{h.o.t}, \tag{17}$$

with $\vec{r}_{ij} = \vec{r}_i - \vec{r}_j$, $r_{ij} = |\vec{r}_{ij}|$, $\mathbb{N} = \{1,2,3,\cdots\}$ being the set of natural numbers, and $i = 0$ denotes the index of the atom at the chosen origin in the solid. The perturbative expansion is formally exact for finite clusters, but is often slowly convergent, or perhaps even divergent as suggested by Heine *et al.*,[57] especially for metallic systems.[36]

In this work, we focus our studies on the two- and three-body interactions, neglecting vibrational and temperature effects, as well as higher order terms (h.o.t.), such as four-body interactions. In the following, we adopt dimensionless units, writing length scales in units of the equilibrium distance r_e of the LJ potential, and energies in units of the LJ dissociation energy ε.

The dimensionless two-body potential in (17) then takes the form,

$$E_{\mathrm{LJ}}^{(2)}(\vec{r}) = \frac{\mathrm{nm}}{n-m}\left(\frac{1}{n}|\vec{r}|^{-n} - \frac{1}{m}|\vec{r}|^{-m}\right), \tag{18}$$

with $n > m > 3$. The resulting cohesive energy can be written in terms of the Epstein zeta function, a generalization of the Riemann zeta function to higher-dimensional lattices. For a lattice Λ, an interaction exponent $v > d$, and a wavevector $\vec{k}$, it reads[27]

$$Z_{\Lambda,v}(\vec{k}) = {\sum_{\vec{x}\in\Lambda}}' \frac{e^{-2\pi i\vec{x}\cdot\vec{k}}}{|\vec{x}|^{v}}, \tag{19}$$

where the lattice sum can be meromorphically continued to $v \in \mathbb{C}$. For the LJ lattice sum, the Epstein zeta function is evaluated at $\vec{k} = 0$ only, where we omit the argument $Z_{\Lambda,v} = Z_{\Lambda,v}(0)$ to simplify the notation. General wavevectors will, however, become crucial in the evaluation of three-body lattice sums. The two-body term in the cohesive energy for a LJ potential can then be rewritten as

$$\begin{aligned} E_{\mathrm{coh}}^{(2)} &= \frac{nm}{2(n-m)}{\sum_{\vec{x}\in\tilde{\Lambda}}}'\left(\frac{|\vec{x}|^{-n}}{nR^n} - \frac{|\vec{x}|^{-m}}{mR^m}\right)\\ &= \frac{nm}{2(n-m)}\left(\frac{Z_{\tilde{\Lambda},n}}{nR^n} - \frac{Z_{\tilde{\Lambda},m}}{mR^m}\right), \end{aligned} \tag{20}$$

where we use the normalized lattice $\tilde{\Lambda} = \Lambda/R$. This normalization is useful, as the distance R (e.g., the nearest neighbor distance) will become a tuning parameter depending along the Bain path on the exponents n and m and on the parameter A as specified in the next sections. It also shows more clearly the link to the LJ potential (18) for a diatomic.

Different computationally efficient methods for evaluating the Epstein zeta function exist. In Appendix E, we evaluate the arising sums for particular lattices $\tilde{\Lambda}(A) = \tilde{B}^{\top}(A)\mathbb{Z}^3$ using Bessel function expansions in Eq. (E38) or Eq. (E39), with the more common notation,

$$L(A, n/2) = Z_{\tilde{\Lambda}(A),n}. \tag{21}$$

As an alternative, for general d-dimensional lattice sums including oscillatory factors and lattice shifts, the recently created high-performance library EpsteinLib (github.com/epsteinlib) can be used.[58] Both approaches allow computing the two-body term to machine precision.

In a similar way, we express the three-body Axilrod–Teller–Muto (ATM) potential in Eq. (3) in dimensionless units. As the ATM potential only depends on relative distance vectors, we can set $\vec{x} = \vec{r}_{0i}$, $\vec{y} = \vec{r}_{0j}$, and $\vec{z} = \vec{r}_{ij} = \vec{y} - \vec{x}$, yielding the potential as a function of two vectors only,

$$E^{(3)}_{\mathrm{ATM}}(\vec{x},\vec{y}) = \lambda \left(\frac{1}{|\vec{x}|^3|\vec{y}|^3|\vec{z}|^3} - 3\frac{(\vec{x}\cdot\vec{y})(\vec{y}\cdot\vec{z})(\vec{z}\cdot\vec{x})}{|\vec{x}|^5|\vec{y}|^5|\vec{z}|^5} \right)\Bigg|_{\vec{z}=\vec{y}-\vec{x}}, \quad (22)$$

where the minus sign on the right-hand side arises due to $\vec{r}_{ji} = -\vec{r}_{ij}$. The cohesive energy contribution due to the three-body interactions is given by the lattice sum,

$$E^{(3)}_{\mathrm{coh}} = \frac{1}{6}\sum_{\vec{x},\vec{y}\in\Lambda}{}' E^{(3)}_{\mathrm{ATM}}(\vec{x},\vec{y}), \quad (23)$$

where the prefactor 1/6 avoids double counting and where the primed sum excludes the undefined cases $\vec{x} = 0$, $\vec{y} = 0$, and $\vec{x} = \vec{y}$. We now normalize the lattice, setting $\tilde{\Lambda} = \Lambda/R$ and subsequently split the three-body lattice sum into a radially isotropic and an anisotropic part,

$$E^{(3)}_{\mathrm{coh}} = \lambda f^{(3)}_{\mathrm{coh}} R^{-9} = \lambda(f^{(3)}_r + f^{(3)}_a)R^{-9}, \quad (24)$$

with the normalized lattice sums,

$$\begin{aligned} f^{(3)}_{\mathrm{coh}} &= f^{(3)}_r + f^{(3)}_a, \\ f^{(3)}_r &= \frac{1}{6}\sum_{\vec{x},\vec{y}\in\tilde{\Lambda}}{}' \frac{1}{|\vec{x}|^3|\vec{y}|^3|\vec{z}|^3}, \\ f^{(3)}_a &= -\frac{1}{2}\sum_{\vec{x},\vec{y}\in\tilde{\Lambda}}{}' \frac{(\vec{x}\cdot\vec{y})(\vec{y}\cdot\vec{z})(\vec{z}\cdot\vec{x})}{|\vec{x}|^5|\vec{y}|^5|\vec{z}|^5}, \end{aligned} \quad (25)$$

where we adopt the convention $\vec{z} = \vec{y} - \vec{x}$ from now on. For simplicity, we leave away the tilde in the following, assuming that the lattices have been appropriately normalized. The above-mentioned form for the three-body lattice form makes it immediately clear that the ATM potential becomes attractive in one dimension, as then $f_a = -3f_r$ and hence $E^{(3)}_{\mathrm{coh}} = -2\lambda f_r R^{-9} < 0$.

E. Efficient computation of the ATM cohesive energy

The efficient computation of three-body lattice sums has been an important open problem, which we solve in this work. In the past, elaborate direct summation methods have been used,[35,59–63] where, however, a single evaluation in three dimensions can demand up to four weeks of single core central processing unit (CPU) time. In this section, we briefly show how general three-body interactions, including the ATM potential, can be computed from singular integrals that involve products of Epstein zeta functions. A deeper discussion, including a rigorous proof as well as numerical benchmarks, is provided in Ref. 30. For a lattice $\Lambda = B^{\mathsf{T}}\mathbb{Z}^d$ with $B \in \mathbb{R}^{d\times d}$ nonsingular, we consider general lattice sums of the form

$$\zeta^{(3)}_\Lambda(\vec{v}) = \sum_{\vec{x},\vec{y}\in\Lambda}{}' |\vec{x}|^{-v_1}|\vec{y}|^{-v_2}|\vec{y}-\vec{x}|^{-v_3}, \quad (26)$$

with $\vec{v} = (v_1, v_2, v_3)^T$, and its meromorphic continuations to $v_i \in \mathbb{C}$ (see Appendix H for details), which we call three-body zeta functions. One can show that the above-mentioned double sum converges absolutely and independently of the summation order if and only if the conditions $v_i + v_j > d$ for $i \neq j$, and $v_1 + v_2 + v_3 > 2d$ hold.

We note in passing that this lattice sum can be extended to the more general n-body zeta function, which will be addressed in our future work.

We first show that the normalized ATM cohesive energy in Eq. (25) can be written as a finite recombination of the above-mentioned zeta functions. The radially symmetric term $f^{(3)}_r$ is already in the desired form with

$$f^{(3)}_r = \frac{1}{6}\zeta^{(3)}_\Lambda(3,3,3). \quad (27)$$

For the anisotropic part $f^{(3)}_a$, we note that the vector products can be rewritten as

$$\begin{aligned} 2\vec{x}\cdot\vec{y} &= |\vec{x}|^2 + |\vec{y}|^2 - |\vec{z}|^2, \\ 2\vec{y}\cdot\vec{z} &= |\vec{y}|^2 + |\vec{z}|^2 - |\vec{x}|^2, \\ 2\vec{z}\cdot\vec{x} &= -(|\vec{z}|^2 + |\vec{x}|^2 - |\vec{y}|^2). \end{aligned} \quad (28)$$

As the above-mentioned lattice sums remain unchanged under permutation of $\vec{x}$, $\vec{y}$, and $\vec{z}$, we find

$$\begin{aligned} f^{(3)}_a &= -\frac{1}{2}\sum_{\vec{x},\vec{y}\in\Lambda}{}' \frac{(\vec{x}\cdot\vec{y})(\vec{y}\cdot\vec{z})(\vec{z}\cdot\vec{x})}{|\vec{x}|^5|\vec{y}|^5|\vec{z}|^5} \\ &= -\frac{1}{16}\sum_{\vec{x},\vec{y}\in\Lambda}{}' \left(3\frac{|\vec{x}|}{|\vec{y}|^5|\vec{z}|^5} - 6\frac{1}{|\vec{x}||\vec{y}|^3|\vec{z}|^5} + 2\frac{1}{|\vec{x}|^3|\vec{y}|^3|\vec{z}|^3} \right). \end{aligned}$$

Rewriting the above-mentioned right-hand side in terms of three-body zeta functions yields

$$f^{(3)}_a = -\frac{1}{16}\left(3\zeta^{(3)}_\Lambda(-1,5,5) - 6\zeta^{(3)}_\Lambda(1,3,5) + 2\zeta^{(3)}_\Lambda(3,3,3) \right). \quad (29)$$

Recombining $f^{(3)}_r$ and $f^{(3)}_a$ finally yields the ATM cohesive energy in terms of three-body zeta functions,

$$f^{(3)}_{\mathrm{coh}} = \frac{1}{24}\zeta^{(3)}_\Lambda(3,3,3) - \frac{3}{16}\zeta^{(3)}_\Lambda(-1,5,5) + \frac{3}{8}\zeta^{(3)}_\Lambda(1,3,5). \quad (30)$$

The three-body zeta function can now be recast as an integral over products of Epstein zeta functions. Recall that for a wavevector $\vec{k} \in \mathbb{R}^d$, the Epstein zeta function reads

$$Z_{\Lambda,v}(\vec{k}) = \sum_{\vec{x}\in\Lambda}{}' \frac{e^{-2\pi i\vec{k}\cdot\vec{x}}}{|\vec{x}|^v}, \quad v > d,$$

which can be meromorphically continued to $v \in \mathbb{C}$. For an extensive discussion of the analytical properties of the Epstein zeta function, see Ref. 58. Using the properties of the Epstein zeta function, one can now show that for any $v_i > 0, i = 1, \ldots, 3$,

$$\zeta^{(3)}_\Lambda(\vec{v}) = V_\Lambda \int_{E^*} Z_{\Lambda,v_1}(\vec{k}) Z_{\Lambda,v_2}(\vec{k}) Z_{\Lambda,v_3}(\vec{k})\, \mathrm{d}\vec{k}, \quad (31)$$

where V_Λ denotes the volume of the elementary lattice cell and $E^* = B^{-1}(-1/2, 1/2)^d$ defines the unit cell of the reciprocal lattice $\Lambda^* = B^{-1}\mathbb{Z}^d$ centered around the Γ-point. The proof of this formula

is based on exchanging summation and integration for sufficiently large v_i and then applying the relation,

$$V_\Lambda \int_{E^*} e^{-2\pi i \vec{k}\cdot\vec{x}}\, \mathrm{d}\vec{k} = \delta_{\vec{x},\vec{0}},$$

with δ being the Kronecker delta. A mathematically rigorous proof as well as details on the numerical computation of the integral will be provided elsewhere.

Special care needs to be taken in evaluating the resulting integral, as the Epstein zeta function exhibits a singularity at $\vec{k} = 0$. We can separate the Epstein zeta function into an analytic function and a singularity as follows:

$$Z_{\Lambda,v}(\vec{k}) = Z^{\mathrm{reg}}_{\Lambda,v}(\vec{k}) + \frac{1}{V_\Lambda}\hat{s}_v(\vec{k}), \tag{32}$$

where the regularized Epstein zeta function $Z^{\mathrm{reg}}_{\Lambda,v}(\vec{k})$ is analytic in the reciprocal unit cell. The function $\hat{s}_v(\vec{k})$ can be understood as the Fourier transform of $|\vec{z}|^{-v}$ (in the distributional sense). It is defined as

$$\hat{s}_v(\vec{k}) = \frac{\pi^{v-d/2}}{\Gamma(v/2)}\Gamma((d-v)/2)|\vec{k}|^{v-d}, \quad v \notin (d+2\mathbb{N}).$$

In case that $v = d + 2n$, $n \in \mathbb{N}$, the Fourier transform is only uniquely defined up to a polynomial of degree $2n$. We adopt the choice,

$$\hat{s}_{d+2n}(\vec{k}) = \frac{\pi^{n+d/2}}{\Gamma(n+d/2)}\frac{(-1)^{n+1}}{n!}(\pi\vec{k}^2)^n \log(\pi\vec{k}^2).$$

Hence, the Epstein zeta function equals the sum of an analytic function and a power-law or logarithmic singularity. Therefore, the integral can be efficiently computed using either a specialized Gauss–Legendre quadrature or a Duffy transformation.[64] Our results are benchmarked against a direct summation approach, presented in Appendix C, where we reach full precision in one and two dimensions, where the direct sum can still be evaluated to machine precision.

F. Minimizing the cohesive energy

In order to analyze the impact of a long-range three-body ATM potential on the stability of lattices with two-body LJ interactions, we need to determine the optimal nearest neighbor distance $R > 0$ that minimizes the cohesive energy,

$$E_{\mathrm{coh}} = c_{n,m}\left(\frac{Z_{\Lambda,n}}{nR^n} - \frac{Z_{\Lambda,m}}{mR^m}\right) + \lambda f^{(3)}_{\mathrm{coh}} R^{-9}, \tag{33}$$

with $n > m$ and

$$c_{n,m} = \frac{nm}{2(n-m)}$$

for a given lattice Λ with distance R. The resulting global minimization problem can be easily solved numerically using standard tools. It is, however, instructive to discuss particular special cases some of which allow for an analytic solution. Here, we distinguish the cases where the repulsive part of the LJ potential dominates the three-body potential for small nearest neighbor distances or not.

1. $n > 9$: after setting $\partial E_{\mathrm{coh}}/\partial R = 0$, this case reduces to solving the following root finding problem:

$$c_{n,m}(Z_{\Lambda,n} - Z_{\Lambda,m}R^{n-m}) + 9\lambda f^{(3)}_{\mathrm{coh}} R^{n-9} = 0. \tag{34}$$

For the special case $n = 9 + k$ and $m = 9 - k$, the energy minimum can be determined analytically as

$$R_{\min}(n,m,\lambda) = \left(\frac{9\lambda f^{(3)}_{\mathrm{coh}}}{2c_{n,m}Z_{\Lambda,m}} + \sqrt{\left(\frac{9\lambda f^{(3)}_{\mathrm{coh}}}{2c_{n,m}Z_{\Lambda,m}}\right)^2 + \frac{Z_{\Lambda,n}}{Z_{\Lambda,m}}}\right)^{1/(n-9)}. \tag{35}$$

The often used (12,6) LJ potential with $k = 3$ belongs to this class.

2. $n = 9$: in this special case, we find from Eq. (34) that

$$R_{\min}(n,m,\lambda) = \left(\frac{Z_{\Lambda,n}}{Z_{\Lambda,m}} + \frac{9\lambda f^{(3)}_{\mathrm{coh}}}{c_{n,m}Z_{\Lambda,m}}\right)^{1/(9-m)}. \tag{36}$$

In case of attractive three-body interactions ($f^{(3)}_{\mathrm{coh}} < 0$), the minimum only exists for sufficiently small ATM coupling strength λ with

$$\lambda \le \frac{c_{n,m}Z_{\Lambda,n}}{9|f^{(3)}_{\mathrm{coh}}|}. \tag{37}$$

3. $n < 9$: this case requires special care. The ATM potential dominates the LJ term for small R. For attractive three-body interactions, this means that the global minimum of the energy is obtained for $R \to 0$, leading to a collapse of the lattice into the origin. Local energy minima can, however, exist for $R > 0$. For the special case $n = 9 - k$, $m = 9 - 2k$, we find extrema at

$$R = \left(\frac{Z_{\Lambda,n}}{2Z_{\Lambda,m}} \pm \sqrt{\left(\frac{Z_{\Lambda,n}}{2Z_{\Lambda,m}}\right)^2 + \frac{9\lambda f^{(3)}_{\mathrm{coh}}}{c_{n,m}Z_{\Lambda,m}}}\right)^{1/(9-n)}. \tag{38}$$

For attractive three-body interactions, a local minimum exists under the condition,

$$\lambda \le c_{n,m}\frac{Z^2_{\Lambda,n}}{36Z_{\Lambda,m}|f^{(3)}_{\mathrm{coh}}|}. \tag{39}$$

In the following, we introduce instructive toy models in one and two dimensions where R is chosen to be the nearest neighbor distance. We then analyze the influence of three-body interactions on the stability of cuboidal phases along a Bain path in three dimensions, where we choose R as the distance from the atom at the origin

to the body-centered atom, which is the nearest neighbor distance in region I ($\frac{1}{3} \le A \le 1$, see Fig. 2).

III. RESULTS AND DISCUSSION

A. LJ + ATM potential for an equidistant infinite linear chain

We begin our investigation with the effect of a three-body ATM potential coupled to a two-body LJ-potential in one dimension for an equidistant linear chain. The cohesive energy for the chain with nearest neighbor distance R and normalized lattice $\Lambda = \mathbb{Z}$ becomes

$$E_{\mathrm{coh}}(R,n,m) = E^{(2)}_{\mathrm{coh}}(R,n,m) + E^{(3)}_{\mathrm{coh}}(R,n,m) = c_{n,m}\left(\frac{2\zeta(n)}{nR^n} - \frac{2\zeta(m)}{mR^m}\right) + \lambda f^{(3)}_{\mathrm{coh}} R^{-9}, \quad (40)$$

where we have used that the Epstein zeta function in 1D reduces to twice the Riemann zeta function, $Z_{\mathbb{Z},n} = 2\zeta(n)$. In this 1D case, the simple pole is situated at $n = 1$ and $Z_{\mathbb{Z},n} \to 2$ for $n \to \infty$ as each atom has two nearest neighbors. The three-body ATM potential in 1D is purely attractive, which follows directly from Eq. (25),

$$f^{(3)}_{\mathrm{coh}} = f^{(3)}_r + f^{(3)}_a = \frac{1}{6}\sum_{x,y\in\mathbb{Z}}{}' \frac{1}{|x|^3|y|^3|z|^3} - \frac{1}{2}\sum_{x,y\in\mathbb{Z}}{}' \frac{(xy)(yz)(zx)}{|x|^5|y|^5|z|^5} = -\frac{1}{3} f^{(3)}_r < 0. \quad (41)$$

The attractive behavior of the ATM potential for three atoms in a line has been discussed already by Axilrod and Teller[32] and will have important consequences in the following.

In one dimension, the three-body cohesive energy can still be evaluated to machine precision using exact summation. We obtain $f^{(3)}_{\mathrm{coh}} = -0.272\,301\,849\,507\,688\,6$, which is in excellent agreement with the result from the Epstein zeta function treatment ($f^{(3)}_{\mathrm{coh}} = -0.272\,301\,849\,507\,688\,65$), as outlined in Sec. II E. This serves as a benchmark for higher dimensional lattices, where exact summation becomes exceedingly numerically expensive.

We now discuss the optimal nearest-neighbor distance $R_{\min}(n,m,\lambda)$ as obtained in the previous Sec. II F for different repulsive LJ exponents n.

1. $n > 9$: in this regime, the repulsive part of the LJ potential dominates the attractive ATM term. The solution to the root finding problem in Eq. (34) can be obtained numerically, with analytical solutions available for special cases, such as the (12,6)-LJ potential in Eq. (35). We obtain $R_{\min}(12,6,0.0) = 0.997\,179\,263\,885\,806$, $R_{\min}(12,6,1.0) = 0.964\,148\,870\,884\,975$, $R_{\min}(12,6,3.0) = 0.902\,526\,982\,458\,744$, and $R_{\min}(12,6,5.0) = 0.847\,847\,116\,323\,818$.

   As expected, the nearest-neighbor distance decreases with increasing coupling strength λ due to the increasing ATM attraction.
2. $n = 9$: here, the repulsive part of the LJ potential and the attractive ATM potential share the same scaling and their prefactors determine the dominant term. The value of R that minimizes the energy is given by Eq. (36) as long as λ obeys the bound,

$$\lambda \le \frac{m\zeta(9)}{|(m-9)f^{(3)}_{\mathrm{coh}}|}. \quad (42)$$

   If this critical value of λ is exceeded, then the energy diverges to $-\infty$ for $R \to 0$ and the chain collapses into the origin.

   For example, for the (9,6)-LJ potential, we get $\lambda \le 7.359\,541\,586\,938\,727$. At larger coupling strengths, the minimum vanishes and the interaction becomes purely attractive and collapse occurs, i.e., $R \to 0$. This has consequences for 2D or 3D lattices as under this model, the crystal may distort into a set of linear chains, as we shall see later on.
3. $n < 9$: here, the attractive ATM potential dominates at small distances R and the global minimum is obtained for $R \to 0$. Local minima can, however, exist for $R > 0$, as described in Sec. II, with analytic solutions available for $n = 9 - k$ and $m = 9 - 2k$. A minimum then exists for sufficiently small λ as described by Eq. (39). For example, for $m = 4$ ($k = \frac{5}{2}$) and $n = \frac{13}{2}$, we obtain $\lambda < 1.003\,897\,458\,750\,910$, which is a rather small value. We find that by lowering the exponent for the repulsive force in the LJ potential, the existence of a minimum for the cohesive energy is achieved at lower critical values of the coupling strength λ.

Figure 3 summarizes our results for cases 1 and 3 for two different LJ potentials. When the two-body potential is of (12,6)-LJ type, the repulsive LJ term dominates at short distances over the ATM term in the cohesive energy. On the other hand, for a softer two-body potential with exponent $n < 9$, as for the (6,4)-LJ potential, the ATM potential completely dominates over the repulsive part of the LJ term for $\lambda > 0.9$ making the total cohesive energy behave like $-R^{-9}$ with a singularity at $R = 0$. When $\lambda \le 0.689$, there is a competition between the attractive and repulsive parts of the cohesive energy, leading to a maximum in the short-range region that makes the cohesive energy slightly positive, followed by a divergence toward $-\infty$ due to the dominance of the attractive three-body term. It is well-known that the simple ATM term is valid only in the long-range[65] and one has to correct the unphysical behavior of the three-body term in the short range in order to avoid the collapse of all atoms toward the origin. On the other hand, one should make sure that the repulsive wall in the two-body potential is described realistically.

B. LJ + ATM potential for a square and hexagonal lattice

After analyzing the one-dimensional chain, we extend our focus to two-dimensional lattices. Among the five possible Bravais lattices, we restrict ourselves to the case of a square (SL) and hexagonal lattice (HL) with a nearest-neighbor distance R, as shown in Fig. 4, and to the rectangular lattices as a mode to distort the square lattice into a set of linear chains. The hexagonal lattice is the densest packing of circles in a two-dimensional plane.

The two- and three-body terms of the cohesive energy for a square lattice $\Lambda = \mathbb{Z}^2$ are given by Eq. (33). Note that the Epstein zeta function for the square lattice appearing in the LJ term can be rewritten in terms of elementary functions,[66]

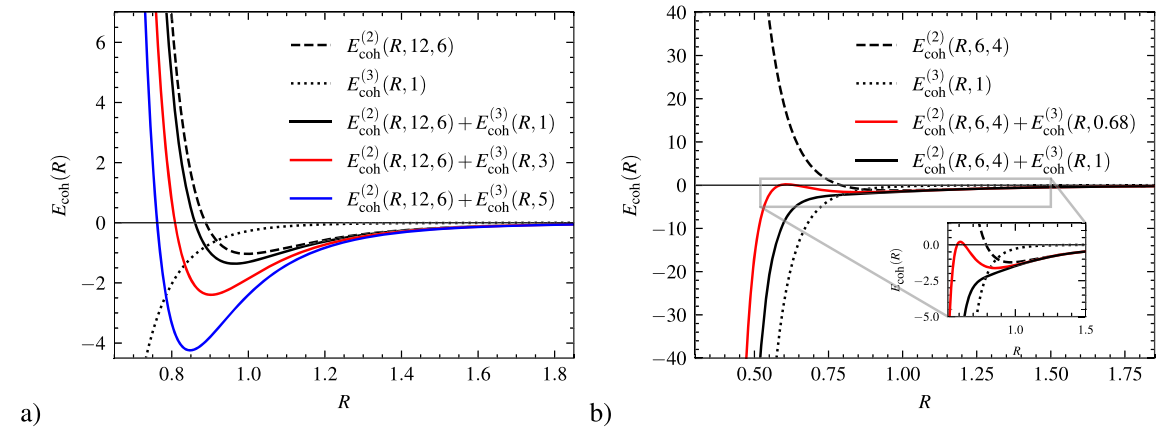

FIG. 3. Cohesive energy of a linear chain with atoms interacting through (a) (12,6)-LJ coupled to an ATM potential and (b) (6,4)-LJ coupled to an ATM potential. Separate two- and three-body contributions are also indicated by the dashed and dotted lines, respectively.

$$Z_{\mathbb{Z}^2,n} = 4\zeta\left(\frac{n}{2}\right)\beta\left(\frac{n}{2}\right), \tag{43}$$

where β denotes the Dirichlet beta function.

The three-body term of the cohesive energy is given by Eq. (25). After an evaluation of the lattice sums through direct summation restricting the sums over integers to $N_{\rm max} = 1600$, the ATM term in the cohesive energy of the square lattice can be written as

$$E^{(3)}_{\rm coh} = \lambda f^{(3)}_{\rm coh} R^{-9}, \tag{44}$$

with $f^{(3)}_{\rm coh} = f^{(3)}_r + f^{(3)}_a = 0.770\,093\,650\,517\,104\,54$ where $f^{(3)}_r = 2.275\,482\,285\,892\,362\,5$ and $f^{(3)}_a = -1.505\,388\,635\,375\,258\,4$; see Eq. (25). This compares well to the more accurate result from the Epstein zeta treatment as outlined in Sec. II E, i.e., we get $f^{(3)}_{\rm coh} = 0.770\,093\,650\,516\,716\,2$ with $f^{(3)}_r = 2.275\,482\,285\,893\,09$ and $f^{(3)}_a = -1.505\,388\,635\,376\,373\,7$. The three-body contribution from an ATM potential to the cohesive energy is now repulsive for any R in the square lattice in contrast to the 1D case.

One can now perform a similar analysis compared to the 1D case. We only mention two examples here. For the (12,6)-LJ potential, the optimal nearest-neighbor distance is given by Eq. (35), where the ATM potential is now positive. This results in $R_{\rm min}(12,6,0.0) = 0.977\,489\,041\,852\,768$, $R_{\rm min}(12,6,1.0) = 1.021\,577\,293\,064\,089$, $R_{\rm min}(12,6,3.0) = 1.112\,586\,607\,942\,759$, and $R_{\rm min}(12,6,5.0) = 1.202\,957\,096\,531\,386$. We see that the distance is increasing rapidly with increasing coupling strength λ.

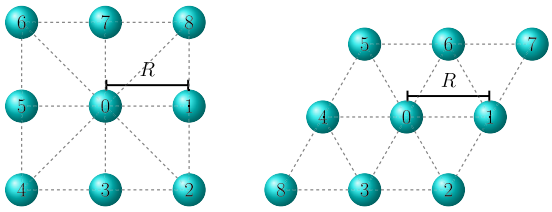

FIG. 4. Square and hexagonal lattices of atoms interacting through LJ + ATM potentials with nearest-neighbor distance R.

The other case we consider here is when the potential becomes completely repulsive over the whole range of R values. This can happen if the attractive R^{-m} term is always dominated by the repulsive ATM term, which can only occur for $m \geq 9$. Consider the case $m = 9$, which leads to the minimum distance,

$$R_{\rm min}(n,9,\lambda) = \left(\frac{Z_{\Lambda,n}}{Z_{\Lambda,9} - 9\lambda f^{(3)}_{\rm coh}/c_{n,9}}\right)^{1/(n-9)} \tag{45}$$

and to the condition that

$$\lambda < \frac{c_{n,9} Z_{\Lambda,9}}{9 f^{(3)}_{\rm coh}}. \tag{46}$$

For example, for $n = 12$, we get $\lambda < 10.885\,087\,443\,434\,88$. With increasing exponent n, the critical λ value decreases as one would expect.

The cohesive energy for the square lattice as a function of R for two different (n,m)-LJ potentials coupled to the ATM potential is shown in Fig. 5. We depict the two-body term $E^{(2)}_{\rm coh}(R,n,m)$, the three-body contribution $E^{(2)}_{\rm coh}(R,\lambda)$, and the full cohesive energy. An example of the long-range region becoming dominated by the repulsive ATM term is for the hard (30,12)-LJ potential, as shown in Fig. 5. For $\lambda = 1$, there is a region in which the square crystal is bounded around the equilibrium distance; however, for $\lambda > 3.1834$, the cohesive energy becomes positive at any distance, meaning that we have a purely repulsive potential energy.

There is one small caveat here to consider as the square lattice might distort to a set of weakly interacting linear chains, which may collapse to the origin for $n \leq 9$ as discussed in Sec. II. In order to

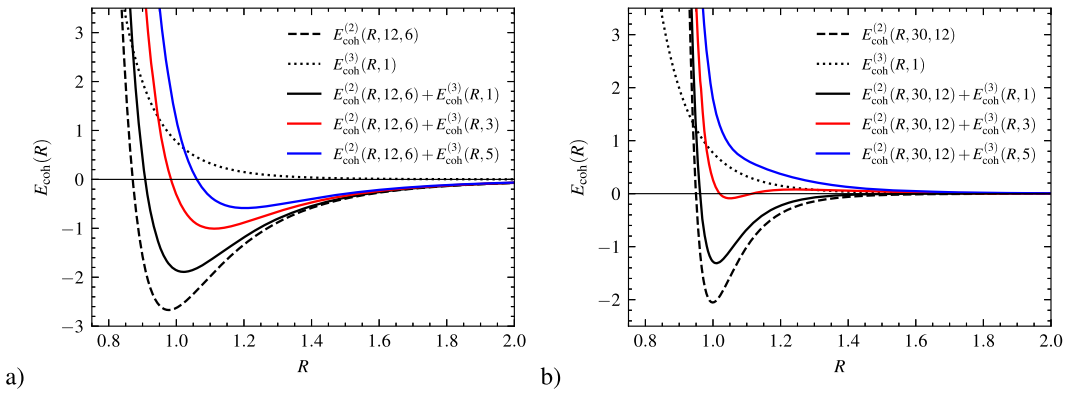

FIG. 5. Cohesive energy of the square lattice with atoms interacting through (a) (12,6)-LJ potential coupled to an ATM potential and (b) (30,12)-LJ coupled to an ATM potential. Separate two- and three-body contributions are represented by the dashed and dotted lines, respectively.

show this, we consider the following generator matrix B^{T} and Gram matrix G:

$$B^{\mathsf{T}} = \begin{pmatrix} 1 & 0 \\ 0 & \gamma \end{pmatrix}, \quad G = \begin{pmatrix} 1 & 0 \\ 0 & \gamma^2 \end{pmatrix}, \tag{47}$$

which allow the square lattice to distort into a rectangular lattice where γ is the distortion parameter. Here, analytical solutions for the corresponding LJ lattice sums exist only for special cases of γ values.[26,67,68] We, therefore, use either the Van der Hoff Benson expansion[69] (see Appendix D) or EpsteinLib for the two-body term, and direct summation for the three-body term, where the latter approximation is sufficiently accurate to demonstrate the effect of such an unphysical distortion.

As it turns out, there exists a critical value of $\gamma_c \approx 1.388$ that makes the three-body term of the cohesive energy neither repulsive nor attractive, i.e., $E_{\rm coh}^{(3)}(R,\gamma,\lambda) = 0, \lambda > 0$. This critical value remains basically constant along different λ values with a (shallow) saddle point appearing at $(\gamma_c,\lambda_c) = (1.388, 1.526)$. γ_c can be seen as the limit between the three-body attractive interaction in the linear chain and the three-body repulsion characteristic of the square lattice as shown before. The (γ,λ)-cohesive energy hypersurface for the difference in cohesive energy with respect to the square lattice with $(\gamma,\lambda) = (1,0)$, i.e.,

$$\Delta E_{\rm coh}(R,\gamma,\lambda) = E_{\rm coh}(R,\gamma,\lambda) - E_{\rm coh}(R,1,0) \tag{48}$$

is shown in Fig. 6. The square lattice without three-body interactions is located at a local minimum of the hypersurface at $(\gamma,\lambda) = (1,0)$, whereas the global minimum in the selected range is found at the upper right corner of the plot.

The point $(\gamma,\lambda) = (2,5)$ corresponds to a rectangular lattice with one of the sides of its unit cell being twice as large as the other. The reason for the high stability of this structure with respect to the square lattice is due to the fact that it is located at the region where the three-body potential becomes attractive, similar to the case of the linear chain. In fact, the square lattice structure is highly destabilized by the repulsive three-body forces, as shown in the lower right corner of Fig. 6, whereas the rectangular lattice in the upper left corner is destabilized due to two-body forces.

In a similar way, the generator matrix and the Gram matrix for the hexagonal lattice $\Lambda_{\rm hex} = B^{\mathsf{T}}\mathbb{Z}^2$, depicted in Fig. 4, are given by

$$B_{\rm hex}^{\mathsf{T}} = \begin{pmatrix} 1 & \frac{1}{2} \\ 0 & \frac{\sqrt{3}}{2} \end{pmatrix}, \quad G_{\rm hex} = \begin{pmatrix} 1 & \frac{1}{2} \\ \frac{1}{2} & 1 \end{pmatrix}. \tag{49}$$

The lattice sum of the hexagonal lattice also has an analytical formula given by Zucker and Robertson,[66]

$$Z_{\Lambda_{\rm hex},n} = 6\zeta\left(\frac{n}{2}\right)\left[3^{-n/2}\left(\zeta\left(\frac{n}{2},\frac{1}{3}\right) - \zeta\left(\frac{n}{2},\frac{2}{3}\right)\right)\right], \tag{50}$$

where $\zeta(n,x)$ is the Hurwitz zeta function; see Appendix A. The full cohesive energy is then given by Eq. (33).

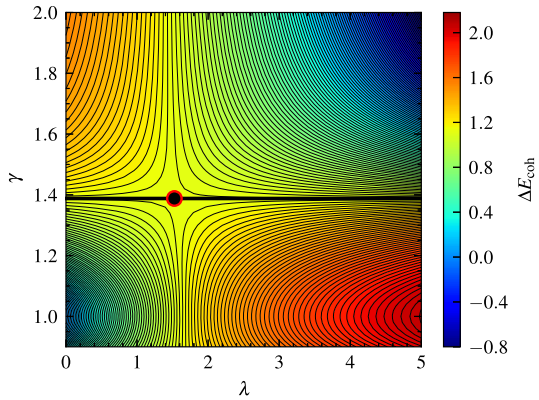

FIG. 6. (γ,λ)-hypersurface for the difference in the cohesive energy of a rectangular lattice at optimized R with respect to the ideal square lattice at $(\gamma,\lambda) = (1,0)$. The horizontal black line indicates the critical value of γ in which the ATM potential is neither repulsive nor attractive, and the black point sits at the saddle point, located at $(\gamma_c,\lambda_c) = (1.388, 1.526)$.

For the three-body term in Eq. (25), we evaluate the 2D lattice sums through direct summation with $N_{\max} = 1600$ to get

$$E^{(3)}_{\rm coh}(R,\lambda) = \lambda f^{(3)}_{\rm coh} R^{-9}, \tag{51}$$

with $f^{(3)}_{\rm coh} = 1.918\,333\,364\,848\,918\,7$ ($f^{(3)}_r = 4.263\,827\,935\,989\,311$, $f^{(3)}_a = -2.345\,494\,571\,140\,392\,3$) From Epstein zeta treatment, we get $f^{(3)}_{\rm coh} = 1.918\,333\,364\,847\,879\,5$ ($f^{(3)}_r = 4.263\,827\,935\,991\,082$ and $f^{(3)}_a = -2.345\,494\,571\,143\,202\,5$). As in the square lattice, the three-body term also results in a repulsive contribution to the total cohesive energy, as shown in Fig. 7. Furthermore, the lattice becomes unstable after a critical value of λ is reached, where the total cohesive energy is positive for any value of R. For example, this limit is obtained for the (30,12)-LJ potential coupled with the ATM when $\lambda > 1.8854$. These results show that the hexagonal lattice is more strongly destabilized by adding three-body interactions compared to the square lattice because $f^{(3)}_{\rm coh,hex} > f^{(3)}_{\rm coh,sq}$. This is due to the hexagonal lattice being a close-packed structure in 2D with the highest packing density and kissing number.

Again, we can do the same analysis as for the square lattice case, but mention only here the minimum distances for the (12,6)-LJ potential for which we get $R_{\min}(12,6,0.0) = 0.990\,193\,636\,287\,356$, $R_{\min}(12,6,1.0) = 1.069\,230\,726\,249\,40$, $R_{\min}(12,6,3.0) = 1.229\,929\,645\,109\,45$, and $R_{\min}(12,6,5.0) = 1.378\,017\,434\,680\,56$. Similar to the square lattice, a distortion into a set of linear chains can occur if $n \le 9$ for large ATM coupling strengths λ.

C. LJ + ATM potential for the cuboidal lattices

We are interested in the Bain minimum energy path $E_{\rm coh}(R_{\min}, A)$ along the A-dependent cuboidal lattices at an optimized distance $R = R_{\min}$. The corresponding cohesive energy is obtained from Eq. (33) as

$$E_{\rm coh}(n,m,A,\lambda,R_{\rm bc}) = \frac{nm}{2(n-m)}\left(\frac{Z_{\Lambda(A),n}}{nR^n_{\rm bc}} - \frac{Z_{\Lambda(A),m}}{mR^m_{\rm bc}}\right) + \lambda f^{(3)}_{\rm coh}(A) R^{-9}_{\rm bc} \tag{52}$$

for the lattice $\Lambda(A)$ along the Bain transformation path,

$$\Lambda(A) = B^{\top}(A)\mathbb{Z}^3,$$
$$B^{\top}(A) = \frac{1}{\sqrt{A+1}}\begin{pmatrix}\sqrt{A} & \sqrt{A} & 0\\ 1 & 0 & 1\\ 0 & 1 & 1\end{pmatrix}, \quad 0 < A \le 1.$$

It is important to notice that the above-mentioned lattice only exhibits unit nearest neighbor distance for $1/3 \le A \le 1$. We here define our measure of distance $R_{\rm bc}$ for all values of A as the distance from the atom in the origin to the body centered atom, otherwise one has to change the lattice sum in region I. In region I in Fig. 2, the resulting nearest neighbor distance can easily be obtained from $R_{\rm bc}$. This choice is made to assure a smooth behavior of the resulting minimized distance $R_{\min}$ across the whole range of A values and facilitates the exploration of region I, where we investigate the distortion of the cubic lattice to a set of weakly interacting linear chains along the c axis. For ease of notation, we set $R = R_{\rm bc}$ in the following.

The two-body contribution to the cohesive energy depends on the Epstein zeta function $Z_{\Lambda(A),n} = L(\frac{n}{2}, A)$, which is either obtained from the Bessel expansion in Appendix E or using EpsteinLib. In the following, we analyze the Bain phase transition for a range of (n,m)-LJ potentials, i.e., (6,4)-LJ, (8,6)-LJ, (12,6)-LJ, and (30,12)-LJ. Note that the Epstein zeta function $Z_{\Lambda(A),n}$ becomes minimal for the bcc structure ($A = \frac{1}{2}$), as discussed in detail in Appendix F.

The three-body lattice sum $f^{(3)}_{\rm coh}(A)$ is depicted in Fig. 8 as a function of the parameter A. For region II, the highest repulsive three-body energy occurs for the densely packed fcc lattice, while the energy minimum is reached for the bcc lattice within the studied parameter range, similar to the lattice sums for the Lennard-Jones (LJ) potential. This suggests that the fcc lattice may become unstable relative to the bcc lattice if the coupling parameter λ becomes sufficiently large. Moreover, at very small A-values in region I, we see that the three-body term has a maximum and starts to go steeply down in energy becoming eventually attractive as discussed for the one- and two-dimensional cases.

In order to assess the stability of the bcc with respect to the fcc phase we need to minimize the cohesive energy (52) with respect to

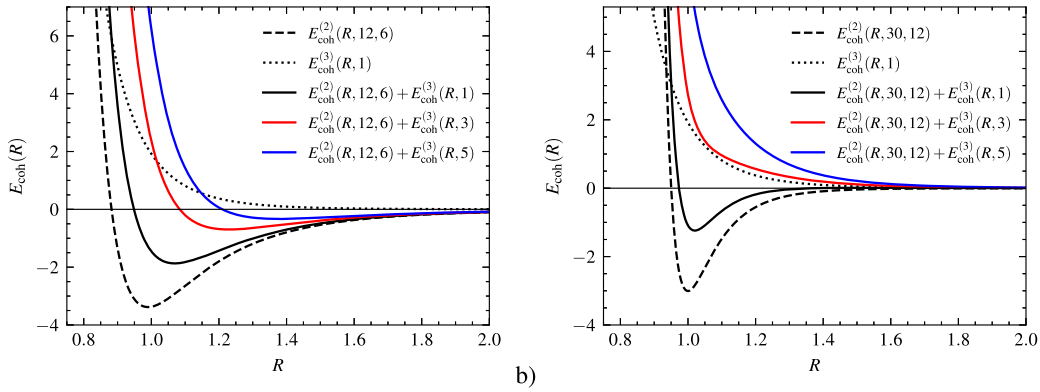

FIG. 7. Cohesive energy of the hexagonal lattice with atoms interacting through (a) (12,6)-LJ potential coupled to an ATM potential and (b) (30,12)-LJ coupled to an ATM potential. Separate two- and three-body contributions are represented by the dashed and dotted lines, respectively.

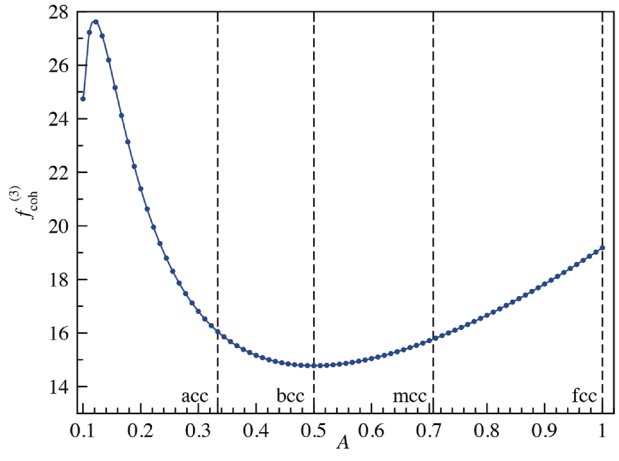

FIG. 8. Normalized ATM cohesive energy $f_{coh}^{(3)}(A) = f_r^{(3)}(A) + f_a^{(3)}(A)$ is displayed along the Bain path as a function of the lattice parameter A.

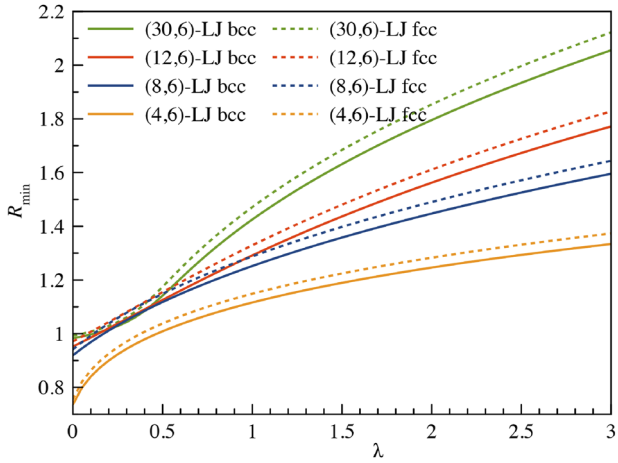

FIG. 9. Minimum distances $R_{min}(A, \lambda)$ for the bcc $(A = \frac{1}{2})$ and fcc $(A = 1)$ structures for different (n, m)-LJ potentials as a function of the ATM coupling parameter λ.

the distance R. The resulting optimization problem is discussed in detail in Sec. II F and can be easily solved numerically with standard tools. However, as already explained in the previous sections, for the (12,6)-LJ potential coupled to an ATM potential, we can derive analytical solutions for the minimum of Eq. (52), which we like to analyze in more detail.

The optimal distance R_{min} to the body-centered atom is obtain from Eq. (35) as

$$R_{min}(12,6,\lambda,A) = \left(\sqrt{\left(\frac{3\lambda f^{(3)}(A)}{4Z_{\Lambda(A),6}}\right)^2 + \frac{Z_{\Lambda(A),12}}{Z_{\Lambda(A),6}}} + \frac{3\lambda f^{(3)}(A)}{4Z_{\Lambda(A),6}}\right)^{\frac{1}{3}}. \tag{53}$$

For $\lambda = 0$ we obtain the well-known result,[70]

$$R_{min}(12,6,\lambda=0,A) = \left(\frac{Z_{\Lambda(A),12}}{Z_{\Lambda(A),6}}\right)^{\frac{1}{6}}, \tag{54}$$

and for $\lambda \to \infty$, we see that $R_{min}(A) \to \infty$ for a repulsive three-body term. A few examples illustrate the behavior of the minimum distance $R_{min}(\lambda)$ with increasing coupling strength: for $A = 1.0$ (fcc), we have $R_{min}(0.0) = 0.971\,233\,690\,959\,646\,2$, $R_{min}(1.0) = 1.329\,165\,159\,071\,515\,7$, $R_{min}(3.0) = 1.828\,126\,388\,924\,327\,8$, and $R_{min}(5.0) = 2.157\,121\,455\,072\,630\,3$, and for $A = 0.5$ (bcc), we have $R_{min}(0.0) = 0.951\,864\,818\,662\,438\,7$, $R_{min}(1.0) = 1.291\,572\,720\,698\,403\,8$, $R_{min}(3.0) = 1.771\,753\,121\,161\,078\,2$, and $R_{min}(5.0) = 2.089\,909\,059\,339\,347\,7$.

Because of $f_{coh}^{(3)}(\text{fcc}) > f_{coh}^{(3)}(\text{bcc})$, the minimum distance is more rapidly increasing for fcc than for bcc with increasing coupling strength λ. This is shown for different (n, m)-LJ potentials in Fig. 9. The minimum properties are also shown in Table II. We note that for the (30,6)-LJ potential, we have $R_{min} = 0.9828$ (bcc) and 0.9923 (fcc) at $\lambda = 0$, which is close to the unit distance for hard spheres. This is expected for a hard-wall potential that approaches the sticky

TABLE II. Minimum distances and cohesive energies at $\lambda = 0$ derived analytically from the lattice sums (also see Ref. 49). For the bcc structure, we have the general condition that $\partial E_{coh}^{(2)}(A = \frac{1}{2})/\partial A = 0$. For the (8,6), (12,6) and (30,6) LJ potentials, the bcc structure is a maximum along the Bain path.

	(6,4)	(8,6)	(12,6)	(30,6)
$R_{min}(A = \frac{1}{2})$	0.735 710 751 1	0.919 276 481 5	0.951 864 818 7	0.982 799 216 6
$R_{min}(A = 1)$	0.755 273 183 8	0.941 120 010 7	0.971 233 691 0	0.992 278 147 8
$E_{coh}^{(2)}(A = \frac{1}{2})$	−38.636 118 884	−10.152 177 739	−8.237 291 910	−6.799 035 350
$E_{coh}^{(2)}(A = 1)$	−38.934 203 192	−10.401 252 415	−8.610 200 157	−7.571 032 638
$\partial^2 E_{coh}^{(2)}(A = \frac{1}{2})/\partial R^2$	3426.261 656 02	1153.288 992 00	1309.171 064 53	2534.079 272 84
$\partial^2 E_{coh}^{(2)}(A = 1)/\partial R^2$	3276.154 677 91	1127.370 985 43	1314.402 151 04	2768.157 295 74
$\partial^2 E_{coh}^{(2)}(A = \frac{1}{2})/\partial A^2$	1.310 611 952 6	−4.007 284 008 6	−8.658 654 168 4	−19.701 773 034
$\partial^2 E_{coh}^{(2)}(A = 1)/\partial A^2$	7.233 240 347 0	4.870 388 425 1	6.870 495 897 0	17.713 990 956

hard-sphere limit.[71] Furthermore, soft potentials (low n and m values) lead to larger contractions in $R_{\min}$ when moving along the cuboidal distortion path from fcc to bcc.

To estimate the range of typical coupling strengths λ, we consider the formula derived from the Drude model describing the triple–dipole interactions between three identical atoms at equilibrium distance r_e,[72,73]

$$\lambda = \frac{9}{16}\frac{I}{\varepsilon}\frac{\alpha^3}{r_e^9}, \tag{55}$$

where I is the first ionization potential of the atom and α the static dipole polarizability. For example, taking known experimental or theoretical values,[74–76] we get for argon $\lambda_{\mathrm{Ar}} = 0.025$, for xenon $\lambda_{\mathrm{Xe}} = 0.034$, for the heaviest noble gas atom $\lambda_{\mathrm{Og}} = 0.101$, and for lithium (due to its large polarizability and small equilibrium distance) $\lambda_{\mathrm{Li}} = 6.0$. However, for bulk lithium, the many-body expansion is not converging smoothly, as this is generally the case for metallic solids.[36,49] This implies that the ATM term is applicable only for small coupling parameters λ, as larger values suggest that higher-order terms in the expansion (17) become important as well. Based on these λ values, we chose the following grid in our computations: $A \in [\frac{1}{10}, 1]$ with step size $\Delta A = \frac{1}{60}$ and $\lambda \in [0, 6.0]$ with step size $\Delta\lambda = 0.05$.

As the differences between the bcc and fcc minimum distances are relatively small compared to $R_{\min}$ at constant λ, we consider the difference in the minimum distances between the cuboidal and the fcc structures, i.e., $\Delta R_{\min}(A,\lambda) = R_{\min}(A,\lambda) - R_{\min}(A=1,\lambda)$. Figure 10 shows $\Delta R_{\min}(A,\lambda)$ values for the four different LJ potentials. They all show a qualitatively similar behavior in the region $\frac{1}{3} \le A \le 1$. The smallest distance is always found at the bcc structure $(A = \frac{1}{2})$. However, we see some significant changes to lower $\Delta R_{\min}$ values with minima occurring in the region $A < \frac{1}{3}$ for larger coupling strengths λ and larger repulsive walls (exponents $n = 12$ and 30), which is due to linear chain formation, as will be discussed in the following.

Figure 11 shows the cohesive energies for a few selected λ values for the (12,6)-LJ potential. The energy curves are shifted toward higher energies with increasing λ value as we expect and become very flat at high energies. At the optimized distance $R_{\min}(A,\lambda)$, it consistently holds that $\Delta E_{\mathrm{coh}}(A,\lambda) < 0$, which is below the atomization limit as expected. With increasing λ, $R_{\min}$ becomes larger to the

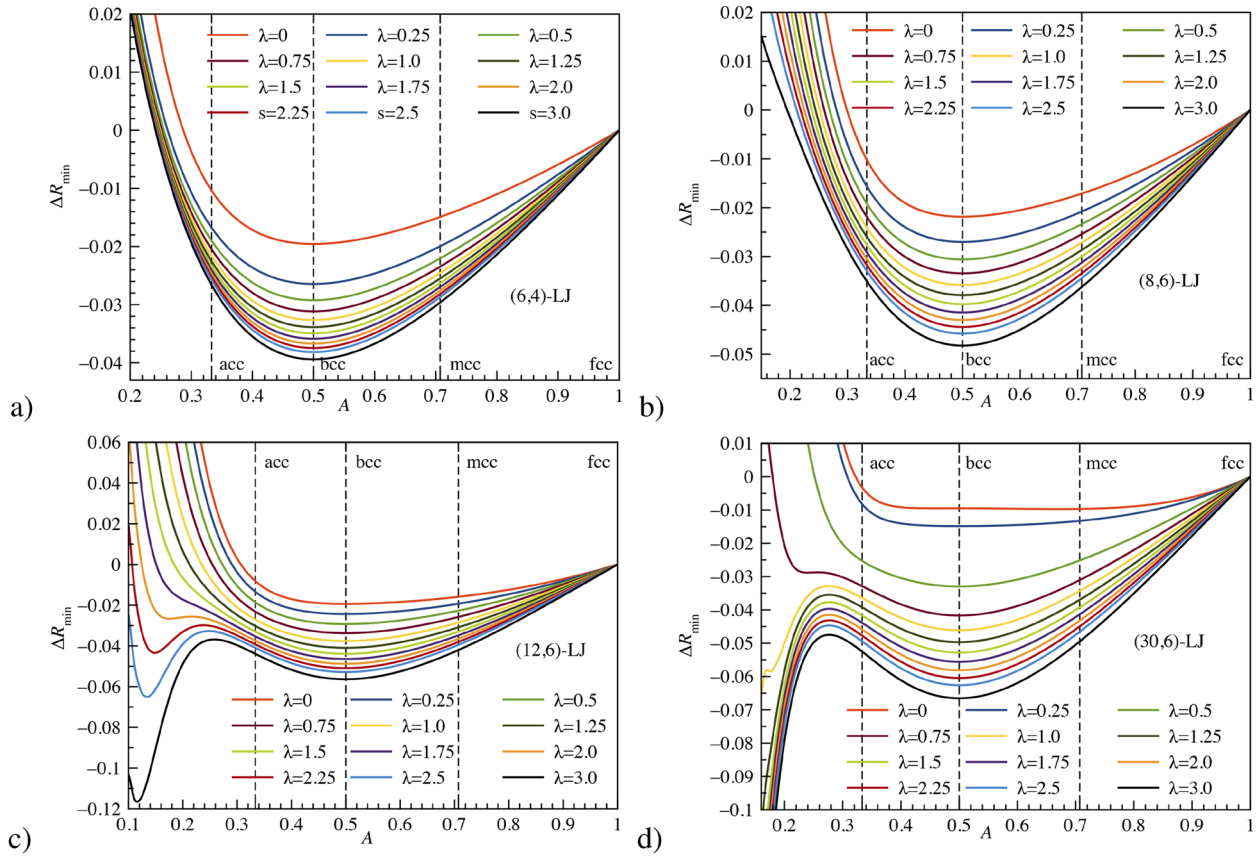

FIG. 10. Difference $\Delta R_{\min}(A,\lambda) = R_{\min}(A,\lambda) - R_{\min}(A=1,\lambda)$ for the (6,4) (a), (8,6) (b), (12,6) (c), and (30,6) (d) LJ potentials for different coupling parameters λ. The four distinct lattices acc $(A = \frac{1}{3})$ on the left, bcc $(A = 1)$ and mcc $(A = \frac{1}{\sqrt{2}})$ at the dashed lines, and fcc $(A = 1)$ on the right are indicated.

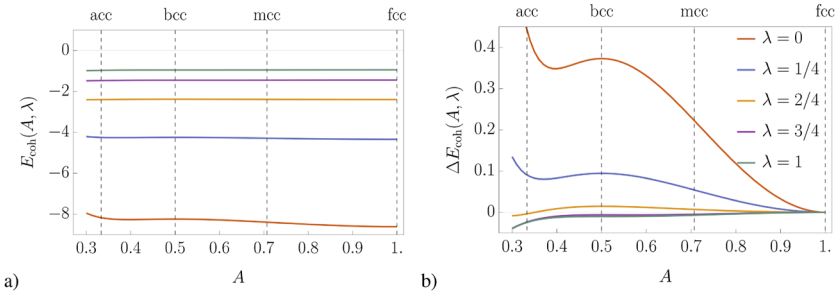

FIG. 11. Cohesive energies $E_{coh}(A,\lambda)$ (a) at the corresponding $R_{min}(A,\lambda)$ values dependent on the parameters A and λ for the (12,6)-LJ potential. The four distinct lattices acc $A = \frac{1}{3}$ on the left, bcc $(A = 1)$ and mcc $(A = \frac{1}{\sqrt{2}})$ indicated by the dashed lines, and fcc $(A = 1)$ on the right are indicated. The difference $\Delta E_{coh}(A,\lambda) = E_{coh}(A,\lambda) - E_{coh}(A = 1,\lambda)$ is shown in panel (b).

point that at long range the dispersive R^{-m} term $(m = 4, 6)$ in the LJ potential dominates over the repulsive ATM force.

Details of the Bain transformation path become more transparent when we plot the difference in cohesive energies with respect to the fcc structure, as shown in Fig. 12. It was pointed out before that for a certain range of (n, m) values with $m < 5.256\,73$, $n > m$ and $\lambda = 0$, the bcc phase becomes metastable, otherwise it will further distort toward lower A values, i.e., the acc structure.[49] However, the bcc structure strictly remains an extremum.[49] The instability of the bcc phase for certain LJ exponents was already discussed in 1940 by Born and Misra,[19,20] and later by Wallace and Patrick.[50] Similar results are obtained for the generalized Morse potential,[77] indicating that many-body forces have substantial influence on the bcc phase. However, a distortion from the ideal bcc phase was also

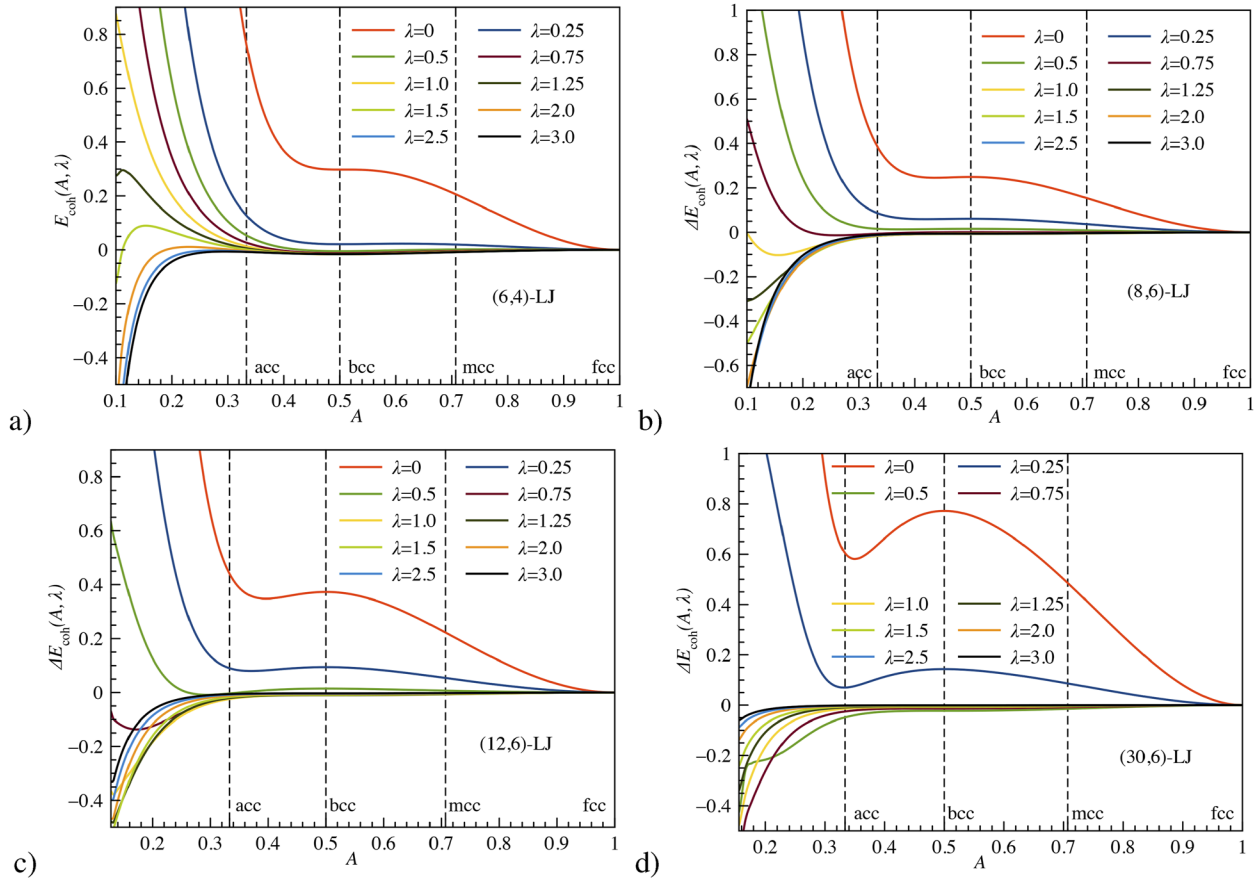

FIG. 12. Cohesive energy differences, $\Delta E_{coh}(A,\lambda) = E_{coh}(A,\lambda) - E_{coh}(A = 1,\lambda)$, at the corresponding $R_{min}(A,\lambda)$ values dependent on the parameters A and λ for the (6,4) (a), (8,6) (b), (12,6) (c), and (30,6) (d) LJ potentials. The four distinct lattices acc $(A = \frac{1}{3})$ on the left, bcc $(A = 1)$, and mcc $(A = \frac{1}{\sqrt{2}})$ represented by the dashed lines, and fcc $(A = 1)$ on the right are indicated.

TABLE III. Minimum distances and LJ and ATM contributions to the cohesive energy at critical λ_c where $E_{coh}(A = \frac{1}{2}, \lambda_c) = E_{coh}(A = 1, \lambda_c)$.

	(6,4)	(8,6)	(12,6)	(30,6)
λ_c	0.419 345 768 6	0.773 357 516 6	0.634 796 849 2	0.388 634 632 2
$R_{min}(A = \frac{1}{2})$	0.985 236 472 2	1.195 870 812 9	1.172 140 515 9	1.079 398 179 5
$R_{min}(A = 1)$	1.013 704 260 1	1.229 545 314 3	1.203 874 540 2	1.103 339 795 9
$E^{(2)}_{coh}(A = \frac{1}{2})$	−22.642 222 548 6	−4.665 534 948 0	−4.047 315 296 8	−4.740 282 456 5
$\lambda_c E^{(3)}_R(A = \frac{1}{2})$	11.685 218 205 6	3.768 346 241 1	3.704 644 569 0	4.762 502 905 8
$\lambda_c E^{(3)}_A(A = \frac{1}{2})$	−4.599 226 677 3	−1.483 196 826 7	−1.458 124 258 5	−1.874 490 491 3
$E_{coh}(A = \frac{1}{2})$	−15.556 231 020 2	−2.380 385 533 6	−1.800 794 986 3	−1.852 270 042 0
$E^{(2)}_{coh}(A = 1)$	−22.673 046 246 3	−4.690 291 651 7	−4.093 343 646 1	−4.928 882 706 0
$\lambda_c E^{(3)}_R(A = 1)$	11.681 664 218 6	3.791 520 053 9	3.763 029 219 9	5.050 005 505 2
$\lambda_c E^{(3)}_A(A = 1)$	−4.564 849 145 1	−1.481 613 985 2	−1.470 480 60 2	−1.973 392 907 2
$E_{coh}(A = 1)$	−15.556 231 020 2	−2.380 385 533 6	−1.800 794 986 3	−1.852 270 042 0
$\partial E_{coh}(A = \frac{1}{2})/\partial A\ [10^{-5}]$	−3.128 265	−1.008 829	−0.991 775	−1.275 000
$\partial^2 E_{coh}(A = \frac{1}{2})/\partial A^2$	1.319 068	−0.194 625	−0.423 196	−0.811 519

found by Craievich *et al.* for several elemental metals.[78] Adding the ATM potential, we see that at a critical coupling strength λ_c [$\lambda_c = 0.635$ for the (12,6)-LJ potential, for example], the bcc phase starts to lie energetically below the fcc phase. The critical λ_c values obtained from a polynomial fit are listed in Table III for the four (n,m)-LJ potentials considered.

Figure 13 shows curves of the critical coupling parameters λ_c for fixed m and variable n for (n,m)-LJ potentials including the ATM potential. The λ_c values given in Table III are indicated as well. For very small values of both exponents (n,m), we see that λ_c is zero. At the other end, in the kissing hard-sphere (KHS) limit $(n,m \to \infty, n > m)$ for a LJ potential, the cohesive energy is given by $E^{(2)}_{coh} = N_{kiss}/2$, where N_{kiss} is the kissing number. Adding the three

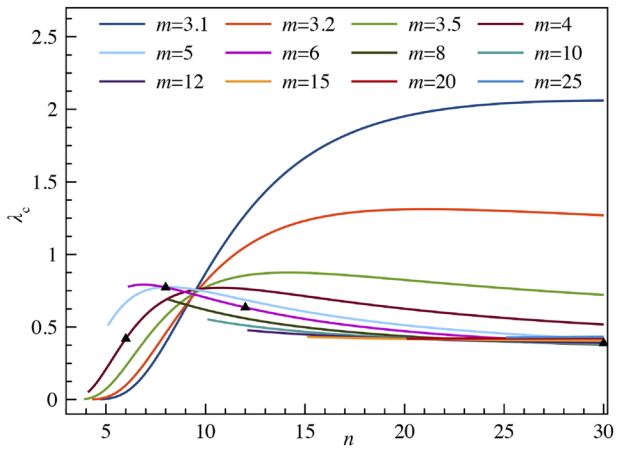

FIG. 13. Critical coupling strength λ_c for different (n,m)-LJ combinations $n > m$. The values for the specific LJ potentials are given in Table III indicated by the black triangles.

body term we get the condition for the critical coupling strength considering that $R = 1$,

$$-6 + \lambda_c E^{(3)}_{coh}(A = 1) = -4 + \lambda_c E^{(3)}_{coh}\left(A = \frac{1}{2}\right), \tag{56}$$

which gives $\lambda_c = 0.454\,307\,399\,567\,58$. This explains the asymptotic behavior of the curves shown in Fig. 13 for large m-values. However, this coupling parameter results in a purely repulsive force for the KHS limit for all cuboidal structures. The main message of this analysis here is that soft two-body interactions and strong repulsive many-body forces favor the bcc over the fcc phase. A prime example for this is lithium where the two phases are almost energetically degenerate.[9] This is also seen in Fig. 14, where for a soft (8,4)-LJ potential, bcc becomes energetically favorable compared to fcc for $\lambda > \lambda_c = 0.687\,403\,812\,123\,84$, with bcc forming a local minimum of the cohesive energy along the Bain path.

The first derivatives are $\partial E_{coh}(A = \frac{1}{2}, \lambda)/\partial A = 0$ at any λ value and a proof that $\partial f^{(3)}_{coh}(A)/\partial A = 0$ at $A = \frac{1}{2}$ is given in Appendix H. This implies that the bcc structure remains an extremum if the ATM term is added. The rather small second derivatives compared to the corresponding values at $\lambda = 0$ show the flatness of the cohesive energy curves $E_{coh}(A = \frac{1}{2}, \lambda_c)$ clearly seen in Fig. 12. However, the bcc structure at λ_c still remains a minimum for the (6,4)-LJ potential and a maximum for the other three potentials considered. At even higher values, $\lambda \gg \lambda_c$, the lattice distorts to much lower A values. While for the (6,4)-LJ potential, we can still locate a very shallow minimum at λ values up to the maximum value considered, for the other potentials we change to a monotonically decreasing function to smaller A-values, that is, the three-body force destabilizes both fcc and bcc.

Kwaadgras *et al.* discussed in detail the formation of linear chains for finite systems within the induced dipole interaction model[79] and commented on the importance of the ATM potential. Figure 15 depicts the behavior at small A-values if the coupling strength λ becomes large. We see a formation of linear chains along

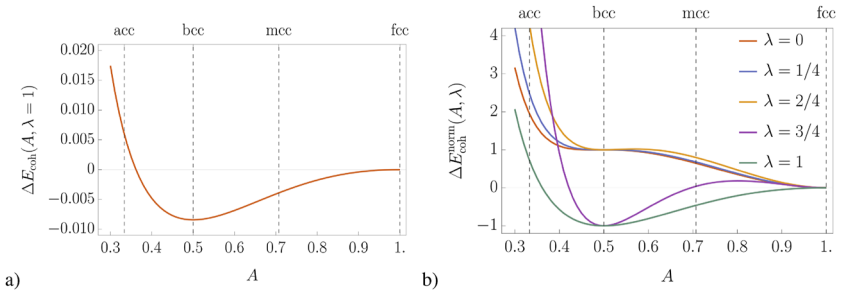

FIG. 14. (a) Cohesive energy differences, $\Delta E_{\rm coh}(A,\lambda) = E_{\rm coh}(A,\lambda) - E_{\rm coh}(A=1,\lambda)$, at the corresponding $R_{\rm min}(A,\lambda)$ values for $\lambda = 1$ as a function of A for the (8,4)-LJ potential. (b) The normalized cohesive energy differences $\Delta E_{\rm coh}^{\rm norm}(A,\lambda) = \Delta E_{\rm coh}(A,\lambda)/|\Delta E_{\rm coh}(A=1/2,\lambda)|$ for different values of $0 \le \lambda \le 1$. Numerically, we observe that bcc becomes energetically favorable compared to fcc for $\lambda > \lambda_c = 0.687\,403\,812\,123\,84$.

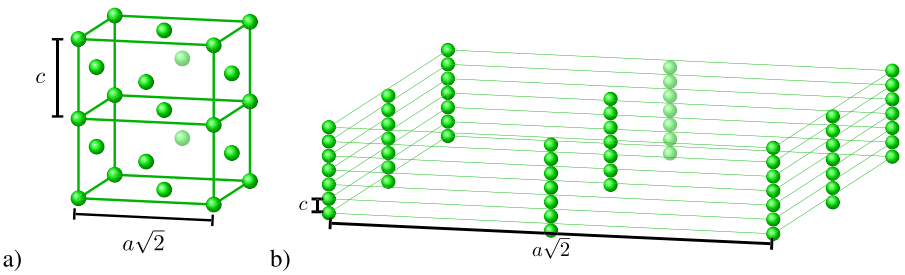

FIG. 15. (a) Conventional cell of the acc structure at $A = 1/3$ showing the linear chain formation parallel to the c axis and (b) weakly interacting linear chains obtained from a cuboidal structure with $A = 0.005$.

the c axis. The kissing number is reduced to 2, as listed in Table I. This is easily explained through Eq. (12): For $A \to 0$, we have $\gamma \to 0$ and $R \to \frac{a}{\sqrt{2}} \to \infty$, which implies that for increasing coupling strength λ keeping c finite, we see the formation of largely separated linear chains where the ATM force becomes attractive, as explained in Sec. III A. Hence, we see exactly the same (unphysical) situation as for the 2D lattice where we allowed for distortion in one direction.

We add some final comments here. First, very large λ values are not realistic as shown above. Second, and more importantly, the ATM potential is only valid in the long range. In the very short range, the three-body force becomes even attractive for the rare gas elements.[80–82] Third, the many-body expansion of the total energy of a lattice described by quantum theory does not converge fast at short distances. This is especially the case for metallic systems as already mentioned.[36] Fourth, if we maintain the use of such a model system, we need to make sure that the exponent of the repulsive force in the LJ potential exceeds the one in the ATM potential; otherwise, we observe a collapse of the linear chain for $n < 9$, as outlined in Sec. III A.

IV. CONCLUSION

In this work, we have explored the influence of three-body interactions on the stability of cuboidal lattices. To this end, we have studied the cohesive energy along a Bain phase transformation path connecting the fcc lattice structure to the mcc, bcc, and finally, the acc lattice, where we have included both a two-body (n,m)-LJ potential and a three-body ATM potential of increasing coupling strength. The two-body lattice sums were computed to full precision using either rapidly converging Bessel function expansions[11,26] or, alternatively, efficient evaluations based on the Epstein zeta function.[58] The challenging computation of the high-dimensional, slowly converging three-body lattice sums has been successfully achieved using a new representation based on singular integrals involving products of Epstein zeta functions. This approach enables, for the first time, the precise evaluation of three-body lattice sums within minutes on a standard laptop and can (most likely) be extended to more general many-body terms and multiple zeta functions, which is part of our future work.[83]

Using our advanced numerical framework, we have been able to precisely evaluate the small energy differences between the cuboidal structures along the Bain path. Our results demonstrate that the three-body potential can destabilize the fcc structure for large ATM coupling strengths. We analytically show and numerically confirm that the ATM potential exhibits a minimum along the Bain path at the bcc structure, resulting in the bcc structure becoming a metastable minimum for soft LJ potentials. For hard-wall LJ potentials, the structure distorts toward, and even beyond, the acc phase. Linear chain formation is observed at high ATM coupling strength, which is due to the short-range behavior of the ATM force.

Our results indicate that, in addition to the softness of the two-body potential, the stability of the bcc lattice may heavily rely on higher than two-body effects. While this study serves as an initial exploration of the martensitic bcc-to-fcc phase transition mechanism, more realistic systems, such as metals, need to be investigated in future work and possible symmetry breaking effects (such as rhombohedral distortions) need to be included.[6] This requires a more precise computation of many-body potentials based on density functional theory, as well as the incorporation of temperature and pressure effects.

ACKNOWLEDGMENTS

P.S. thanks Professor Paul Indelicato (Kastler lab, Paris) for a visiting professorship at Sorbonne and acknowledges the Sir Neil Waters Fund at Massey University for financial support. JB acknowledges the support from the Quantum Fellowship Program of the German Aerospace Center (DLR) for funding their contribution to this work.

AUTHOR DECLARATIONS

Conflict of Interest

The authors have no conflicts to disclose.

Author Contributions

Andres Robles-Navarro: Conceptualization (equal); Data curation (equal); Formal analysis (equal); Investigation (equal); Methodology (equal); Project administration (equal); Software (equal); Validation (equal); Visualization (equal); Writing – original draft (equal); Writing – review & editing (equal). **Shaun Cooper**: Conceptualization (equal); Data curation (equal); Formal analysis (equal); Investigation (equal); Methodology (equal); Validation (equal); Visualization (equal); Writing – original draft (equal); Writing – review & editing (equal). **Andreas A. Buchheit**: Conceptualization (equal); Data curation (equal); Formal analysis (equal); Investigation (equal); Methodology (equal); Software (equal); Validation (equal); Visualization (equal); Writing – original draft (equal); Writing – review & editing (equal). **Jonathan K. Busse**: Data curation (equal); Formal analysis (equal); Investigation (equal); Methodology (equal); Software (equal); Writing – original draft (equal); Writing – review & editing (equal). **Antony Burrows**: Conceptualization (equal); Data curation (equal); Formal analysis (equal); Investigation (equal); Software (equal); Validation (equal); Visualization (equal); Writing – original draft (equal). **Odile Smits**: Conceptualization (equal); Formal analysis (equal); Investigation (equal); Project administration (equal); Software (equal); Validation (equal); Visualization (equal); Writing – original draft (equal); Writing – review & editing (equal). **Peter Schwerdtfeger**: Conceptualization (equal); Data curation (equal); Formal analysis (equal); Funding acquisition (equal); Investigation (equal); Methodology (equal); Project administration (equal); Resources (equal); Software (equal); Supervision (equal); Validation (equal); Visualization (equal); Writing – original draft (equal); Writing – review & editing (equal).

DATA AVAILABILITY

The data that support the findings of this study are available within the article.

APPENDIX A: FORMULAS FOR SPECIAL FUNCTIONS

In this appendix, we give a detailed description of the mathematical tools to derive the lattice sums and properties for the cuboidal lattices studied here. We start with defining the required standard functions and theta series used in the theory of lattice sums here. We then introduce the quadratic forms, integral transforms, and expansions in terms of Bessel functions. This is followed by a discussion of some important lattice sum properties and their analytic continuation.

A few special functions have been used in this work. For clarity and ease of use, they are stated here along with references.

The *gamma function* may be defined for $s > 0$ by

$$\Gamma(s) = \int_{[0,\infty)} t^{s-1}\, e^{-t}\, \mathrm{d}t. \tag{A1}$$

By the change of variable $t = wx$, this can be rewritten in the form [see Ref. 84, (1.1.18)]

$$\frac{1}{w^s} = \frac{1}{\Gamma(s)} \int_{[0,\infty)} x^{s-1}\, e^{-wx}\, \mathrm{d}x. \tag{A2}$$

The following integral may be evaluated in terms of the *modified Bessel function*:

$$\int_{[0,\infty)} x^{s-1} e^{-ax-b/x} \mathrm{d}x = 2\left(\frac{b}{a}\right)^{s/2} K_s(2\sqrt{ab}). \tag{A3}$$

By the change of variable $x = u^{-1}$, it can be shown that

$$K_s(z) = K_{-s}(z). \tag{A4}$$

When $s = 1/2$, the modified Bessel function reduces to an elementary function,

$$K_{1/2}(z) = \sqrt{\frac{\pi}{2z}}\, e^{-z}. \tag{A5}$$

The asymptotic formula holds

$$K_s(z) \sim \sqrt{\frac{\pi}{2z}}\, e^{-z} \quad \text{as} \quad z \to \infty, \quad (|\arg z| < 3\pi/2). \tag{A6}$$

For all of these properties, see Ref. 84, pp. 223, 237 or Ref. 85, pp. 233–248.

The transformation formula for *theta functions* is Ref. 84, p. 119 [Ref. 86, (2.2.5)],

$$\sum_{n\in\mathbb{Z}} e^{-\pi n^2 t + 2\pi i n a} = \frac{1}{\sqrt{t}} \sum_{n\in\mathbb{Z}} e^{-\pi(n+a)^2/t}, \quad \text{assuming } \mathrm{Re}(t) > 0. \tag{A7}$$

We will need the special cases $a = 0$ and $a = 1/2$, which are

$$\sum_{n\in\mathbb{Z}} e^{-\pi n^2 t} = \frac{1}{\sqrt{t}} \sum_{n\in\mathbb{Z}} e^{-\pi n^2/t} \tag{A8}$$

and

$$\sum_{n\in\mathbb{Z}} (-1)^n e^{-\pi n^2 t} = \frac{1}{\sqrt{t}} \sum_{n\in\mathbb{Z}} e^{-\pi\left(n+\frac{1}{2}\right)^2/t}, \tag{A9}$$

respectively. The sum of two squares formula is Ref. 87, (3.111),

$$\left(\sum_{j\in\mathbb{Z}} q^{j^2}\right)^2 = \sum_{j,k\in\mathbb{Z}} q^{j^2+k^2} = \sum_{N\in\mathbb{N}_0} r_2(N) q^N, \tag{A10}$$

where

$$r_2(N) = \#\{j^2 + k^2 = N\} = \begin{cases} 1 & \text{if } N = 0, \\ 4\sum_{d|N} \chi_{-4}(d) & \text{if } N \geq 1, \end{cases} \tag{A11}$$

with the sum being over the positive divisors d of N. For example,

$$\begin{aligned} r_2(18) &= 4(\chi_{-4}(1) + \chi_{-4}(2) + \chi_{-4}(3) + \chi_{-4}(6) + \chi_{-4}(9) + \chi_{-4}(18)) \\ &= 4(1 + 0 - 1 + 0 + 1 + 0) = 4. \end{aligned}$$

By Ref. 87, (3.15) and (3.111), we also have

$$\left(\sum_{j\in\mathbb{Z}} q^{(j+\frac{1}{2})^2}\right)^2 = \sum_{N\in\mathbb{N}_0} r_2(4N+1) q^{(4N+1)/2}. \tag{A12}$$

The *Riemann zeta function* $\zeta(s)$ and *Dirichlet L function* are defined by

$$\zeta(s) = \sum_{j\in\mathbb{N}} \frac{1}{j^s}, \tag{A13}$$

$$L_{-4}(s) = \sum_{j\in\mathbb{N}} \frac{\chi_{-4}(j)}{j^s} = 1 - \frac{1}{3^s} + \frac{1}{5^s} - \frac{1}{7^s} + \cdots. \tag{A14}$$

For even integers, the Riemann zeta function can be expressed as $\zeta(2n) = \pi^{2n} B_n / A_n$, where A_n and B_n are positive integers, e.g., we have $\zeta(2) = \pi^2/6$, $\zeta(4) = \pi^4/90$, $\zeta(6) = \pi^6/945$, $\zeta(8) = \pi^8/9450$, $\zeta(10) = \pi^{10}/93\,555$, $\zeta(12) = 691\pi^{12}/638\,512\,875$, $\zeta(14) = 2\pi^{14}/18\,243\,225$, and $\zeta(16) = 3617\pi^{16}/325\,641\,566\,250$. The coefficients A_n and B_n are listed in the On-Line Encyclopedia of Integer Sequences A002432 and A046988, respectively.[88]

For an integer n, the *Dirichlet character* $\chi_{-4}(n)$ is defined by

$$\chi_{-4}(n) = \sin(\pi n/2) = \begin{cases} 1 & \text{if } n \equiv 1 \pmod 4, \\ -1 & \text{if } n \equiv 3 \pmod 4, \\ 0 & \text{otherwise.} \end{cases} \tag{A15}$$

The Riemann zeta function has a pole of order 1 at $s = 1$ and, in fact,

$$\lim_{s\to 1} (s-1)\zeta(s) = 1. \tag{A16}$$

This is a consequence of Ref. 84, (1.3.2); also see Ref. 85, p. 58.

We require the following functional equations:

$$\pi^{-s/2}\Gamma(s/2)\zeta(s) = \pi^{-(1-s)/2}\Gamma((1-s)/2)\zeta(1-s) \tag{A17}$$

and

$$\pi^{-s}\Gamma(s)\zeta(s)L_{-4}(s) = \pi^{-(1-s)}\Gamma(1-s)\zeta(1-s)L_{-4}(1-s) \tag{A18}$$

and the special values,

$$\begin{aligned} &\zeta(2) = \frac{\pi^2}{6}, \quad \zeta(0) = -\frac{1}{2}, \\ &\zeta(-1) = -\frac{1}{12}, \quad \zeta(-2) = \zeta(-4) = \zeta(-6) = \cdots = 0, \end{aligned} \tag{A19}$$

$$\begin{aligned} &L_{-4}(1) = \frac{\pi}{4}, \quad L_{-4}(0) = \frac{1}{2}, \\ &L_{-4}(-1) = L_{-4}(-3) = L_{-4}(-5) = \cdots = 0. \end{aligned} \tag{A20}$$

See Ref. 89, Chap. 12 or Ref. 67 Other equalities used are

$$\sum_{j\in\mathbb{N}_0} \frac{1}{(j+\frac{1}{2})^s} = (2^s - 1)\zeta(s), \tag{A21}$$

$$\sum_{j\in\mathbb{N}} \frac{(-1)^j}{j^s} = -(1 - 2^{1-s})\zeta(s), \tag{A22}$$

$$\sum_{j,k\in\mathbb{Z}}{}' \frac{1}{(j^2+k^2)^s} = 4\zeta(s)L_{-4}(s), \tag{A23}$$

$$\sum_{j,k\in\mathbb{Z}}{}' \frac{(-1)^{j+k}}{(j^2+k^2)^s} = -4(1 - 2^{1-s})\zeta(s)L_{-4}(s). \tag{A24}$$

The identities (A21) and (A22) follow from the definition of $\zeta(s)$ by series rearrangements. For (A23) and (A24), see (1.4.14) and (1.7.5) respectively, of Ref. 11.

Given a positive definite quadratic form $g(i,j,k)$, the corresponding *theta series* is defined for $|q| < 1$ by

$$\theta_g(q) = \sum_{i,j,k\in\mathbb{Z}} q^{g(i,j,k)}. \tag{A25}$$

For the quadratic form in (E3), the theta series is

$$\theta(A;q) = \sum_{i,j,k\in\mathbb{Z}} q^{(A(i+j)^2+(j+k)^2+(i+k)^2)/(A+1)} \quad \text{where } 1/3 \leq A \leq 1. \tag{A26}$$

The first few terms in the theta series for fcc, mcc, bcc, and acc as far as q^9 are given, respectively, by

$$\theta(1;q) = 1 + 12q + 6q^2 + 24q^3 + 12q^4 + 24q^5 + 8q^6 + 48q^7 + 6q^8 + 36q^9 + \cdots,$$
$$\theta\left(\frac{1}{\sqrt{2}};q\right) = 1 + 8q + 4q^{4-2\sqrt{2}} + 2q^{4\sqrt{2}-4} + 4q^{8-4\sqrt{2}} + 8q^{2\sqrt{2}} + 16q^{-4\sqrt{2}+9} + 8q^4 + 8q^{8\sqrt{2}-7} + 4q^{16-8\sqrt{2}} + 8q^{-8\sqrt{2}+17}$$
$$+ 8q^{20-10\sqrt{2}} + 8q^{-4\sqrt{2}+12} + 2q^{16\sqrt{2}-16} + 16q^{4\sqrt{2}+1} + 16q^{-6\sqrt{2}+16} + 8q^{14\sqrt{2}-12} + 16q^{-12\sqrt{2}+25} + 8q^{-8+12\sqrt{2}} + 8q^9 + \cdots,$$
$$\theta\left(\frac{1}{2};q\right) = 1 + 8q + 6q^{4/3} + 12q^{8/3} + 8q^4 + 24q^{11/3} + 6q^{16/3} + 24q^{19/3} + 24q^{20/3} + 24q^8 + 32q^9 + \cdots,$$
$$\theta\left(\frac{1}{3};q\right) = 1 + 10q + 4q^{3/2} + 8q^{5/2} + 12q^3 + 26q^4 + 8q^{11/2} + 20q^6 + 32q^7 + 8q^{15/2} + 16q^{17/2} + 10q^9 + \cdots.$$

Since the quadratic form $g(A;\ i,j,k)$ has been normalized to make the minimum distance 1, the kissing number occurs in each theta series as the coefficient of q. That is, we have kiss(fcc) = 12, kiss(mcc) = 8, kiss(bcc) = 8, and kiss(acc) = 10.

Finally, we mention the d-dimensional Epstein zeta function[27,90] in its most general form for a matrix A, vectors $\vec{c}$ and $\vec{v}$, and exponent $\rho \in \mathbb{C}$,

$$Z_d(A,\rho) = \sum_{\vec{k}\in\mathbb{Z}^d}{}' \frac{e^{2\pi i\vec{c}\cdot A\vec{k}}}{|A\vec{k}-\vec{v}|^\rho}. \tag{A27}$$

The connection to the generator matrix B in lattices is by setting $A = B^\top$, and the Gram matrix becomes $G = BB^\top = A^\top A$. The vector $\vec{v}$ is often called the shift vector in lattice theory.

APPENDIX B: CONNECTION TO ALTERNATIVE GRAM MATRICES IN THE LITERATURE

In this appendix, we discuss a few important properties of the generator and Gram matrices used in this work.[91] Two generator matrices B_1 and B_2 are equivalent if $B_2 = cUB_1\mathcal{O}$; c is a non-zero real number; $\mathcal{O}$ a real orthogonal matrix ($\mathcal{O}\mathcal{O}^\top = 1$) with $\det\mathcal{O} = \pm 1$ describing rotation, reflection, or roto-reflection of the lattice; and U is a matrix containing integers with $\det U = 1$ describing, for example, permutations of the lattice basis vectors. Given two equivalent generator matrices, B_1 and B_2, the corresponding (equivalent) Gram matrices $G_1 = B_1B_1^\top$ and $G_2 = B_2B_2^\top$ are related by

$$G_2 = B_2B_2^\top = cUB_1\mathcal{O}\,(cUB_1\mathcal{O})^\top = c^2UB_1\mathcal{O}\mathcal{O}^\top B_1^\top U^\top = c^2UG_1U^\top. \tag{B1}$$

We now reconcile the Gram matrix G in (8) with two matrices given by Conway and Sloane.[51] Let

$$U_1 = \begin{pmatrix} 1 & 0 & 0 \\ -1 & 0 & 1 \\ 0 & -1 & 0 \end{pmatrix} \quad \text{and} \quad U_2 = \begin{pmatrix} 1 & 1 & -1 \\ 1 & 0 & 0 \\ 0 & 1 & 0 \end{pmatrix} \tag{B2}$$

and consider the equivalent matrices G_1 and G_2 defined by

$$G_1 = U_1\,G\,U_1^\top = \begin{pmatrix} u^2+v^2 & -u^2 & -u^2 \\ -u^2 & u^2+v^2 & u^2-v^2 \\ -u^2 & u^2-v^2 & u^2+v^2 \end{pmatrix} \tag{B3}$$

and

$$G_2 = U_2\,G\,U_2^\top = \begin{pmatrix} 4u^2 & 2u^2 & 2u^2 \\ 2u^2 & u^2+v^2 & u^2 \\ 2u^2 & u^2 & u^2+v^2 \end{pmatrix}. \tag{B4}$$

When $u = 1/\sqrt{2}$ and $v = 1/\sqrt[4]{2}$, the matrix G_1 in (B3) is the Gram matrix for the mcc lattice given by Conway and Sloane [Ref. 51, (10)]. Moreover, when $u = \sqrt{1/3}$ and $v = \sqrt{2/3}$, the matrix G_1 leads to another known quadratic form for the bcc lattice, e.g., see Ref. 26, (8b). When $u = 1$ and $v = \sqrt{3}$, the matrix G_2 in (B4) is the Gram matrix for the acc lattice given in Ref. 51, p. 378. Since $\det U_1^2 = \det U_2^2 = 1$, it follows that

$$\det G_1 = \det G_2 = \det G = (\det B)^2 = 4u^2v^4 = 4v^6A. \tag{B5}$$

The corresponding quadratic forms g_1 and g_2 are defined by

$$g_1(i,j,k) = (i,j,k)\,G_1(i,j,k)^\top = (u^2+v^2)i^2 + (u^2+v^2)j^2 + (u^2+v^2)k^2 - 2u^2ij - 2u^2ik + 2(u^2-v^2)jk$$

and

$$g_2(i,j,k) = (i,j,k)\,G_2(i,j,k)^\top = 4u^2i^2 + (u^2+v^2)j^2 + (u^2+v^2)k^2 + 4u^2ij + 4u^2ik + 2u^2jk.$$

They are related to the quadratic form g in Eq. (5) by

$$g_1(i,j,k) = g((i,j,k)U_1) = g(i-j,-k,j) \tag{B6}$$

and

$$g_2(i,j,k) = g((i,j,k)U_2) = g(i+j,i+k,-i). \tag{B7}$$

These quadratic forms are an essential ingredient for the lattice sums $L(G)$ in (2) used to obtain the cohesive energy of a lattice for the case of inverse power potentials $V(r) = r^{-n}$. This is outlined in the following sections.

APPENDIX C: DIRECT SUMMATION APPROACH TO THREE-BODY LATTICE SUMS

Unfortunately, the three-body sum is slowly convergent and cannot be analytically expressed in terms of lattice sums containing a single quadratic form as for the Epstein zeta function.[27] It has, therefore, been treated in the past by using direct summation methods. Along the Bain path, we can express the ATM potential in terms of lattice sums dependent on the parameter A similar to the two-body potential, such that

$$E_{\rm coh}^{(3)}(R,A,\lambda) = \lambda\{E_R(R,A) + E_A(R,A)\}, \tag{C1}$$

with $E_R = f_r/R^9$ and $E_A = f_a/R^9$.

In our previous work,[35,59–63] where more complicated forms of three-body forces were used, we produced the Cartesian coordinates of the vectors $\vec{R}_{0i}$ for a specific lattice first and stored them for further use in (17). For this, one could use the fcc lattice basis vectors $(1,1,0)^\top$, $(1,0,0)^\top$, and $(0,1,1)^\top$, as a starting point and for the different cuboidal lattices scale the Cartesian coordinates (x_n, y_n, z_n), such that we have $\frac{R}{\sqrt{A+1}}(x_n\sqrt{A}, y_n, z_n)$.[35,82,92] However, for the simple ATM potential, this offers no advantage in terms of computer time and memory requirements. Moreover, as we shall see the simple form has some advantage for the determination of the minimum distance for a λ dependent energy (C1) at a specific A value. We, therefore, decided to use (C1) directly by utilizing the permutation symmetry $i_1 \leftrightarrow j_1$ for the vectors $\vec{i}$ and $\vec{j}$.

The convergence for the two individual three-body terms as well as the sum of both in Eq. (C1) is shown in Fig. 16 for the bcc lattice ($A = \frac{1}{2}$), setting $\lambda = 1$ and $R_{\rm min}$ to the minimum nearest-neighbor distance of a (12,6)-LJ potential. The rather slow convergence of both terms $E_R^{(3)}(R_{\rm min}, A)$ and $E_A^{(3)}(R_{\rm min}, A)$ with increasing $N_{\rm max}$ is obvious. Nevertheless, the sum of these terms exhibits significantly faster convergence, and $N_{\rm max} = 100$ proves in principle to be sufficiently accurate for our analysis. However, due to the computational time scaling of $\mathcal{O}(N_{\rm max}^6)$, calculating the ATM term for a specific A value already demands four weeks of CPU time on a single processor. We, therefore, use a far more efficient evaluation of the three-body term through the Epstein zeta function, as introduced originally by Crandall and put into a computer efficient form by Buchheit *et al.*[58] This allows evaluating general three-body lattice sums to machine precision within minutes on a standard laptop.

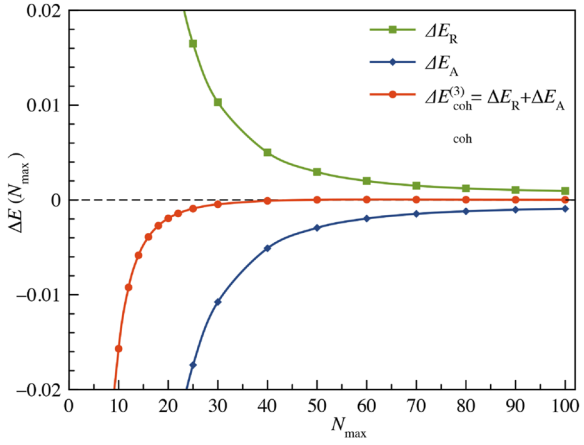

FIG. 16. Convergence of the ATM terms $E_R(N_{\rm max}, R_{\rm min}, A)$, $E_A(N_{\rm max}, R_{\rm min}, A)$, and $E_{\rm coh}^{(3)}(N_{\rm max}, R_{\rm min}, A)$ [Eq. (C1)] for the bcc lattice $A = \frac{1}{2}$ using a (12,6)-LJ potential. $R_{\rm min}$ is set to 0.951 864 818 662 439, the minimum distance for the bcc lattice of a (12,6)-LJ potential. The values show the difference in energies $\Delta E = E(N_{\rm max} \to \infty) - E(N_{\rm max})$ to the extrapolated value $N_{\rm max} \to \infty$. The limit for $N_{\rm max} \to \infty$ was obtained from a linear extrapolation over $N_{\rm max}^{-1}$ of the last two values at $N_{\rm max} = 90$ and 100. This gives $\Delta E_R(N_{\rm max} = 100) = -9.283\,159 \times 10^{-4}$, $\Delta E_A(N_{\rm max} = 100) = 9.461\,724 \times 10^{-4}$, and $\Delta E_R(N_{\rm max} = 100) + E_A(N_{\rm max} = 100) = 1.785\,654 \times 10^{-5}$.

For our detailed analysis, we tabulate the following properties along the Bain path: $E_{\rm coh}(A, R_{\rm min})$, $\partial E_{\rm coh}(A)/\partial R|_{R_{\rm min}}$, $\partial^2 E_{\rm coh}(A)/\partial R^2|_{R_{\rm min}}$, $\partial E_{\rm coh}(A)/\partial A|_{R_{\rm min}}$, and $\partial^2 E_{\rm coh}(A)/\partial A^2|_{R_{\rm min}}$. The latter two derivatives are obtained analytically for the two-body force (see Ref. 49 for details) and numerically for the three-body force. For the general LJ potential, we used the (n,m) combinations (6,4), (8,6), (12,6), and (30,6). The latter represents a hard-wall potential accompanied by an attractive long-range dispersive r^{-6} term.

APPENDIX D: EVALUATION OF THE TWO-BODY LATTICE SUM FOR A RECTANGULAR 2D LATTICE

For the lattice sum with Gram matrix (47),

$$\sum_{i\in\mathbb{Z}}{}'\left[i^2 + (\gamma j)^2\right]^{-s} = 2\zeta(2s)\left\{1 + \gamma^{-2s} + 2\left(1+\gamma^2\right)^{-s}\right\} + 4\sum_{i,j\in\mathbb{N},i\neq j}{}'\left[i^2 + (\gamma j)^2\right]^{-s}, \tag{D1}$$

we use Van der Hoff and Benson's original expression derived from a Mellin transformation and the use of theta functions,[69]

$$\sum_{i\in\mathbb{Z}}{}'\left[x^2 + (i+a)^2\right]^{-s} = \frac{\sqrt{\pi}\Gamma\left(s-\frac{1}{2}\right)}{\Gamma(s)|x|^{2s-1}} + \frac{4\pi^s}{\Gamma(s)}\sum_{n\in\mathbb{N}}\left(\frac{n}{|x|}\right)^{s-\frac{1}{2}} \times \cos(2\pi n a) K_{s-\frac{1}{2}}(2\pi n|x|), \tag{D2}$$

with $a \in (0,1)$. For the special case of $a = 0$ and $x = \gamma j$ ($\gamma > 0$), we get a fast converging series in terms of Bessel functions,

$$\sum_{i,j\in\mathbb{Z}}{}'\left[i^2 + (\gamma j)^2\right]^{-s} = 2\zeta(2s) + \sum_{j\in\mathbb{Z}}{}'\frac{\sqrt{\pi}\Gamma\left(s-\frac{1}{2}\right)}{\Gamma(s)|\gamma j|^{2s-1}} + \frac{4\pi^s}{\Gamma(s)}\sum_{j\in\mathbb{Z}}{}'\sum_{n\in\mathbb{N}}\left(\frac{n}{|\gamma j|}\right)^{s-\frac{1}{2}} K_{s-\frac{1}{2}}(2\pi n\gamma|j|), \tag{D3}$$

which simplifies to

$$\sum_{i,j\in\mathbb{Z}}{}'\left[i^2 + (\gamma j)^2\right]^{-s} = 2\zeta(2s) + \frac{2\sqrt{\pi}\Gamma\left(s-\frac{1}{2}\right)\zeta(2s-1)}{\Gamma(s)\gamma^{2s-1}} + \frac{8\pi^s}{\Gamma(s)}\sum_{n,j\in\mathbb{N}}\left(\frac{n}{\gamma j}\right)^{s-\frac{1}{2}} K_{s-\frac{1}{2}}(2\pi\gamma n j). \tag{D4}$$

The additional Riemman zeta function comes from the case when $(j = 0, i \neq 0)$. As the Bessel function $K_n(x)$ decays exponentially with the argument x, for $\gamma < 1$, it is computationally advantageous to rewrite the sum into

$$\sum_{i,j\in\mathbb{Z}}{}'\left[i^2 + (\gamma j)^2\right]^{-s} = \gamma^{-2s}\sum_{i,j\in\mathbb{Z}}{}'\left[\gamma^{-2}i^2 + j^2\right]^{-s} = \gamma^{-2s}\sum_{i,j\in\mathbb{Z}}{}'\left[i^2 + (j/\gamma)^2\right]^{-s}, \tag{D5}$$

and we get in a similar fashion,

$$\gamma^{-2s}\sum_{i,j\in\mathbb{Z}}{}'\left[i^2 + (j/\gamma)^2\right]^{-s} = 2\gamma^{-2s}\zeta(2s) + \frac{2\sqrt{\pi}\Gamma\left(s-\frac{1}{2}\right)\zeta(2s-1)}{\Gamma(s)\gamma} + \frac{8\pi^s}{\Gamma(s)\gamma^{s+\frac{1}{2}}}\sum_{n,j\in\mathbb{N}}\left(\frac{n}{j}\right)^{s-\frac{1}{2}} \times K_{s-\frac{1}{2}}(2\pi\gamma^{-1}nj). \tag{D6}$$

This formula is identical to the one given by Bateman and Grosswald.[93] For computational efficiency, we rewrite Eq. (D4),

$$\sum_{i,j\in\mathbb{Z}}{}'\left[i^2 + (\gamma j)^2\right]^{-s} = \zeta(2s) + \frac{2\sqrt{\pi}\Gamma\left(s-\frac{1}{2}\right)\zeta(2s-1)}{\Gamma(s)\gamma^{2s-1}} + \frac{8\pi^s}{\Gamma(s)\gamma^{s-\frac{1}{2}}}\sum_{n\in\mathbb{N}}K_{s-\frac{1}{2}}(2\pi\gamma n^2) + \frac{8\pi^s}{\Gamma(s)\gamma^{s-\frac{1}{2}}}\sum_{n<j\in\mathbb{N}}\left\{\left(\frac{n}{j}\right)^{s-\frac{1}{2}} + \left(\frac{j}{n}\right)^{s-\frac{1}{2}}\right\} \times K_{s-\frac{1}{2}}(2\pi\gamma nj) \tag{D7}$$

and we can do the same for Eq. (D6).

APPENDIX E: EVALUATION OF THE LATTICE SUM $L(A; s)$

Consider the quadratic form

$$g(i,j,k) = (i,j,k)G(i,j,k)^{\top}, \tag{E1}$$

with the Gram matrix in Eq. (8). To eliminate v, we divide the above-mentioned equation by the squared nearest-neighbor distance R^2, yielding

$$g(A;i,j,k) = \frac{g(i,j,k)}{R^2} = \begin{cases} \frac{1}{4A}\left(A(i+j)^2 + (j+k)^2 + (i+k)^2\right) & \text{if } 0 < A < 1/3, \\ \frac{1}{A+1}\left(A(i+j)^2 + (j+k)^2 + (i+k)^2\right) & \text{if } 1/3 \le A \le 1, \\ \frac{1}{2}\left(A(i+j)^2 + (j+k)^2 + (i+k)^2\right) & \text{if } A > 1. \end{cases} \tag{E2}$$

The cases that we are mainly interested in are fcc, mcc, bcc, and acc, all of which satisfy $1/3 \le A \le 1$, but we will go slightly beyond this limit to mainly discuss distortions toward the acc structure. In the important range $1/3 \le A \le 1$, we have

$$g(A;i,j,k) = \frac{1}{A+1}\left(A(i+j)^2 + (j+k)^2 + (i+k)^2\right), \tag{E3}$$

corresponding to the rescaled Gram matrix,

$$G(A) = \frac{1}{A+1}\begin{pmatrix} A+1 & A & 1 \\ A & A+1 & 1 \\ 1 & 1 & 2 \end{pmatrix}, \tag{E4}$$

which is used throughout this work.

The lattice sum for inverse power potentials in terms of the quadratic form $g(A;\ i,j,k)$ defined in (E3) is then given by[11,26]

$$L(A;s) = \sum_{i,j,k\in\mathbb{Z}}{}'\left(\frac{1}{g(A;i,j,k)}\right)^s = \sum_{i,j,k\in\mathbb{Z}}{}'\left(\frac{A+1}{A(i+j)^2 + (j+k)^2 + (i+k)^2}\right)^s, \tag{E5}$$

where $1/3 \le A \le 1$. Here and throughout this work, a prime on the summation symbol will denote that the sum ranges over all integer values except for the term when all of the summation indices are simultaneously zero, i.e., the sums in (E5) are over all integer values of i, j, and k except for the term $(i,j,k) = (0,0,0)$, which is omitted. This lattice sum smoothly connects four different lattices along a cuboidal transition path (the Bain transformation), i.e., when $A = 1$, $1/\sqrt{2}$, $1/2$, or $1/3$ we obtain the expressions for the lattice sums of fcc, mcc, bcc, and acc respectively (face-centered cubic, mean centered-cuboidal, body-centered cubic, and axial centered cuboidal). In these cases, we also write $L_3^{\mathrm{fcc}}(s) = L(1;s)$, $L_3^{\mathrm{mcc}}(s) = L(1/\sqrt{2};s)$, $L_3^{\mathrm{bcc}}(s) = L(1/2;s)$, and $L_3^{\mathrm{acc}}(s) = L(1/3;s)$.

Our objective is to find formulas for $L(A;\ s)$ that are both simple and computationally efficient. The formulas we obtain can be used to show that $L(A;\ s)$ can be analytically continued to complex values of s, with a simple pole at $s = 3/2$ and no other singularities.

One method of evaluating the sum $L(A;\ s)$ is to use the Terras decomposition.[94] This was done in our previous work for the fcc and bcc lattices[26] and can in principle also be applied for general $L(A;\ s)$ with symmetric Gram matrices related to the Epstein zeta function.[27] Here, we use an easier method that works for the entire parameter range $1/3 \le A \le 1$ along the Bain transformation path and

hence gives the lattice sum for all four lattices fcc, mcc, bcc, and acc. The advantage is that we obtain two formulas, which not only can be used as checks but also provide distinct information about their analytic continuation.

We begin by writing the lattice sum in the form

$$\begin{aligned} L(A;s) &= \sum_{i,j,k\in\mathbb{Z}}{}'\left(\frac{A+1}{A(i+j)^2+(j+k)^2+(i+k)^2}\right)^s \\ &= \sum_{\substack{I,J,K\in\mathbb{Z}\\ I+J+K\,\text{even}}}{}'\left(\frac{A+1}{AI^2+J^2+K^2}\right)^s \\ &= \frac{(A+1)^s}{2}\sum_{i,j,k\in\mathbb{Z}}{}'\frac{1+(-1)^{i+j+k}}{(Ai^2+j^2+k^2)^s} \\ &= \frac{(A+1)^s}{2}(T_1(A;s)+T_2(A;s)), \end{aligned} \tag{E6}$$

with the two sums,

$$T_1(A;s) := \sum_{i,j,k\in\mathbb{Z}}{}'\frac{1}{(Ai^2+j^2+k^2)^s} \tag{E7}$$

and

$$T_2(A;s) := \sum_{i,j,k\in\mathbb{Z}}{}'\frac{(-1)^{i+j+k}}{(Ai^2+j^2+k^2)^s}, \tag{E8}$$

which we evaluate separately. For $A = 1$, T_1 is identical to the lattice sum of a simple cubic lattice and T_2 to the Madelung constant.

The lattice sum is $T_1(A;s)$. We shall consider two ways for handling the sum in (E7). The first is to separate the terms according to whether $i = 0$ or $i \neq 0$, which gives rise to

$$T_1(A;s) = f(s) + 2F(s), \tag{E9}$$

where

$$f(s) = \sum_{j,k\in\mathbb{Z}}{}'\frac{1}{(j^2+k^2)^s} \quad\text{and}\quad F(s) = \sum_{i\in\mathbb{N}}\sum_{j,k\in\mathbb{Z}}\frac{1}{(Ai^2+j^2+k^2)^s}, \tag{E10}$$

and $\mathbb{N}$ is the set of positive integers. For simplicity, we omit the parameter A from the notation and just write $f(s)$ and $F(s)$ in place of $f(A;\ s)$ and $F(A;\ s)$, respectively. This is the starting point of the approach taken by Selberg and Chowla (Ref. 95, Sec. 7). Using theta series and Mellin transforms, Zucker showed that the double sum can be expressed in terms of standard functions,[66]

$$f(s) = \sum_{j,k\in\mathbb{Z}}{}'\frac{1}{(j^2+k^2)^s} = 4\zeta(s)L_{-4}(s), \tag{E11}$$

where $\zeta(s)$ is the Riemann zeta function defined in (A13) and $L_{-4}(s)$ is the Dirichlet beta series from (A14) described in Appendix A. It remains to analyze $F(s)$. Using the integral formula for the gamma function (A2), we get

$$\begin{aligned} \pi^{-s}\Gamma(s)F(s) &= \int_{[0,\infty)} x^{s-1}\sum_{i\in\mathbb{N}} e^{-\pi Axi^2}\sum_{j,k\in\mathbb{Z}} e^{-\pi x(j^2+k^2)}\,dx \\ &= \int_{[0,\infty)} x^{s-1}\sum_{i\in\mathbb{N}} e^{-\pi Axi^2}\left(\sum_{j\in\mathbb{Z}} e^{-\pi xj^2}\right)^2 dx. \end{aligned} \tag{E12}$$

Now apply the modular transformation for theta functions (A10) to obtain

$$\begin{aligned} \pi^{-s}\Gamma(s)F(s) &= \int_{[0,\infty)} x^{s-1}\sum_{i\in\mathbb{N}} e^{-\pi Axi^2}\left(\frac{1}{\sqrt{x}}\sum_{j\in\mathbb{Z}} e^{-\pi j^2/x}\right)^2 dx \\ &= \int_{[0,\infty)} x^{s-2}\sum_{i\in\mathbb{N}} e^{-\pi Axi^2}\sum_{N\in\mathbb{N}_0} r_2(N)e^{-\pi N/x}\,dx, \end{aligned} \tag{E13}$$

where $r_2(N)$ is the number of representations of N as a sum of two squares; e.g., see (A11) and $\mathbb{N}_0 = \mathbb{N}\cup\{0\}$. Separating out the $N = 0$ term and evaluating the resulting integrals, we find that

$$\begin{aligned} \pi^{-s}\Gamma(s)F(s) &= \sum_{i\in\mathbb{N}}\int_{[0,\infty)} x^{s-2}e^{-\pi Axi^2}\,dx \\ &\quad + \sum_{i,N\in\mathbb{N}} r_2(N)\int_{[0,\infty)} x^{s-2}e^{-\pi Axi^2-\pi N/x}\,dx \\ &= \frac{\Gamma(s-1)\zeta(2s-2)}{A^{s-1}\pi^{s-1}} + 2\sum_{i,N\in\mathbb{N}} r_2(N) \\ &\quad\times\left(\frac{N}{Ai^2}\right)^{(s-1)/2} K_{s-1}\left(2\pi i\sqrt{AN}\right), \end{aligned}$$

where we have used the formula (A3) for the K-Bessel function. On using all of the above back in (E9), we obtain

$$\begin{aligned} \sum_{i,j,k\in\mathbb{Z}}{}'\frac{1}{(Ai^2+j^2+k^2)^s} &= 4\zeta(s)L_{-4}(s) + \frac{2\pi}{(s-1)}\frac{\zeta(2s-2)}{A^{s-1}} \\ &\quad + \frac{4\pi^s}{\Gamma(s)}A^{(1-s)/2}\sum_{i,N\in\mathbb{N}} r_2(N) \\ &\quad\times\left(\frac{N}{i^2}\right)^{(s-1)/2} K_{s-1}\left(2\pi i\sqrt{AN}\right). \end{aligned} \tag{E14}$$

This is essentially Selberg and Chowla's formula,[95] although they write it in terms of a sum over the divisors of N to minimize the number of Bessel function evaluations. We will leave it as it is for simplicity.

Second formula for the sum is $T_1(A;s)$. Another way is to separate the terms according to whether $(j,k) = (0,0)$ or $(j,k) \neq (0,0)$ and write

$$T_1(A;s) = 2g(s) + G(s), \tag{E15}$$

where

$$g(s) = \sum_{i\in\mathbb{N}}\frac{1}{(Ai^2)^s} \quad\text{and}\quad G(s) = \sum_{j,k\in\mathbb{Z}}{}'\sum_{i\in\mathbb{Z}}\frac{1}{(Ai^2+j^2+k^2)^s}. \tag{E16}$$

For simplicity, we omit the parameter A from the notation and just write $g(s)$ and $G(s)$ in place of $g(A;\ s)$ and $G(A;\ s)$, respectively. Now, apply the integral formula for the gamma function (A2)

and then the modular transformation for the theta function (A7) to obtain

$$\pi^{-s}\Gamma(s)G(s) = \int_{[0,\infty)} x^{s-1} {\sum_{j,k\in\mathbb{Z}}}' e^{-\pi(j^2+k^2)x} \sum_{i\in\mathbb{Z}} e^{-\pi i^2 A x}\, dx$$
$$= \frac{1}{\sqrt{A}} \int_{[0,\infty)} x^{s-3/2} {\sum_{j,k\in\mathbb{Z}}}' e^{-\pi(j^2+k^2)x} \sum_{i\in\mathbb{Z}} e^{-\pi i^2/Ax}\, dx. \tag{E17}$$

Separate the $i = 0$ term, to get

$$\pi^{-s}\Gamma(s)G(s) = \frac{1}{\sqrt{A}} \int_{[0,\infty)} x^{s-3/2} {\sum_{j,k\in\mathbb{Z}}}' e^{-\pi(j^2+k^2)x}\, dx$$
$$+ \frac{2}{\sqrt{A}} \int_{[0,\infty)} x^{s-3/2} {\sum_{j,k\in\mathbb{Z}}}' e^{-\pi(j^2+k^2)x}$$
$$\times \sum_{i\in\mathbb{N}} e^{-\pi i^2/Ax}\, dx. \tag{E18}$$

The first integral can be evaluated in terms of the gamma function by (A2), while the second integral can be expressed in terms of the modified Bessel function by (A3). The result is

$$\pi^{-s}\Gamma(s)G(s) = \frac{\Gamma\left(s-\frac{1}{2}\right)}{\sqrt{A}\,\pi^{s-\frac{1}{2}}} {\sum_{j,k\in\mathbb{Z}}}' \frac{1}{(j^2+k^2)^{s-\frac{1}{2}}}$$
$$+ \frac{4}{A^{\frac{s}{2}+\frac{1}{4}}} {\sum_{j,k\in\mathbb{Z}}}' \sum_{i\in\mathbb{N}} \left(\frac{i}{\sqrt{j^2+k^2}}\right)^{s-\frac{1}{2}}$$
$$\times K_{s-\frac{1}{2}}\left(2\pi i\sqrt{\frac{j^2+k^2}{A}}\right)$$
$$= \frac{4}{\sqrt{A}}\,\pi^{-\left(s-\frac{1}{2}\right)}\,\Gamma\left(s-\frac{1}{2}\right)\zeta\left(s-\frac{1}{2}\right)L_{-4}\left(s-\frac{1}{2}\right)$$
$$+ \frac{4}{A^{\frac{s}{2}+\frac{1}{4}}} \sum_{N,i\in\mathbb{N}} r_2(N)\left(\frac{i}{\sqrt{N}}\right)^{s-\frac{1}{2}}$$
$$\times K_{s-\frac{1}{2}}\left(2\pi i\sqrt{\frac{N}{A}}\right). \tag{E19}$$

On using all of the above back in (E15), we obtain

$${\sum_{i,j,k\in\mathbb{Z}}}' \frac{1}{(Ai^2+j^2+k^2)^s} = 2A^{-s}\zeta(2s) + 4\sqrt{\frac{\pi}{A}}\,\frac{\Gamma\left(s-\frac{1}{2}\right)}{\Gamma(s)}$$
$$\times \zeta\left(s-\frac{1}{2}\right)L_{-4}\left(s-\frac{1}{2}\right)$$
$$+ \frac{4}{A^{\frac{s}{2}+\frac{1}{4}}}\,\frac{\pi^s}{\Gamma(s)} \sum_{N,i\in\mathbb{N}} r_2(N)$$
$$\times \left(\frac{i}{\sqrt{N}}\right)^{s-\frac{1}{2}} K_{s-\frac{1}{2}}\left(2\pi i\sqrt{\frac{N}{A}}\right). \tag{E20}$$

The terms in (E14) involve K_{s-1} Bessel functions, whereas $K_{s-\frac{1}{2}}$ Bessel functions occur in (E20). That is because each application of the theta function transformation formula lowers the subscript in the resulting Bessel function by 1/2 due to the creation of an $x^{-1/2}$ factor in the integral. The theta function transformation formula is used twice (i.e., the formula is squared) in the derivation of (E14) and only once in the derivation of (E20). Each of (E14) and (E20) turns out to have its own advantages when it comes to convergence for specific A and s values.

The alternating lattice sum is $T_2(A;s)$. Analysis in the previous sections can be modified to handle the alternating series (E8) which has the term $(-1)^{i+j+k}$ in the numerator, as follows. Separating the terms according to whether $i = 0$ or $i \neq 0$ gives

$$T_2(A;s) = h(s) + 2H(s), \tag{E21}$$

where

$$h(s) = {\sum_{j,k\in\mathbb{Z}}}' \frac{(-1)^{j+k}}{(j^2+k^2)^s} \quad \text{and} \quad H(s) = \sum_{i\in\mathbb{N}} \sum_{j,k\in\mathbb{Z}} \frac{(-1)^{i+j+k}}{(Ai^2+j^2+k^2)^s}. \tag{E22}$$

Using (A14), we obtain $h(s) = -4(1-2^{1-s})\zeta(s)L_{-4}(s)$. Next, using the integral formula for the gamma function (A2), we obtain

$$\pi^{-s}\Gamma(s)H(s) = \int_{[0,\infty)} x^{s-1} \sum_{i\in\mathbb{N}} (-1)^i e^{-\pi A x i^2}$$
$$\times \sum_{j,k\in\mathbb{Z}} (-1)^{j+k} e^{-\pi x(j^2+k^2)}\, dx, \tag{E23}$$

$$= \int_{[0,\infty)} x^{s-1} \sum_{i\in\mathbb{N}} (-1)^i e^{-\pi A x i^2}$$
$$\times \left(\sum_{j\in\mathbb{Z}} (-1)^j e^{-\pi x j^2}\right)^2 dx. \tag{E24}$$

Applying the modular transformation for theta functions leads to

$$\pi^{-s}\Gamma(s)H(s) = \int_{[0,\infty)} x^{s-1} \sum_{i\in\mathbb{N}} (-1)^i$$
$$\times e^{-\pi A x i^2} \left(\frac{1}{\sqrt{x}} \sum_{j\in\mathbb{Z}} e^{-\pi\left(j+\frac{1}{2}\right)^2/x}\right)^2 dx. \tag{E25}$$

By formula (A12), this can be expressed as

$$\pi^{-s}\Gamma(s)H(s) = \int_{[0,\infty)} x^{s-2} \sum_{i\in\mathbb{N}} (-1)^i e^{-\pi A x i^2}$$
$$\times \sum_{N\in\mathbb{N}_0} r_2(4N+1) e^{-\pi(4N+1)/2x}\, dx$$
$$= \sum_{i\in\mathbb{N}} \sum_{N\in\mathbb{N}_0} (-1)^i r_2(4N+1)$$
$$\times \int_{[0,\infty)} x^{s-2} e^{-\pi A x i^2 - \pi(4N+1)/2x}\, dx. \tag{E26}$$

The integral can be expressed in terms of Bessel functions using (A3),

$$\pi^{-s}\Gamma(s)H(s) = 2\sum_{i\in\mathbb{N}}\sum_{N\in\mathbb{N}_0}(-1)^i r_2(4N+1)\left(\frac{2N+\frac{1}{2}}{Ai^2}\right)^{(s-1)/2} \times K_{s-1}\left(2\pi i\sqrt{A\left(2N+\frac{1}{2}\right)}\right). \tag{E27}$$

Incorporating all of the above back in (E21) results in

$$\sum_{i,j,k\in\mathbb{Z}}{}' \frac{(-1)^{i+j+k}}{(Ai^2+j^2+k^2)^s} = -4(1-2^{1-s})\zeta(s)L_{-4}(s) + \frac{4\pi^s}{\Gamma(s)}A^{(1-s)/2}\sum_{i\in\mathbb{N}}\sum_{N\in\mathbb{N}_0}(-1)^i \times r_2(4N+1)\left(\frac{2N+\frac{1}{2}}{i^2}\right)^{(s-1)/2} \times K_{s-1}\left(2\pi i\sqrt{A\left(2N+\frac{1}{2}\right)}\right). \tag{E28}$$

Second formula for $T_2(A;s)$: this time, we separate the terms according to whether $(j,k) = (0,0)$ or $(j,k) \neq (0,0)$ and write

$$T_2(A;s) = 2\sum_{i\in\mathbb{N}}\frac{(-1)^i}{(Ai^2)^s} + J(s), \tag{E29}$$

where

$$J(s) = \sum_{j,k\in\mathbb{Z}}{}'\sum_{i\in\mathbb{Z}}\frac{(-1)^{i+j+k}}{(Ai^2+j^2+k^2)^s}. \tag{E30}$$

Using (A22) gives

$$2\sum_{i\in\mathbb{N}}\frac{(-1)^i}{(Ai^2)^s} = -2A^{-s}(1-2^{1-2s})\zeta(2s). \tag{E31}$$

It remains to analyze the sum for $J(s)$. Using the integral formula for the gamma function (A2) leads to

$$\pi^{-s}\Gamma(s)J(s) = \int_{[0,\infty)}x^{s-1}\sum_{j,k\in\mathbb{Z}}{}'(-1)^{j+j}e^{-\pi(j^2+k^2)x} \times \sum_{i\in\mathbb{Z}}(-1)^i e^{-\pi i^2 Ax}\,dx. \tag{E32}$$

Applying the modular transformation (A9) gives

$$\pi^{-s}\Gamma(s)J(s) = \frac{1}{\sqrt{A}}\int_{[0,\infty)}x^{s-3/2}\sum_{j,k\in\mathbb{Z}}{}'(-1)^{j+k}e^{-\pi(j^2+k^2)x} \times \sum_{i\in\mathbb{Z}}e^{-\pi\left(i+\frac{1}{2}\right)^2/Ax}\,dx. \tag{E33}$$

Setting $N = j^2 + k^2$ and using

$$\sum_{i\in\mathbb{Z}}e^{-\pi\left(i+\frac{1}{2}\right)^2/Ax} = 2\sum_{i\in\mathbb{N}_0}^{\infty}e^{-\pi\left(i+\frac{1}{2}\right)^2/Ax} = 2\sum_{i\in\mathbb{N}}e^{-\pi\left(i-\frac{1}{2}\right)^2/Ax} \tag{E34}$$

gives

$$\pi^{-s}\Gamma(s)J(s) = \frac{2}{\sqrt{A}}\sum_{N,i\in\mathbb{N}}(-1)^N r_2(N) \times \int_{[0,\infty)}x^{s-3/2}e^{-\pi Nx-\pi\left(i-\frac{1}{2}\right)^2/Ax}\,dx. \tag{E35}$$

The integral can be evaluated in terms of the modified Bessel function, (A3),

$$\pi^{-s}\Gamma(s)J(s) = \frac{4}{A^{\frac{s}{2}+\frac{1}{4}}}\sum_{N,i\in\mathbb{N}}(-1)^N r_2(N)\left(\frac{i-\frac{1}{2}}{\sqrt{N}}\right)^{s-\frac{1}{2}} \times K_{s-\frac{1}{2}}\left(2\pi\left(i-\frac{1}{2}\right)\sqrt{\frac{N}{A}}\right). \tag{E36}$$

It follows that

$$\sum_{i,j,k\in\mathbb{Z}}{}'\frac{(-1)^{i+j+k}}{(Ai^2+j^2+k^2)^s} = -2A^{-s}(1-2^{1-2s})\zeta(2s) + \frac{4}{A^{\frac{s}{2}+\frac{1}{4}}}\frac{\pi^s}{\Gamma(s)}\sum_{N,i\in\mathbb{N}}(-1)^N r_2(N) \times \left(\frac{i-\frac{1}{2}}{\sqrt{N}}\right)^{s-\frac{1}{2}}K_{s-\frac{1}{2}}\left(2\pi\left(i-\frac{1}{2}\right)\sqrt{\frac{N}{A}}\right). \tag{E37}$$

Two formulas for $L(A;s)$: on substituting the results of (E14) and (E28) back into (E6), we obtain a formula for $L(A;s)$ in terms of K_{s-1} Bessel functions,

$$L(A;s) = 4\left(\frac{A+1}{2}\right)^s\zeta(s)L_{-4}(s) + \frac{\pi A}{s-1}\left(1+\frac{1}{A}\right)^s\zeta(2s-2) + \frac{2\pi^s\sqrt{A}}{\Gamma(s)}\left(\sqrt{A}+\frac{1}{\sqrt{A}}\right)^s\sum_{N,i\in\mathbb{N}}r_2(N) \times \left(\frac{N}{i^2}\right)^{(s-1)/2}K_{s-1}\left(2\pi i\sqrt{AN}\right) + \frac{2\pi^s\sqrt{A}}{\Gamma(s)}\left(\sqrt{A}+\frac{1}{\sqrt{A}}\right)^s\sum_{i\in\mathbb{N}}\sum_{N\in\mathbb{N}_0}(-1)^i r_2(4N+1) \times \left(\frac{2N+\frac{1}{2}}{i^2}\right)^{(s-1)/2}K_{s-1}\left(2\pi i\sqrt{A\left(2N+\frac{1}{2}\right)}\right). \tag{E38}$$

On the other hand, if the results of (E20) and (E37) are used in (E6), the resulting formula for $L(A;s)$ involves $K_{s-1/2}$ Bessel functions,

$$L(A;s) = 2\left(\frac{A+1}{4A}\right)^s\zeta(2s) + 2\sqrt{\frac{\pi}{A}}(A+1)^s\frac{\Gamma\left(s-\frac{1}{2}\right)}{\Gamma(s)} \times \zeta\left(s-\frac{1}{2}\right)L_{-4}\left(s-\frac{1}{2}\right) + \frac{2}{A^{1/4}}\left(\sqrt{A}+\frac{1}{\sqrt{A}}\right)^s\frac{\pi^s}{\Gamma(s)}\sum_{N,i\in\mathbb{N}}N^{(1-2s)/4}r_2(N) \times \left\{i^{s-\frac{1}{2}}K_{s-\frac{1}{2}}\left(2\pi i\sqrt{\frac{N}{A}}\right) + (-1)^N\left(i-\frac{1}{2}\right)^{s-\frac{1}{2}} \times K_{s-\frac{1}{2}}\left(2\pi\left(i-\frac{1}{2}\right)\sqrt{\frac{N}{A}}\right)\right\}. \tag{E39}$$

The formulas (E38) and (E39) can be used as checks against one another. Moreover, the formulas offer different information about special values of the lattice sum, as will be seen in Appendix G.

APPENDIX F: A MINIMUM PROPERTY OF THE LATTICE SUM $L(A;\ s)$

It was noted that on the interval $1/3 \le A \le 1$, the packing density function Δ_Λ has a minimum value when $A = 1/2$. Provided that $s > 3/2$, the corresponding lattice sum $L(A;\ s)$ also attains a minimum at the same value $A = 1/2$. The proof for this condition is provided in Ref. 56.

Theorem F.1. *Let $L(A;\ s)$ be the lattice defined by (E5), that is,*

$$L(A;s) = \sum_{i,j,k\in\mathbb{Z}}{}'\left(\frac{1}{g(A;i,j,k)}\right)^s = \sum_{i,j,k\in\mathbb{Z}}{}'\left(\frac{A+1}{A(i+j)^2+(j+k)^2+(i+k)^2}\right)^s, \tag{F1}$$

where $s > 3/2$ and $1/3 \le A \le 1$. Then,

$$\frac{\partial}{\partial A}L(A;s)\Big|_{A=1/2} = 0 \quad \text{and} \quad \frac{\partial^2}{\partial A^2}L(A;s)\Big|_{A=1/2} > 0. \tag{F2}$$

As a consequence, for any fixed value $s > 3/2$, the lattice sum $L(A;\ s)$ attains a minimum when $A = 1/2$. Graphs of $L(A;\ s)$ to illustrate this minimum property are shown in Fig. 17. In the limiting case $s \to \infty$, we have

$$L(A;\infty) = \lim_{s\to\infty} L(A;s) = \mathrm{kiss}(\Lambda) = \begin{cases} 10 & \text{if } A = 1/3, \\ 8 & \text{if } 1/3 < A < 1, \\ 12 & \text{if } A = 1. \end{cases} \tag{F3}$$

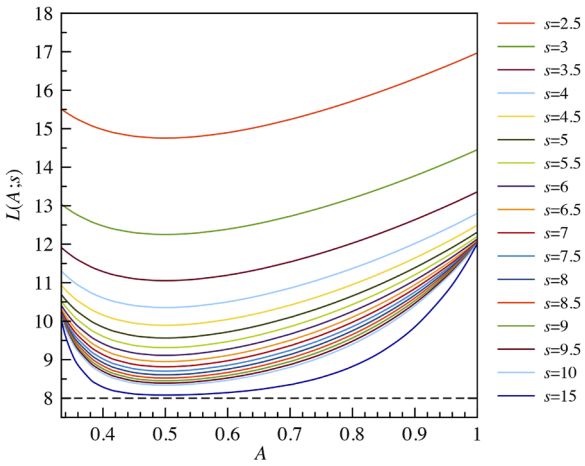

FIG. 17. Graph of $L(A;\ s)$ vs A for various values of s For $s \to \infty$, we have at both ends of the interval $L(A = \frac{1}{3};\infty) = 10$ and $L(A = 1;\ \infty) = 12$.

We find an interesting relation between the lattice sum and its first derivative,

$$\frac{\partial}{\partial A}L(A;s)\Big|_{A=1} = \frac{s}{6}L(A;s)\Big|_{A=1} \tag{F4}$$

which can be proved as follows: on calculating the derivative using (F1), we obtain

$$\frac{\partial}{\partial A}L(A;s) = \frac{2s}{(A+1)^2}\sum_{i,j,k\in\mathbb{Z}}{}'(k^2+ik+jk-ij) \times\left(\frac{A+1}{A(i+j)^2+(j+k)^2+(i+k)^2}\right)^{s+1}$$

and on setting $A = 1$, it follows that

$$\frac{\partial}{\partial A}L(A;s)\Big|_{A=1} = \frac{s}{2}\sum_{i,j,k\in\mathbb{Z}}{}'\frac{k^2+ik+jk-ij}{\left(i^2+j^2+k^2+ij+jk+ki\right)^{s+1}}.$$

Now, replace the summation indices (i,j,k) with the cyclic permutations (j,k,i) and (k,i,j) and add the three equations to obtain

$$\begin{aligned} 3\frac{\partial}{\partial A}L(A;s)\Big|_{A=1} &= \frac{s}{2}\sum_{i,j,k\in\mathbb{Z}}{}'\frac{i^2+j^2+k^2+ij+jk+ki}{\left(i^2+j^2+k^2+ij+jk+ki\right)^{s+1}} \\ &= \frac{s}{2}\sum_{i,j,k\in\mathbb{Z}}{}'\frac{1}{\left(i^2+j^2+k^2+ij+jk+ki\right)^{s}} \\ &= \frac{s}{2}L(A;s)\Big|_{A=1}. \end{aligned}$$

This proves (F4).

APPENDIX G: ANALYTIC CONTINUATIONS OF THE LATTICE SUMS $L(A;\ s)$

We will now show that the lattice sums $L(A;\ s)$ can be continued analytically to the whole s-plane and that the resulting functions have a single simple pole at $s = 3/2$ and no other singularities. We do this in steps. First, we show that the lattice sums each have a simple pole at $s = 3/2$ and determine the residue. Then, we show that the analytic continuations obtained are valid for the whole s-plane and there are no other singularities. Finally, values of the analytic continuations at the points $s = 1/2$ and $s = 1, 0, -1, -2, \ldots$ are computed. In particular, the evaluation of $T_2(A;\ s)$ at $s = 1/2$ in the case $A = 1$ gives the Madelung constant, e.g., see Ref. 31, (Ref. 11, pp. xiii, 39–51).[18]

We start by showing that $L(A;\ s)$ has a simple pole at $s = 3/2$ and determine the residue. In formula (E38), all of the terms are analytic at $s = 3/2$, except for the term involving $\zeta(2s-2)$. It follows that

$$\lim_{s\to 3/2}(s-3/2)L(A;s) = \lim_{s\to 3/2}(s-3/2)\frac{\pi A}{s-1}\left(1+\frac{1}{A}\right)^s\zeta(2s-2)$$
$$= 2\pi A\left(1+\frac{1}{A}\right)^{3/2}\lim_{s\to 3/2}(s-3/2)\zeta(2s-2)$$
$$= \frac{2\pi}{\sqrt{A}}(A+1)^{3/2}\times\frac{1}{2}\lim_{u\to 1}(u-1)\zeta(u)$$
$$= \frac{\pi}{\sqrt{A}}(A+1)^{3/2}, \tag{G1}$$

where (A16) was used in the last step of the calculation. It follows further that $L(A;\, s)$ has a simple pole at $s = 3/2$ and the residue is given by

$$\mathrm{Res}(L(A;s),3/2) = \frac{\pi}{\sqrt{A}}(A+1)^{3/2}. \tag{G2}$$

This corresponds to 12 times the packing density, i.e.,

$$\mathrm{Res}(L(A;s),3/2) = 12\Delta_\Lambda. \tag{G3}$$

For example, taking $A = 1$ gives

$$\mathrm{Res}(L_3^{\mathrm{FCC}}(s),3/2) = 2\sqrt{2}\,\pi, \tag{G4}$$

while taking $A = 1/2$ gives

$$\mathrm{Res}(L_3^{\mathrm{BCC}}(s),3/2) = 3\sqrt{3}\,\pi/2. \tag{G5}$$

Laurent's theorem implies that there is an expansion of the form

$$L(A;s) = \frac{c_{-1}}{s-3/2} + c_0 + \sum_{n=1}^{\infty} c_n(s-3/2)^n, \tag{G6}$$

where

$$c_{-1} = \mathrm{Res}(L(A;s),3/2) = \frac{\pi}{\sqrt{A}}(A+1)^{3/2}, \tag{G7}$$

and the coefficients c_0, c_1, and $c_2, \ldots$ depend on A but not on s. To calculate c_0, start with the fact that

$$\lim_{s\to 3/2}\left(\frac{\pi A}{s-1}\left(1+\frac{1}{A}\right)^s\zeta(2s-2) - \frac{c_{-1}}{s-3/2}\right)$$
$$= \frac{\pi}{\sqrt{A}}(A+1)^{3/2}\left(2\gamma - 2 + \log\left(1+\frac{1}{A}\right)\right), \tag{G8}$$

where $\gamma = 0.577\,215\,664\,901\,532\,86\,060\ldots$ is the Euler–Mascheroni constant. Then, use (E38) and (A5) to deduce

$$c_0 = \lim_{s\to 3/2}\left(L(A;s) - \frac{c_{-1}}{s-3/2}\right) = \sqrt{2}(A+1)^{3/2}\zeta\left(\frac{3}{2}\right)L_{-4}\left(\frac{3}{2}\right)$$
$$+ \frac{\pi}{\sqrt{A}}(A+1)^{3/2}\left(2\gamma - 2 + \log\left(1+\frac{1}{A}\right)\right)$$
$$+ \frac{2\pi}{\sqrt{A}}(A+1)^{3/2}\sum_{k,N\in\mathbb{N}}\frac{1}{k}\,r_2(N)\exp\left(-2\pi k\sqrt{AN}\right)$$
$$+ \frac{2\pi}{\sqrt{A}}(A+1)^{3/2}\sum_{k,N\in\mathbb{N}}\frac{(-1)^k}{k}\,r_2(4N+1)$$
$$\times\exp\left(-2\pi k\sqrt{A\left(2N+\frac{1}{2}\right)}\right). \tag{G9}$$

Interchanging the order of summation and evaluating the sum over k gives

$$c_0 = \sqrt{2}(A+1)^{3/2}\zeta\left(\frac{3}{2}\right)L_{-4}\left(\frac{3}{2}\right)$$
$$+ \frac{\pi}{\sqrt{A}}(A+1)^{3/2}\left(2\gamma - 2 + \log\left(1+\frac{1}{A}\right)\right)$$
$$- \frac{2\pi}{\sqrt{A}}(A+1)^{3/2}\sum_{N\in\mathbb{N}} r_2(N)\log\left(1-e^{-2\pi\sqrt{AN}}\right)$$
$$- \frac{2\pi}{\sqrt{A}}(A+1)^{3/2}\sum_{N\in\mathbb{N}_0} r_2(4N+1)\log\left(1+e^{-\pi\sqrt{2A(4N+1)}}\right). \tag{G10}$$

Numerical evaluation in the case $A = 1$ gives

$$c_0|_{A=1} = 6.984\,05\,25\,503\,22\,247\,93\,406\ldots. \tag{G11}$$

We now evaluate the analyticity of the lattice sums at other values of s. By (A6), the double series of Bessel functions in (E38) converges absolutely and uniformly on compact subsets of the s-plane and, therefore, represents an entire function of s. It follows that $L(A;\, s)$ has an analytic continuation to a meromorphic function which is analytic except possibly at the singularities of the terms,

$$4\left(\frac{A+1}{2}\right)^s\zeta(s)L_{-4}(s) \tag{G12}$$

and

$$\frac{\pi A}{s-1}\left(1+\frac{1}{A}\right)^s\zeta(2s-2). \tag{G13}$$

The function in (G12) is analytic except at $s = 1$ due to the pole of $\zeta(s)$. The function $L_{-4}(s)$ and the exponential function are both entire. The function in (G13) is analytic except at $s = 1$ and $s = 3/2$.

The singularity at $s = 3/2$ was already studied before.[26,70] Using (A16) and the values of $\zeta(0)$ and $L_{-4}(1)$ in (A19) and (A20), we find that

$$4\left(\frac{A+1}{2}\right)^s\zeta(s)L_{-4}(s) = \frac{(A+1)\pi}{2(s-1)} + O(1) \quad \text{as } s\to 1 \tag{G14}$$

and

$$\frac{\pi A}{s-1}\left(1+\frac{1}{A}\right)^s\zeta(2s-2) = -\frac{(A+1)\pi}{2(s-1)} + O(1) \quad \text{as } s \to 1. \tag{G15}$$

It follows that the sum of the functions in (G12) and (G13) has a removable singularity at $s = 1$ and thus $L(A; s)$ is also analytic at $s = 1$. The analyticity at $s = 1$ can also be seen directly from the alternative formula for $L(A; s)$ in (E39). We thus showed that $L(A; s)$ has an analytic continuation to a meromorphic function of s, which has a simple pole at $s = 3/2$ and no other singularities. Because $L(A; s)$ has only one singularity, namely, $s = 3/2$, the Laurent expansion (G6) is valid in the annulus $0 < |s - 3/2| < \infty$, i.e., for all $s \neq 3/2$.

By the theory of complex variables, the analytic continuation, if one exists, is unique; e.g., see Ref. 96. Therefore, analytic continuation formulas can be used to assign values to divergent series. For example, the Madelung constant is defined by

$$M = {\sum_{i,j,k\in\mathbb{Z}}}' \left.\frac{(-1)^{i+j+k}}{(i^2+j^2+k^2)^s}\right|_{s=1/2}. \tag{G16}$$

This is interpreted as being the value of the analytic continuation of the series at $s = 1/2$ because the sum diverges if $s = 1/2$. From now on, we shall use the expression "the value of a series at a point s" to mean "the value of the analytic continuation of the series at the point s."

For the A-dependent case, on putting $s = 1/2$ in (E28), we obtain an analytic expression for the value of

$$M(A) = {\sum_{i,j,k\in\mathbb{Z}}}' \left.\frac{(-1)^{i+j+k}}{(Ai^2+j^2+k^2)^s}\right|_{s=1/2}, \tag{G17}$$

which specializes to the Madelung constant in the case $A = 1$.[97] We have

$$\begin{aligned} M(A) = & -4(1-2^{1-s})\zeta(s)L_{-4}(s)\big|_{s=1/2} \\ & + \frac{4\pi^s}{\Gamma(s)} A^{(1-s)/2} \sum_{i\in\mathbb{N}}\sum_{N\in\mathbb{N}_0} (-1)^i r_2(4N+1) \\ & \times \left(\frac{2N+\frac{1}{2}}{i^2}\right)^{(s-1)/2} K_{s-1}\left(2\pi i\sqrt{A\left(2N+\frac{1}{2}\right)}\right)\Bigg|_{s=1/2}. \end{aligned} \tag{G18}$$

Now, we use (A4) and (A5) to express the Bessel functions in terms of exponential functions. The result simplifies to

$$\begin{aligned} M(A) = & 4(\sqrt{2}-1)\zeta\left(\frac{1}{2}\right)L_{-4}\left(\frac{1}{2}\right) \\ & + 2\sum_{i\in\mathbb{N}}\sum_{N\in\mathbb{N}_0} (-1)^i \frac{r_2(4N+1)}{\sqrt{2N+\frac{1}{2}}} e^{-2\pi i\sqrt{A(2N+1/2)}}. \end{aligned} \tag{G19}$$

On interchanging the order of summation and summing the geometric series, we obtain

$$\begin{aligned} M(A) = & 4(\sqrt{2}-1)\zeta\left(\frac{1}{2}\right)L_{-4}\left(\frac{1}{2}\right) \\ & - 2\sqrt{2}\sum_{N\in\mathbb{N}_0} \frac{r_2(4N+1)}{\sqrt{4N+1}}\left(\frac{1}{e^{\pi\sqrt{2A(4N+1)}}+1}\right). \end{aligned} \tag{G20}$$

When $A = 1$, this gives the Madelung constant defined by (G16). Numerical evaluation gives

$$M = M(1) = -1.747\,56\,45\,946\,33\,182\,19\,063\ldots, \tag{G21}$$

which is in agreement with Ref. 11, p. xiii (apart from the minus sign which we have corrected here) and matches the value of $d(1)$ in Ref. 11, pp. 39–51.

In a similar way, starting from (E14) and using (A5) and (A19), we obtain

$$\begin{aligned} & {\sum_{i,j,k\in\mathbb{Z}}}' \left.\frac{1}{(Ai^2+j^2+k^2)^s}\right|_{s=1/2} \\ & = 4\zeta\left(\frac{1}{2}\right)L_{-4}\left(\frac{1}{2}\right) + \frac{\pi\sqrt{A}}{3} + 2\sum_{i,N\in\mathbb{N}} \frac{r_2(N)}{\sqrt{N}} e^{-2\pi i\sqrt{AN}} \\ & = 4\zeta\left(\frac{1}{2}\right)L_{-4}\left(\frac{1}{2}\right) + \frac{\pi\sqrt{A}}{3} + 2\sum_{N\in\mathbb{N}} \frac{r_2(N)}{\sqrt{N}}\left(\frac{1}{e^{2\pi\sqrt{AN}}-1}\right). \end{aligned} \tag{G22}$$

Numerical evaluation in the case $A = 1$ gives

$$\left.{\sum_{i,j,k\in\mathbb{Z}}}' \frac{1}{(i^2+j^2+k^2)^s}\right|_{s=1/2} = -2.837\,29\,74\,794\,80\,619\,47\,666\ldots. \tag{G23}$$

Now, from (E6) we have for the fcc lattice,

$$\begin{aligned} L\left(A=1;\frac{1}{2}\right) = & \frac{1}{\sqrt{2}}{\sum_{i,j,k\in\mathbb{Z}}}' \left.\frac{1}{(i^2+j^2+k^2)^s}\right|_{s=1/2} \\ & + \frac{1}{\sqrt{2}}{\sum_{i,j,k\in\mathbb{Z}}}' \left.\frac{(-1)^{i+j+k}}{(i^2+j^2+k^2)^s}\right|_{s=1/2}. \end{aligned} \tag{G24}$$

Hence, using the values from (G21) and (G23), we obtain

$$L\left(A=1;\frac{1}{2}\right) = -3.241\,98\,70\,634\,10\,888\,39\,428\ldots. \tag{G25}$$

We now turn to the value of the lattice sum at $s = 1$. It was noted above that (E38), which involves K_{s-1} Bessel functions, contains terms with singularities at $s = 1$ and, therefore, is not suitable for calculations at that value of s. Instead, we can use (E39), which involves $K_{s-1/2}$ Bessel functions. As in Appendix F, two steps are involved. First, the $K_{1/2}$ Bessel functions can be expressed in terms of the exponential function by (A5). Then, the double sum can be reduced to a single sum by geometric series. We omit the details and just record the final results and corresponding numerical values. From (E20), we have

$$\begin{aligned} {\sum_{i,j,k\in\mathbb{Z}}}' \left.\frac{1}{(Ai^2+j^2+k^2)^s}\right|_{s=1} = & \frac{\pi^2}{3A} + \frac{4\pi}{\sqrt{A}}\zeta\left(\frac{1}{2}\right)L_{-4}\left(\frac{1}{2}\right) \\ & + \frac{2\pi}{\sqrt{A}}\sum_{N\in\mathbb{N}} \frac{r_2(N)}{\sqrt{N}}\left(\frac{1}{e^{2\pi\sqrt{N/A}}-1}\right), \end{aligned} \tag{G26}$$

while (E37) gives

$$\sum_{i,j,k\in\mathbb{Z}}{}' \left.\frac{(-1)^{i+j+k}}{(Ai^2+j^2+k^2)^s}\right|_{s=1} = \frac{-\pi^2}{6A} + \frac{2\pi}{\sqrt{A}}\sum_{N\in\mathbb{N}}(-1)^N\frac{r_2(N)}{\sqrt{N}} \times\left(\frac{1}{e^{\pi\sqrt{N/A}}-e^{-\pi\sqrt{N/A}}}\right). \quad \text{(G27)}$$

Then, (E6) can be used to write down the value of $L(A;\ s)$. For example, when $A=1$, the above-mentioned formulas give

$$\sum_{i,j,k\in\mathbb{Z}}{}' \left.\frac{1}{(i^2+j^2+k^2)^s}\right|_{s=1} = -8.913\,63\ 29\,175\ 85\,151\ 27\,268\ldots \quad \text{(G28)}$$

and

$$\sum_{i,j,k\in\mathbb{Z}}{}' \left.\frac{(-1)^{i+j+k}}{(i^2+j^2+k^2)^s}\right|_{s=1} = -2.519\,35\ 61\,520\ 89\,445\ 31\,334\ldots. \quad \text{(G29)}$$

Then, taking $s=1$ in (E6) gives for the fcc lattice,

$$L(A=1,1) = \sum_{i,j,k}{}' \left.\frac{1}{(i^2+j^2+k^2)^s}\right|_{s=1} + \sum_{i,j,k}{}' \left.\frac{(-1)^{i+j+k}}{(i^2+j^2+k^2)^s}\right|_{s=1}, \quad \text{(G30)}$$

$$= -11.432\,98\ 90\,696\ 74\,596\ 58\,602\ldots. \quad \text{(G31)}$$

We note a connection between two of the values in the above-mentioned analysis. By setting $A=1$ in each of (G22) and (G26), we obtain the remarkable result,

$$\sum_{i,j,k\in\mathbb{Z}}{}' \left.\frac{1}{(i^2+j^2+k^2)^s}\right|_{s=1} = \pi\sum_{i,j,k\in\mathbb{Z}}{}' \left.\frac{1}{(i^2+j^2+k^2)^s}\right|_{s=1/2}. \quad \text{(G32)}$$

This is consistent with Ref. 11, p. 46 (1.3.44) and is the special case $s=1$ of the functional equation,

$$\pi^{-s}\Gamma(s)T_1(1;s) = \pi^{-\left(\frac{3}{2}-s\right)}\Gamma\left(\frac{3}{2}-s\right)T_1\left(1;\frac{3}{2}-s\right). \quad \text{(G33)}$$

This functional equation can be deduced from the two formulas for $T_1(A;\ s)$ in (E14) and (E20), as follows: replace s with $\frac{3}{2}-s$ in (E14) and then multiply by $\pi^{s-\frac{3}{2}}\Gamma(\frac{3}{2}-s)$ and set $A=1$ to get

$$\begin{aligned}\pi^{s-\frac{3}{2}}\Gamma\left(\frac{3}{2}-s\right)T_1\left(1;\frac{3}{2}-s\right) &= 4\pi^{s-\frac{3}{2}}\Gamma\left(\frac{3}{2}-s\right)\zeta\left(\frac{3}{2}-s\right)L_{-4}\left(\frac{3}{2}-s\right)\\ &+ 2\pi^{s-\frac{1}{2}}\Gamma\left(\frac{1}{2}-s\right)\zeta(1-2s) + 4\sum_{i,N\in\mathbb{N}} r_2(N)\\ &\times\left(\frac{N}{i^2}\right)^{\left(\frac{1}{2}-s\right)/2} K_{\frac{1}{2}-s}\left(2\pi i\sqrt{N}\right),\end{aligned} \quad \text{(G34)}$$

where we have used the functional equation for the gamma function in the form $\Gamma(3/2-s)=(1/2-s)\Gamma(1/2-s)$ to obtain the second term on the right-hand side. Now, apply the functional Eqs. (A4), (A17), and (A18) to deduce

$$\begin{aligned}\pi^{-\left(\frac{3}{2}-s\right)}\Gamma\left(\frac{3}{2}-s\right)T_1\left(1;\frac{3}{2}-s\right) &= 4\pi^{\frac{1}{2}-s}\Gamma\left(s-\frac{1}{2}\right)\zeta\left(s-\frac{1}{2}\right)L_{-4}\left(s-\frac{1}{2}\right) + 2\pi^{-s}\Gamma(s)\zeta(2s)\\ &+ 4\sum_{i,N\in\mathbb{N}} r_2(N)\left(\frac{i}{\sqrt{N}}\right)^{s-\frac{1}{2}} K_{s-\frac{1}{2}}\left(2\pi i\sqrt{N}\right).\end{aligned} \quad \text{(G35)}$$

The functional equation (G33) follows from this by using (E20). In addition to providing another proof of the functional equation, the calculation above also demonstrates the interconnection between the formulas (E14) and (E20). Further functional equations of this type are considered in Ref. 11, p. 46.

We now evaluate the values at $s=0,-1,-2,-3,\ldots$ for the lattice sum. Recall from (E38) that

$$\begin{aligned}L(A;s) &= 4\left(\frac{A+1}{2}\right)^s\zeta(s)L_{-4}(s) + \frac{\pi A}{s-1}\left(1+\frac{1}{A}\right)^s\zeta(2s-2)\\ &+ \frac{2\pi^s\sqrt{A}}{\Gamma(s)}\left(\sqrt{A}+\frac{1}{\sqrt{A}}\right)^s\sum_{i,N\in\mathbb{N}} r_2(N)\left(\frac{N}{i^2}\right)^{(s-1)/2}\\ &\times K_{s-1}\left(2\pi i\sqrt{AN}\right) + \frac{2\pi^s\sqrt{A}}{\Gamma(s)}\left(\sqrt{A}+\frac{1}{\sqrt{A}}\right)^s\\ &\times\sum_{i\in\mathbb{N}}\sum_{N\in\mathbb{N}_0}(-1)^i r_2(4N+1)\left(\frac{2N+\frac{1}{2}}{i^2}\right)^{(s-1)/2}\\ &\times K_{s-1}\left(2\pi i\sqrt{A\left(2N+\frac{1}{2}\right)}\right).\end{aligned} \quad \text{(G36)}$$

On using the values $\zeta(0)=-\frac{1}{2}$, $\zeta(-2)=0$, and $L_{-4}(0)=\frac{1}{2}$ and the limiting value $\lim_{s\to 0}1/\Gamma(s)=0$, we readily obtain the result $L(A;\ 0)=-1$. Moreover, since

$$\zeta(-2)=\zeta(-4)=\zeta(-6)=\cdots=0, \quad \text{(G37)}$$

$$L_{-4}(-1)=L_{-4}(-3)=\zeta(-5)=\cdots=0, \quad \text{(G38)}$$

$$\text{and}\quad \lim_{s\to N}\frac{1}{\Gamma(s)}=0 \quad \text{if } N=0,-1,-2,\ldots, \quad \text{(G39)}$$

it follows that

$$L(A;-1)=L(A;-2)=L(A;-3)=\cdots=0. \quad \text{(G40)}$$

The graph of $L(A=1,s)$ obtained from the formulas (E38) and (E39) on the intervals $-10<s<10$ and $-7<s<0$ is shown in Fig. 18, which illustrates the properties discussed in this section.

We briefly consider the behavior of the lattices in the limiting cases $A\to 0^+$ and $A\to+\infty$. For example, from Eq. (13), we can easily see that one of the basis vectors become zero in the limit $A\to 0^+$, leaving a sub-lattice of lower dimension. We, therefore, discuss each case $A\to 0^+$ and $A\to+\infty$ both in terms of theta functions and then in terms of the lattice basis vectors.

First, consider the limit $A\to 0^+$. In the interval $0<A<1/3$, the theta function is

$$\theta(A;q) = \sum_{i,j,k\in\mathbb{Z}} q^{g(A;i,j,k)} = \sum_{i,j,k\in\mathbb{Z}} q^{(A(i+j)^2+(j+k)^2+(i+k)^2)/4A}. \quad \text{(G41)}$$

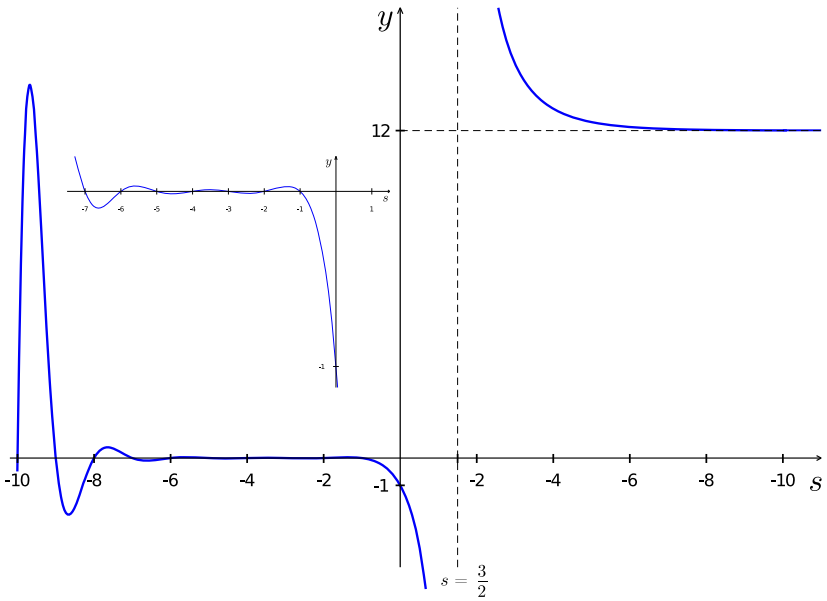

FIG. 18. Graph of $y = L(A = 1;\ s)$ for $-10 < s < 10$ for the fcc structure. The inlet shows $y = L(A = 1;\ s)$ for $-7 < s < 0$.

As $A \to 0^+$, we have $q^{(j+k)^2/4A} \to 0$ and $q^{(i+k)^2/4A} \to 0$ unless $j = -k$ and $i = -k$, respectively. Hence,

$$\lim_{A\to 0^+} \theta(A;q) = \lim_{A\to 0^+} \sum_{k\in\mathbb{Z}} \left(\sum_{i=-k} \sum_{j=-k} q^{(A(i+j)^2+(j+k)^2+(i+k)^2)/4A} \right)$$
$$= \lim_{A\to 0^+} \sum_{k\in\mathbb{Z}} q^{A(-k-k)^2/4A} = \sum_{k=-\infty}^{\infty} q^{k^2}. \tag{G42}$$

This corresponds to the one-dimensional lattice with minimal distance 1. The kissing number is 2, which is in agreement with the other lattices in the range $0 < A < 1/3$, as indicated in Table I. In terms of the lattice basis vectors for the bct lattice, we have

$$\vec{b}_1 = \left(\frac{1}{2}, \frac{1}{2\sqrt{A}}, 0\right)^\top,$$
$$\vec{b}_2 = \left(\frac{1}{2}, 0, \frac{1}{2\sqrt{A}}\right)^\top, \tag{G43}$$
$$\vec{b}_3 = \left(0, \frac{1}{2\sqrt{A}}, \frac{1}{2\sqrt{A}}\right)^\top.$$

The only linear combinations $\vec{v} = i\vec{b}_1 + j\vec{b}_2 + k\vec{b}_3$ (for $i, j, k \in \mathbb{Z}$) that remain finite in the limit $A \to 0^+$ occur when $i = -k$ and $j = -k$, in which case we obtain $\vec{v} = -k\vec{b}_1 - k\vec{b}_2 + k\vec{b}_3 = -k(1,0,0)^\top$. That is, the limiting lattice is just the one-dimensional lattice consisting of integer multiples of $(1,0,0)^\top$.

Now, consider the limit $A \to +\infty$. For $A > 1$, the theta function is

$$\theta(A;q) = \sum_{i,j,k\in\mathbb{Z}} q^{g(A;i,j,k)} = \sum_{i,j,k\in\mathbb{Z}} q^{(A(i+j)^2+(j+k)^2+(i+k)^2)/2}. \tag{G44}$$

Since $q^{A(i+j)^2/2} \to 0$ as $A \to +\infty$ unless $i = -j$, it follows that

$$\lim_{A\to+\infty} \theta(A;q) = \sum_{j,k\in\mathbb{Z}} \left(\sum_{i=-j} q^{(A(i+j)^2+(j+k)^2+(i+k)^2)/2} \right)$$
$$= \sum_{j,k\in\mathbb{Z}} q^{((j+k)^2+(-j+k)^2)/2} = \sum_{j,k\in\mathbb{Z}} q^{j^2+k^2}. \tag{G45}$$

This is the theta series for the two-dimensional square close packing lattice with minimal distance 1. The kissing number is 4, in agreement with other values in the range $A > 1$ given by Table I. In terms of the lattice basis vectors, we have

$$\vec{b}_1 = \frac{1}{\sqrt{2}}(\sqrt{A}, 1, 0)^\top, \quad \vec{b}_2 = \frac{1}{\sqrt{2}}(\sqrt{A}, 0, 1)^\top, \quad \vec{b}_3 = \frac{1}{\sqrt{2}}(0, 1, 1)^\top. \tag{G46}$$

The only linear combinations $\vec{v} = i\vec{b}_1 + j\vec{b}_2 + k\vec{b}_3$ (for $i, j, k \in \mathbb{Z}$) that remain finite in the limit $A \to +\infty$ occur when $i = -j$, in which case we obtain

$$\vec{v} = -j\vec{b}_1 + j\vec{b}_2 + k\vec{b}_3 = \frac{1}{\sqrt{2}}\left[j(0,-1,1)^\top + k(0,1,1)^\top\right]. \tag{G47}$$

This is isomorphic to the two-dimensional square close packing lattice with minimal distance 1, rotated from the coordinate axes by 45°.

APPENDIX H: THREE-BODY LATTICE SUMS

The three-body lattice sums for the ATM potential for different A-values according to Eq. (25) are listed in Table IV. The data were obtained from the treatment of the Epstein zeta function, as described in Sec. II E.

TABLE IV. Values for ATM three-body lattice sums.

A	$f_r^{(3)}(A)$	$f_a^{(3)}(A)$	$f_{\text{coh}}^{(3)} = f_r^{(3)}(A) + f_r^{(3)}(A)$
0.100 000 000 000 000 00	94.323 511 425 615 860	−69.582 608 619 579 300	24.740 902 806 036 560
0.111 111 111 111 111 11	78.996 234 807 153 090	−51.772 409 380 650 180	27.223 825 426 502 913
0.122 222 222 222 222 22	68.141 987 707 984 340	−40.523 230 176 857 204	27.618 757 531 127 130
0.133 333 333 333 333 33	60.127 931 145 011 650	−33.031 920 833 977 730	27.096 010 311 033 922
0.144 444 444 444 444 44	54.014 423 818 716 900	−27.821 816 896 120 083	26.192 606 922 596 810
0.155 555 555 555 555 55	49.227 632 547 044 850	−24.065 452 623 566 330	25.162 179 923 478 533
0.166 666 666 666 666 66	45.399 641 069 773 320	−21.274 409 710 807 973	24.125 231 358 965 350
0.177 777 777 777 777 77	42.284 826 583 051 180	−19.147 330 114 086 900	23.137 496 468 964 287
0.188 888 888 888 888 88	39.713 541 043 931 286	−17.491 030 258 502 235	22.222 510 785 429 050
0.200 000 000 000 000 00	37.565 176 004 82 040	−16.177 483 733 401 676	21.387 692 271 180 384
0.211 111 111 111 111 11	35.751 832 524 862 300	−15.119 334 299 395 149	20.632 498 225 467 145
0.222 222 222 222 222 22	34.208 057 391 103 196	−14.255 421 758 422 894	19.952 635 632 680 300
0.233 333 333 333 333 33	32.884 186 353 006 996	−13.541 936 344 866 237	19.342 250 008 140 766
0.244 444 444 444 444 44	31.741 906 110 675 053	−12.946 849 917 296 078	18.795 056 193 378 983
0.255 555 555 555 555 55	30.751 222 581 342 716	−12.446 315 486 424 176	18.304 907 094 918 548
0.266 666 666 666 666 66	29.888 344 501 346 580	−12.022 282 828 652 422	17.866 061 672 694 160
0.277 777 777 777 777 77	29.134 177 122 870 604	−11.660 884 764 889 580	17.473 292 357 981 023
0.288 888 888 888 888 88	28.473 231 311 321 676	−11.351 323 228 504 182	17.121 908 082 817 498
0.300 000 000 000 000 00	27.892 820 967 578 835	−11.085 086 344 259 825	16.807 734 623 319 007
0.311 111 111 111 111 11	27.382 464 087 618 917	−10.855 388 996 987 124	16.527 075 090 631 797
0.322 222 222 222 222 22	26.933 429 942 612 158	−10.656 766 985 644 794	16.276 662 956 967 370
0.333 333 333 333 333 33	26.538 392 635 746 654	−10.484 778 456 088 293	16.053 614 179 658 368
0.344 444 444 444 444 44	26.191 163 135 730 186	−10.335 781 403 352 645	15.855 381 732 377 538
0.355 555 555 555 555 55	25.886 479 914 810 245	−10.206 765 870 266 250	15.679 714 044 544 000
0.366 666 666 666 666 66	25.619 843 846 530 660	−10.095 225 986 419 386	15.524 617 860 111 277
0.377 777 777 777 777 77	25.387 386 879 598 203	−9.999 061 377 931 273 0	15.388 325 501 666 927
0.388 888 888 888 888 88	25.185 766 737 800 538	−9.916 500 474 040 106 0	15.269 266 263 760 429
0.400 000 000 000 000 00	25.012 081 855 389 425	−9.846 040 310 479 587 0	15.166 041 544 909 831
0.411 111 111 111 111 11	24.863 802 178 265 250	−9.786 398 883 876 206 0	15.077 403 294 389 043
0.422 222 222 222 222 22	24.738 712 502 866 125	−9.736 477 143 320 062 0	15.002 235 359 546 063
0.433 333 333 333 333 33	24.634 865 795 888 576	−9.695 328 445 993 656 0	14.939 537 349 894 920
0.444 444 444 444 444 44	24.550 544 514 439 906	−9.662 133 840 829 120 0	14.888 410 673 610 792
0.455 555 555 555 555 55	24.484 228 380 961 902	−9.636 181 937 706 048 0	14.848 046 443 255 853
0.466 666 666 666 666 66	24.434 567 397 857 776	−9.616 852 410 735 849 0	14.817 714 987 121 931
0.477 777 777 777 777 77	24.400 359 140 141 877	−9.603 602 401 199 240 0	14.796 756 738 942 634
0.488 888 888 888 888 88	24.380 529 560 080 320	−9.595 955 249 133 514 0	14.784 574 310 946 809
0.500 000 000 000 000 00	24.374 116 689 926 883	−9.593 491 106 415 080 0	14.780 625 583 511 807
0.511 111 111 111 111 11	24.380 256 747 943 890	−9.595 839 078 803 330 0	14.784 417 669 140 566
0.522 222 222 222 222 22	24.398 172 246 700 100	−9.602 670 617 391 109 0	14.795 501 629 308 987
0.533 333 333 333 333 33	24.427 161 776 971 960	−9.613 693 936 256 187 0	14.813 467 840 715 774
0.544 444 444 444 444 44	24.466 591 199 811 035	−9.628 649 277 177 047 0	14.837 941 922 633 988
0.555 555 555 555 555 55	24.515 886 026 805 056	−9.647 304 876 902 943 0	14.868 581 149 902 113
0.566 666 666 666 666 66	24.574 524 806 789 046	−9.669 453 519 681 912 0	14.905 071 287 107 134
0.577 777 777 777 777 77	24.642 033 368 202 980	−9.694 909 579 441 795 0	14.947 123 788 761 190
0.588 888 888 888 888 88	24.717 979 791 452 187	−9.723 506 473 302 120 0	14.994 473 318 150 071
0.600 000 000 000 000 00	24.801 970 006 178 507	−9.755 094 462 032 037 0	15.046 875 544 146 474
0.611 111 111 111 111 11	24.893 643 925 210 420	−9.789 538 744 131 757 0	15.104 105 181 078 666
0.622 222 222 222 222 22	24.992 672 040 848 475	−9.826 717 799 403 035 0	15.165 954 241 445 434
0.633 333 333 333 333 33	25.098 752 420 626 415	−9.866 521 945 181 134 0	15.232 230 475 445 277
0.644 444 444 444 444 44	25.211 608 049 226 257	−9.908 852 074 419 482 0	15.302 755 974 806 772
0.655 555 555 555 555 55	25.330 984 471 164 940	−9.953 618 549 838 264 0	15.377 365 921 326 671
0.666 666 666 666 666 66	25.456 647 695 517 326	−10.000 740 232 325 285	15.455 907 463 192 048
0.677 777 777 777 777 77	25.588 382 329 509 372	−10.050 143 625 200 935	15.538 238 704 308 440

TABLE IV. (*Continued*.)

A	$f_r^{(3)}(A)$	$f_a^{(3)}(A)$	$f_{\text{coh}}^{(3)} = f_r^{(3)}(A) + f_r^{(3)}(A)$
0.688 888 888 888 888 88	25.725 989 912 504 650	−10.101 762 118 796 010	15.624 227 793 708 641
0.700 000 000 000 000 00	25.869 287 425 869 180	−10.155 535 322 025 365	15.713 752 103 843 817
0.711 111 111 111 111 11	26.018 105 957 551 953	−10.211 408 469 676 325	15.806 697 487 875 624
0.722 222 222 222 222 22	26.172 289 503 063 816	−10.269 331 895 722 843	15.902 957 607 340 980
0.733 333 333 333 333 33	26.331 693 886 967 138	−10.329 260 564 360 926	16.002 433 322 606 210
0.744 444 444 444 444 44	26.496 185 791 055 442	−10.391 153 651 638 422	16.105 032 139 417 020
0.755 555 555 555 555 55	26.665 641 877 180 228	−10.454 974 171 488 043	16.210 667 705 692 188
0.766 666 666 666 666 66	26.839 947 994 200 763	−10.520 688 640 873 030	16.319 259 353 327 737
0.777 777 777 777 777 77	27.018 998 459 845 170	−10.588 266 779 406 624	16.430 731 680 438 555
0.788 888 888 888 888 88	27.202 695 409 400 450	−10.657 681 239 450 945	16.545 014 169 949 510
0.800 000 000 000 000 00	27.390 948 204 127 140	−10.728 907 363 179 943	16.662 040 840 947 200
0.811 111 111 111 111 11	27.583 672 893 138 015	−10.801 922 963 620 449	16.781 749 929 517 560
0.822 222 222 222 222 22	27.780 791 723 221 473	−10.876 708 126 908 810	16.904 083 596 312 660
0.833 333 333 333 333 33	27.982 232 691 721 270	−10.953 245 033 538 540	17.028 987 658 182 730
0.844 444 444 444 444 44	28.187 929 138 152 157	−11.031 517 796 468 115	17.156 411 341 684 050
0.855 555 555 555 555 55	28.397 819 370 709 860	−11.111 512 314 338 800	17.286 307 056 371 058
0.866 666 666 666 666 66	28.611 846 324 266 285	−11.193 216 138 171 746	17.418 630 186 094 546
0.877 777 777 777 777 77	28.829 957 246 812 050	−11.276 618 350 194 180	17.553 338 896 617 873
0.888 888 888 888 888 88	29.052 103 411 639 130	−11.361 709 453 496 548	17.690 393 958 142 580
0.900 000 000 000 000 00	29.278 239 852 844 173	−11.448 481 271 471 891	17.829 758 581 372 290
0.911 111 111 111 111 11	29.508 325 121 990 370	−11.536 926 856 036 661	17.971 398 265 953 710
0.922 222 222 222 222 22	29.742 321 063 989 510	−11.627 040 403 757 988	18.115 280 660 231 520
0.933 333 333 333 333 33	29.980 192 610 464 800	−11.718 817 179 160 165	18.261 375 431 304 643
0.944 444 444 444 444 44	30.221 907 589 035 680	−11.812 253 444 459 664	18.409 654 144 576 024
0.955 555 555 555 555 55	30.467 436 547 115 813	−11.907 346 395 178 287	18.560 090 151 937 530
0.966 666 666 666 666 66	30.716 752 588 962 620	−12.004 094 101 029 036	18.712 658 487 933 580
0.977 777 777 777 777 77	30.969 831 224 834 856	−12.102 495 451 618 665	18.867 335 773 216 197
0.988 888 888 888 888 88	31.226 650 231 227 172	−12.202 550 106 530 040	19.024 100 124 697 128
1.000 000 000 000 000 00	31.487 189 521 251 523	−12.304 258 449 363 747	19.182 931 071 887 780

The total lattice sum shows a minimum at the bcc structure ($A = \frac{1}{2}$), as shown in Fig. 8. In order to prove this, we show that for any $\nu_i \in \mathbb{C}$,

$$\frac{\partial}{\partial A}\zeta^{(3)}_{\Lambda(A)}(\vec{\nu})\Big|_{A=1/2} = 0 \tag{H1}$$

holds. As the ATM potential is a finite sum of three-body zeta functions, its derivative, therefore, also vanishes. Let $\vec{x}(A) = B^{\top}(A)\vec{n}$ with $\vec{n} \in \mathbb{Z}^d$. Then,

$$\frac{\partial}{\partial A}\frac{1}{|B^{\top}(A)\vec{n}|^{\nu}}\Big|_{A=1/2} = -\nu\frac{\vec{x}(1/2)^T D\vec{x}(1/2)}{|\vec{x}(1/2)|^{\nu+1}},$$

with the diagonal traceless matrix,

$$D = B^{\top\prime}(1/2)\big(B^{\top}(1/2)\big)^{-1} = \begin{pmatrix} -2/3 & 0 & 0 \\ 0 & 1/3 & 0 \\ 0 & 0 & 1/3 \end{pmatrix}.$$

which is convenient for our proof as we shall see. Thus,

$$\begin{aligned}\frac{\partial}{\partial A}\zeta^{(3)}_{\Lambda(A)}(\vec{\nu})\Big|_{A=1/2} &= -\sum_{\vec{x},\vec{y}\in\Lambda(1/2)}{}' \Bigg(\nu_1\frac{\vec{x}^T D\vec{x}}{|\vec{x}|^{\nu_1+1}}\frac{1}{|\vec{y}|^{\nu_2}}\frac{1}{|\vec{z}|^{\nu_3}} + \nu_2\frac{1}{|\vec{x}|^{\nu_1}}\frac{\vec{y}^T D\vec{y}}{|\vec{y}|^{\nu_2+1}}\frac{1}{|\vec{z}|^{\nu_3}} \\ &\quad + \nu_3\frac{1}{|\vec{x}|^{\nu_1}}\frac{1}{|\vec{y}|^{\nu_2}}\frac{\vec{z}^T D\vec{z}}{|\vec{z}|^{\nu_3+1}}\Bigg),\end{aligned} \tag{H2}$$

with the convention $\vec{z} = \vec{y} - \vec{x}$. As $\Lambda(1/2)$ is the bcc lattice, we can choose a rotated lattice Λ_0, such that $\Lambda_0 = c\big(\mathbb{Z}^d \cup (\mathbb{Z}^d + 1/2)\big)$, and the resulting lattice sums do of course not depend on this particular choice.

The bcc lattice Λ_0 in this representation now exhibits the property that for $\vec{z} \in \Lambda_0$ also its cyclic permutation,

$$\sigma\vec{z} = (z_2, \ldots, z_d, z_1)^T$$

is an element of Λ_0. Thus, we have $\sigma^n\Lambda_0 = \Lambda_0$ for any $n \in \mathbb{N}$.

We now show that sum over the first term in Eq. (H2) vanishes and thus, in complete analogy, the two remaining sums as well.

Averaging over cyclic permutations and using that permutations of the elements of $\vec{z}$ do not change the norm, we find

$$-\nu_1 \sum_{\vec{x},\vec{y}\in\Lambda_0} \frac{\vec{x}^T D\vec{x}}{|\vec{x}|^{\nu_1+1}} \frac{1}{|\vec{y}|^{\nu_2}} \frac{1}{|\vec{z}|^{\nu_3}} = -\nu_1 \frac{1}{3} \sum_{\vec{x},\vec{y}\in\Lambda_0}{}' \sum_{n=0}^{2} \left((\sigma^n\vec{x})^T D(\sigma^n\vec{x})\right) \times \frac{1}{|\vec{x}|^{\nu_1+1}} \frac{1}{|\vec{y}|^{\nu_2}} \frac{1}{|\vec{z}|^{\nu_3}}.$$

However, as D is diagonal, we have

$$\sum_{n=0}^{2} \left((\sigma^n\vec{x})^T D(\sigma^n\vec{x})\right) = |\vec{x}|^2 \operatorname{Tr}(D) = 0,$$

as D is traceless. With the same argument for the remaining two sums, we have thus shown that all three terms in Eq. (H2) vanish. Thus, also

$$\frac{\partial}{\partial A} \zeta^{(3)}_{\Lambda(A)}(\vec{\nu})\Big|_{A=1/2} = 0.$$

Finally, recall that the three-body cohesive energy is a recombination of three-body zeta functions,

$$E^{(3)}_{\mathrm{coh}}/\lambda = \frac{1}{24}\zeta^{(3)}_{\Lambda(A)}(3,3,3) - \frac{3}{16}\zeta^{(3)}_{\Lambda(A)}(-1,5,5) + \frac{3}{8}\zeta^{(3)}_{\Lambda(A)}(1,3,5),$$

and therefore,

$$\frac{\partial}{\partial A} E^{(3)}_{\mathrm{coh}}\Big|_{A=1/2} = 0.$$

The defining integral for $\zeta^{(3)}_\Lambda$ can be meromorphically continued to $\nu_i \in \mathbb{C}$ by means of the Hadamard integral. This, however, requires the computation of derivatives of the Epstein zeta function, which can be avoided for the special case of the ATM potential. Here, only the $\vec{\nu} = (-1,3,5)^T$ term leads to a hypersingular Hadamard integral, which can be reduced to a standard integral as follows. We readily find that

$$\int_{E^*} Z_{\Lambda,\nu}(\vec{k})\,\mathrm{d}\vec{k} = 0, \quad \nu > d,$$

and thus also the meromorphic continuation to $\nu \in \mathbb{C}$ equals zero. Hence, we have

$$\zeta^{(3)}_\Lambda(-1,1,3) = \frac{1}{V_\Lambda}\int_{E^*} Z_{\Lambda,-1}(\vec{k}) \times \left(Z_{\Lambda,1}(\vec{k})Z_{\Lambda,3}(\vec{k}) - Z_{\Lambda,1}(\vec{0})Z_{\Lambda,3}(\vec{0})\right)\mathrm{d}\vec{k},$$

where the right-hand side is defined as a regular integral as the term in brackets scales as $\vec{k}^2$ around $\vec{k} = \vec{0}$ due to reflection symmetry as $\vec{k} \to -\vec{k}$. In conclusion, the ATM potential for any lattice and any dimension can be written in terms of three generalized zeta functions that can, in turn, be efficiently computed to machine precision from singular integrals that involve products of Epstein zeta functions.

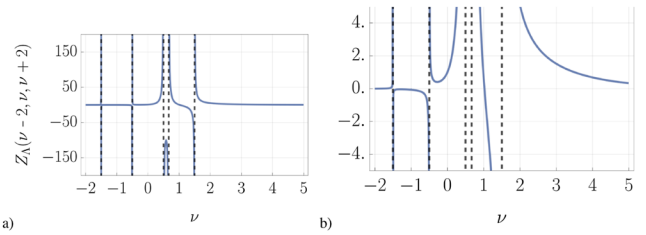

FIG. 19. Three-body zeta function for $\Lambda = \mathbb{Z}$ computed via the Epstein integral representation for $\vec{\nu} = (\nu-2, \nu, \nu+2)^T$, including its meromorphic continuation (a). The dashed gray lines indicate the simple poles at $\nu \in 3/2 - \mathbb{N}$, corresponding to the condition $\nu_i + \nu_j \in d + 2\mathbb{N}$ for $i \neq j$, and $\nu = 2/3$, corresponding to $\nu_1 + \nu_2 + \nu_3 = 2d$. Panel (b) offers a magnified view of the region close to the origin.

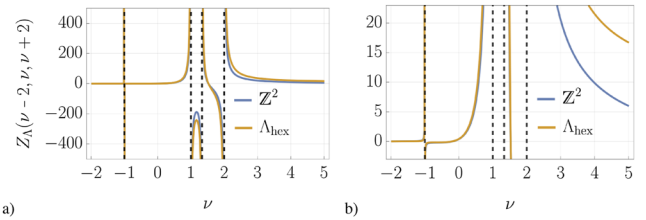

FIG. 20. Two dimensional three-body zeta function (a) for the square lattice $\Lambda = \mathrm{SL} = \mathbb{Z}^2$ (blue) and the hexagonal lattice $\Lambda = \mathrm{HL}$ (orange) shown in Fig. 4 for $R = 1$ via the Epstein integral representation for $\vec{\nu} = (\nu-2, \nu, \nu+2)^T$, including its meromorphic continuation. For $\nu \leq 1$, the three-body zeta function for the square lattice and the three-body zeta function for the hexagonal lattice are visually indistinguishable. The dashed gray lines indicate the simple poles at $\nu \in 1 - 2\mathbb{N}$, corresponding to the condition $\nu_i + \nu_j \in d + 2\mathbb{N}$ for $i \neq j$, and $\nu = 4/3$, corresponding to $\nu_1 + \nu_2 + \nu_3 = 2d$. Panel (b) offers a magnified view of the region close to the origin.

We display the behavior of the one-dimensional three-body zeta function $Z^{(3)}_{\mathbb{Z}}$ and two-dimensional three-body zeta functions $Z^{(3)}_{\mathrm{SL}}$ for $\mathrm{SL} = \mathbb{Z}^2$ and $Z^{(3)}_{\mathrm{HL}}$ for

$$\mathrm{HL} = \begin{bmatrix} 1 & 1/2 \\ 0 & \sqrt{3}/2 \end{bmatrix}\mathbb{Z}^2$$

as a function of $\vec{\nu}$, including its meromorphic continuation, in Figs. 19 and 20. We observe simple poles at $\nu_1 + \nu_2 + \nu_3 = 2d$ and $\nu_i + \nu_j = d - 2n$, $n \in \mathbb{N}$, where $i \neq j$.

APPENDIX I: CONVERGENCE OF THE LATTICE SUM OF THE THREE-BODY ZETA FUNCTION

In this section, we show that the defining lattice sum for the three-body zeta function,

$$\zeta^{(3)}_\Lambda(\vec{\nu}) = \sum_{\vec{x},\vec{y}\in\Lambda}{}' |\vec{x}|^{-\nu_1} |\vec{y}|^{-\nu_2} |\vec{y}-\vec{x}|^{-\nu_3}$$

converges if all of the following conditions hold:

$$\nu_i + \nu_j > d, \quad i \neq j, \quad \text{and} \quad \nu_1 + \nu_2 + \nu_3 > 2d$$

for $i \in \{1,2,3\}$. Note that all summands are non-negative, so convergence of the sum does not depend on the order of summation. We first investigate the sum over $\vec{y}$, which converges if and only if

$$\nu_2 + \nu_3 > d. \tag{I1}$$

We then cast the sum over $\vec{y}$ in terms of Epstein zeta functions,

$$\sum_{\vec{y}\in\Lambda}{}' |\vec{y}|^{-\nu_2}|\vec{y}-\vec{x}|^{-\nu_3} = \sum_{\vec{y},\vec{z}\in\Lambda}{}' |\vec{y}|^{-\nu_2}|\vec{z}|^{-\nu_3}\delta_{\vec{y}-\vec{x},\vec{z}} = V_\Lambda \int_{E^*} Z_{\Lambda,\nu_2}(\vec{k})Z_{\Lambda,\nu_3}(\vec{k})e^{2\pi i\vec{y}\cdot\vec{k}}\,\mathrm{d}\vec{k}$$

using that

$$V_\Lambda \int_{E^*} e^{-2\pi i\vec{z}\cdot\vec{k}} = \delta_{\vec{z},0}$$

for a lattice vector $\vec{z} \in \Lambda$, as well as the lattice symmetry $\Lambda = -\Lambda$. We will now use knowledge of the singularity of the Epstein zeta function at $\vec{k} = 0$ as well as standard results from Fourier analysis to derive the asymptotic decay of the above-mentioned sum in $\vec{x}$.

Let $\chi(\vec{k})$ be a smooth cutoff function with

$$\chi(\vec{k}) = \begin{cases} 1, & |\vec{k}| < r/2, \\ 0, & |\vec{k}| > r \end{cases}$$

and $r > 0$ chosen small enough that the support lies within an open subset of the reciprocal unit cell. Adding and subtracting the cutoff in the integrand, we find

$$V_\Lambda \int_{E^*} Z_{\Lambda,\nu_2}(\vec{k})Z_{\Lambda,\nu_3}(\vec{k})e^{2\pi i\vec{y}\cdot\vec{k}}\,\mathrm{d}\vec{k} = f(\vec{x}) + V_\Lambda \int_{\mathbb{R}^d} \chi(\vec{k})Z_{\Lambda,\nu_2} \times (\vec{k})Z_{\Lambda,\nu_3}(\vec{k})e^{2\pi i\vec{y}\cdot\vec{k}}\,\mathrm{d}\vec{k},$$

with f decaying superalgebraically as the Fourier integral of a smooth function and where we could extend the integral on the right to $\mathbb{R}^d$ due to the compact support of the cutoff. The term on the right-hand side is then a standard inverse Fourier transform.

Now, separate the Epstein zeta function into an analytic function and the singularity $\hat{s}_\nu$, see Eq. (32), yielding

$$V_\Lambda \mathscr{F}^{-1}\Big(\chi(\vec{k})(Z^{\mathrm{reg}}_{\Lambda,\nu_2}(\vec{k}) + c_{\nu_2}|\vec{k}|^{\nu_2-d})(Z^{\mathrm{reg}}_{\Lambda,\nu_3}(\vec{k}) + c_{\nu_3}|\vec{k}|^{\nu_3-d})\Big),$$

with constants $c_\nu \in \mathbb{R}$ and $\nu_2, \nu_3 \notin d + 2\mathbb{N}$. If ν_2 or $\nu_3 \in d + 2\mathbb{N}$, then powers of $\log(\vec{k})$ need to be included that do not alter convergence behavior and the proof proceeds in complete analogy. We then find that the above-mentioned Fourier integral can be rewritten as

$$\mathscr{F}^{-1}(h_0)(\vec{x}) + \mathscr{F}^{-1}(h_1|\cdot|^{\nu_2-d})(\vec{x}) + \mathscr{F}^{-1}(h_2|\cdot|^{\nu_3-d})(\vec{x}) + \mathscr{F}^{-1}(h_3|\cdot|^{(\nu_2+\nu_3-d)-d})(\vec{x})$$

with $h_0, \ldots, h_3$ smooth compactly supported functions, whose Fourier transforms decay superalgebraically. Thus, we only need to analyze the asymptotic decay in $\vec{x}$ of

$$\mathscr{F}^{-1}(h|\cdot|^{\nu-d}),$$

for h, a smooth compactly supported function. This is, however, a standard result,

$$\left|\mathscr{F}^{-1}(h|\cdot|^{\nu-d})\right| \leq C|\vec{x}|^{-\nu}, \quad |\vec{x}| > R$$

for some $C, R > 0$. Inserting these bounds into the sum over $\vec{x}$, we obtain the addition constraints,

$$\nu_1 + \nu_2 > d, \quad \nu_1 + \nu_3 > d, \quad \nu_1 + \nu_2 + \nu_3 - d > d. \tag{I2}$$

The conditions in Eqs. (I1) and (I2) then yield the convergence criteria for the three-body zeta lattice sum.

REFERENCES

[1] H. E. Stanley, *Phase Transitions and Critical Phenomena* (Clarendon Press, Oxford, 1971), Vol. 7.
[2] F. Falk, "Landau theory and martensitic phase transitions," J. Phys. Colloq. **43**, C4-3 (1982).
[3] Y. A. Izyumov, V. M. Laptve, and V. N. Syromyatnikov, "Phenomenological theory of martensitic and reconstructive phase transitions," Phase Transitions **49**, 1–55 (1994).
[4] K. Otsuka and C. M. Wayman, *Shape Memory Materials* (Cambridge University Press, Cambridge, UK, 1999).
[5] G. J. Ackland, A. P. Jones, and R. Noble-Eddy, "Molecular dynamics simulations of the martensitic phase transition process," Mater. Sci. Eng.: A **481–482**, 11–17 (2008), part of Special Issue: Proceedings of the 7th European Symposium on Martensitic Transformations, ESOMAT 2006.
[6] G. Grimvall, B. Magyari-Köpe, V. Ozoliņš, and K. A. Persson, "Lattice instabilities in metallic elements," Rev. Mod. Phys. **84**, 945–986 (2012).
[7] G. Torrents, X. Illa, E. Vives, and A. Planes, "Geometrical model for martensitic phase transitions: Understanding criticality and weak universality during microstructure growth," Phys. Rev. E **95**, 013001 (2017).
[8] D. A. Young, *Phase Diagrams of the Elements* (University of California Press, 1991).
[9] G. J. Ackland, M. Dunuwille, M. Martinez-Canales, I. Loa, R. Zhang, S. Sinogeikin, W. Cai, and S. Deemyad, "Quantum and isotope effects in lithium metal," Science **356**, 1254–1259 (2017).
[10] K. J. Caspersen and E. A. Carter, "Finding transition states for crystalline solid–solid phase transformations," Proc. Natl. Acad. Sci. U. S. A. **102**, 6738–6743 (2005).
[11] J. M. Borwein, M. Glasser, R. McPhedran, J. Wan, and I. Zucker, *Lattice Sums Then and Now* (Cambridge University Press, 2013), Vol. 150.
[12] E. Grüneisen, "Theorie des festen Zustandes einatomiger Elemente," Ann. Phys. **344**, 257–306 (1912).
[13] R. Fürth, "On the equation of state for solids," Proc. R. Soc. London, Ser. A **183**, 87–110 (1944).
[14] F. H. Stillinger, "Lattice sums and their phase diagram implications for the classical Lennard-Jones model," J. Chem. Phys. **115**, 5208–5212 (2001).
[15] P. Schwerdtfeger, A. Burrows, and O. R. Smits, "The Lennard-Jones potential revisited: Analytical expressions for vibrational effects in cubic and hexagonal close-packed lattices," J. Phys. Chem. A **125**, 3037–3057 (2021).
[16] J. E. Jones and A. E. Ingham, "On the calculation of certain crystal potential constants, and on the cubic crystal of least potential energy," Proc. R. Soc. London, Ser. A **107**, 636–653 (1925).
[17] P. Schwerdtfeger and D. J. Wales, "100 years of the Lennard-Jones potential," J. Chem. Theory Comput. **20**, 3379–3405 (2024).
[18] E. Madelung, "Das elektrische Feld in Systemen von regelmäßig angeordneten Punktladungen," Phys. Z. **19**, 32 (1918).
[19] M. Born, "On the stability of crystal lattices. I," Math. Proc. Cambridge Philos. Soc. **36**, 160–172 (1940).

[20]R. D. Misra, "On the stability of crystal lattices. II," Math. Proc. Cambridge Philos. Soc. **36**, 173–182 (1940).
[21]J.-P. Hansen and L. Verlet, "Phase transitions of the Lennard-Jones system," Phys. Rev. **184**, 151–161 (1969).
[22]M. P. Allen and D. J. Tildesley, *Computer Simulation of Liquids*, *Oxford Science Publications* (Clarendon Press, New York, NY, 1989).
[23]H. Watanabe, N. Ito, and C.-K. Hu, "Phase diagram and universality of the Lennard-Jones gas-liquid system," J. Chem. Phys. **136**, 204102 (2012).
[24]E. H. Abramson, "Melting curves of argon and methane," High Pressure Res. **31**, 549–554 (2011).
[25]A. Hajibabaei and K. S. Kim, "First-order and continuous melting transitions in two-dimensional Lennard-Jones systems and repulsive disks," Phys. Rev. E **99**, 022145 (2019).
[26]A. Burrows, S. Cooper, E. Pahl, and P. Schwerdtfeger, "Analytical methods for fast converging lattice sums for cubic and hexagonal close-packed structures," J. Math. Phys. **61**, 123503 (2020).
[27]P. Epstein, "Zur Theorie allgemeiner Zetafunktionen," Math. Ann. **56**, 615–644 (1903).
[28]E. Elizalde, "Analysis of an inhomogeneous generalized Epstein–Hurwitz zeta function with physical applications," J. Math. Phys. **35**, 6100–6122 (1994).
[29]E. Elizalde, "Zeta functions: Formulas and applications," J. Comput. Appl. Math. **118**, 125–142 (2000).
[30]A. A. Buchheit and J. K. Busse, "Epstein zeta method for many-body lattice sums," arXiv:2504.11989 [math.NA] (2025).
[31]D. Borwein, J. M. Borwein, and C. Pinner, "Convergence of Madelung-like lattice sums," Trans. Am. Math. Soc. **350**, 3131–3167 (1998).
[32]B. M. Axilrod and E. Teller, "Interaction of the van der Waals type between three atoms," J. Chem. Phys. **11**, 299–300 (1943).
[33]Y. Muto, "Force between nonpolar molecules," Proc. Phys.-Math. Soc. Jpn. **17**, 629–631 (1943).
[34]P. Attard, "Simulation results for a fluid with the Axilrod-Teller triple dipole potential," Phys. Rev. A **45**, 5649 (1992).
[35]P. Schwerdtfeger, R. Tonner, G. E. Moyano, and E. Pahl, "Towards J/mol accuracy for the cohesive energy of solid argon," Angew. Chem., Int. Ed. **55**, 12200–12205 (2016).
[36]A. Hermann, R. P. Krawczyk, M. Lein, P. Schwerdtfeger, I. P. Hamilton, and J. J. P. Stewart, "Convergence of the many-body expansion of interaction potentials: From van der Waals to covalent and metallic systems," Phys. Rev. A **76**, 013202 (2007).
[37]B. Li, G. Qian, A. R. Oganov, S. E. Boulfelfel, and R. Faller, "Mechanism of the fcc-to-hcp phase transformation in solid Ar," J. Chem. Phys. **146**, 214502 (2017).
[38]K. J. Caspersen, A. Lew, M. Ortiz, and E. A. Carter, "Importance of shear in the bcc-to-hcp transformation in iron," Phys. Rev. Lett. **93**, 115501 (2004).
[39]D. F. Johnson and E. A. Carter, "Nonadiabaticity in the iron bcc to hcp phase transformation," J. Chem. Phys. **128**, 104703 (2008).
[40]S. Ono and T. Ito, "Theory of dynamical stability for two- and three-dimensional Lennard-Jones crystals," Phys. Rev. B **103**, 075406 (2021).
[41]P. Schwerdtfeger and A. Burrows, "Cuboidal bcc to fcc transformation of Lennard-Jones phases under high pressure derived from exact lattice summations," J. Phys. Chem. C **126**, 8874–8882 (2022).
[42]S. Alexander and J. McTague, "Should all crystals be bcc? Landau theory of solidification and crystal nucleation," Phys. Rev. Lett. **41**, 702–705 (1978).
[43]B. Groh and B. Mulder, "Why all crystals need not be bcc: Symmetry breaking at the liquid-solid transition revisited," Phys. Rev. E **59**, 5613–5620 (1999).
[44]A. Travesset, "Phase diagram of power law and Lennard-Jones systems: Crystal phases," J. Chem. Phys. **141**, 164501 (2014).
[45]E. Bain, "A new orientation relationship between fcc and bcc," Trans. Metall. Soc. AIME **70**, 25 (1924).
[46]C. Zener, "Theory of strain interaction of solute atoms," Phys. Rev. **74**, 639–647 (1948).
[47]J. Rifkin, "Equivalence of Bain and Zener transformations," Philos. Mag. A **49**, L31–L34 (1984).
[48]P. Jerabek, A. Burrows, and P. Schwerdtfeger, "Solving a problem with a single parameter: A smooth bcc to fcc phase transition for metallic lithium," Chem. Commun. **58**, 13369–13372 (2022).
[49]A. Burrows, S. Cooper, and P. Schwerdtfeger, "Instability of the body-centered cubic lattice within the sticky hard sphere and Lennard-Jones model obtained from exact lattice summations," Phys. Rev. E **104**, 035306 (2021).
[50]D. C. Wallace and J. L. Patrick, "Stability of crystal lattices," Phys. Rev. **137**, A152–A160 (1965).
[51]J. H. Conway and N. J. A. Sloane, "On lattices equivalent to their duals," J. Number Theory **48**, 373–382 (1994).
[52]J. H. Conway and N. J. Sloane, "The optimal isodual lattice quantizer in three dimensions," Adv. Math. Commun. **1**, 257–260 (2007).
[53]A. L. Patterson, "Crystal lattice models based on the close packing of spheres," Rev. Sci. Instrum. **12**, 206–211 (1941).
[54]K. L. Fields, "The fragile lattice packings of spheres in three-dimensional space," Acta Crystallogr., Sect. A: Found. Adv. **36**, 194–197 (1980).
[55]S. Torquato and F. H. Stillinger, "Toward the jamming threshold of sphere packings: Tunneled crystals," J. Appl. Phys. **102**, 093511 (2007).
[56]S. Cooper and P. Schwerdtfeger, "A minimum property for cuboidal lattice sums," SIGMA **21**, 019 (2025).
[57]V. Heine, I. J. Robertson, and M. C. Payne, "Many-atom interactions in solids," Philos. Trans.: Phys. Sci. Eng. **334**, 393–405 (1991).
[58]A. A. Buchheit, J. Busse, and R. Gutendorf, "Computation and properties of the Epstein zeta function with high-performance implementation in EpsteinLib," arXiv:2412.16317 (2024).
[59]O. R. Smits, P. Jerabek, E. Pahl, and P. Schwerdtfeger, "A hundred-year-old experiment re-evaluated: Accurate ab initio Monte Carlo simulations of the melting of radon," Angew. Chem., Int. Ed. **57**, 9961–9964 (2018).
[60]P. Jerabek, O. R. Smits, J.-M. Mewes, K. A. Peterson, and P. Schwerdtfeger, "Solid oganesson via a many-body interaction expansion based on relativistic coupled-cluster theory and from plane-wave relativistic density functional theory," J. Phys. Chem. A **123**, 4201–4211 (2019).
[61]O. R. Smits, P. Jerabek, E. Pahl, and P. Schwerdtfeger, "First-principles melting of krypton and xenon based on many-body relativistic coupled-cluster interaction potentials," Phys. Rev. B **101**, 104103 (2020).
[62]O. R. Smits, J.-M. Mewes, P. Jerabek, and P. Schwerdtfeger, "Oganesson: A noble gas element that is neither noble nor a gas," Angew. Chem., Int. Ed. **59**, 23636–23640 (2020).
[63]E. Florez, O. R. Smits, J.-M. Mewes, P. Jerabek, and P. Schwerdtfeger, "From the gas phase to the solid state: The chemical bonding in the superheavy element flerovium," J. Chem. Phys. **157**, 064304 (2022).
[64]M. G. Duffy, "Quadrature over a pyramid or cube of integrands with a singularity at a vertex," SIAM J. Numer. Anal. **19**, 1260–1262 (1982).
[65]Y. Xie, Z. L. Glick, and C. D. Sherrill, "Assessment of three-body dispersion models against coupled-cluster benchmarks for crystalline benzene, carbon dioxide, and triazine," J. Chem. Phys. **158**, 094110 (2023).
[66]I. J. Zucker, "Exact results for some lattice sums in 2, 4, 6 and 8 dimensions," J. Phys. A: Math. Nucl. Gen. **7**, 1568–1575 (1974).
[67]I. J. Zucker and M. M. Robertson, "Exact values of some two-dimensional lattice sums," J. Phys. A: Math. Gen. **8**, 874–881 (1975).
[68]I. J. Zucker, "The exact evaluation of some new lattice sums," Symmetry **9**, 314 (2017).
[69]B. M. E. van der Hoff and G. C. Benson, "A method for the evaluation of some lattice sums occurring in calculations of physical properties of crystals," Can. J. Phys. **31**, 1087–1094 (1953).
[70]P. Schwerdtfeger, N. Gaston, R. P. Krawczyk, R. Tonner, and G. E. Moyano, "Extension of the Lennard-Jones potential: Theoretical investigations into rare-gas clusters and crystal lattices of He, Ne, Ar, and Kr using many-body interaction expansions," Phys. Rev. B **73**, 064112 (2006).
[71]R. J. Baxter, "Percus–Yevick equation for hard spheres with surface adhesion," J. Chem. Phys. **49**, 2770–2774 (1968).
[72]W. L. Bade, "Drude-model calculation of dispersion forces. I. General theory," J. Chem. Phys. **27**, 1280–1284 (1957).
[73]E. E. Polymeropoulos, P. Bopp, J. Brickmann, L. Jansen, and R. Block, "Molecular-dynamics simulations in systems of rare gases using Axilrod-Teller and exchange three-atom interactions," Phys. Rev. A **31**, 3565–3569 (1985).

[74]C. E. Moore, *Atomic Energy Levels as Derived from the Analyses of Optical Spectra, 467* (U.S. Department of Commerce, National Bureau of Standards, 1949).
[75]K. Huber and G. Herzberg, *Molecular Spectra and Molecular Structure Constants of Diatomic Molecules* (Van Nostrand, 1979).
[76]P. Schwerdtfeger and J. K. Nagle, "2018 Table of static dipole polarizabilities of the neutral elements in the periodic table," Mol. Phys. **117**, 1200–1225 (2019).
[77]F. Milstein, "Applicability of exponentially attractive and repulsive interatomic potential functions in the description of cubic crystals," J. Appl. Phys. **44**, 3825–3832 (1973).
[78]P. J. Craievich, J. M. Sanchez, R. E. Watson, and M. Weinert, "Structural instabilities of excited phases," Phys. Rev. B **55**, 787–797 (1997).
[79]B. W. Kwaadgras, M. W. J. Verdult, M. Dijkstra, and R. v. Roij, "Can nonadditive dispersion forces explain chain formation of nanoparticles?," J. Chem. Phys. **138**, 104308 (2013).
[80]E. Ermakova, J. Solca, G. Steinebrunner, and H. Huber, "Ab initio calculation of a three-body potential to be applied in simulations of fluid neon," Chem. Eur. J. **4**, 377–382 (1998).
[81]Y. A. Freiman and S. M. Tretyak, "Many-body interactions and high-pressure equations of state in rare-gas solids," Low Temp. Phys. **33**, 545–552 (2007).
[82]P. Schwerdtfeger and A. Hermann, "Equation of state for solid neon from quantum theory," Phys. Rev. B **80**, 064106 (2009).
[83]J. Zhao, *Multiple Zeta Functions, Multiple Polylogarithms and Their Special Values* (World Scientific, Singapore, 2016).
[84]G. E. Andrews, R. Askey, and R. Roy, *Special Functions* (Cambridge University Press, Cambridge, 1999), Vol. 71.
[85]N. M. Temme, *Special Functions: An Introduction to the Classical Functions of Mathematical Physics* (John Wiley & Sons, 1996).
[86]J. M. Borwein and P. B. Borwein, "A cubic counterpart of Jacobi's identity and the AGM," Trans. Am. Math. Soc. **323**, 691–701 (1991).
[87]S. Cooper, *Ramanujan's Theta Functions* (Springer, Berlin, 2017).
[88]N. J. A. Sloane and S. Plouffe, *The Encyclopedia of Integer Sequences*(Academic Press, 1995); online version available at https://oeis.org/.
[89]T. M. Apostol, *Introduction to Analytic Number Theory* (Springer Science & Business Media, Berlin, 1998).
[90]R. E. Crandall, "Fast evaluation of Epstein zeta functions," https://www.reed.edu/physics/faculty/crandall/papers/epstein.pdf (1998).
[91]J. H. Conway and N. J. A. Sloane, *Sphere Packings, Lattices and Groups* (Springer, New York, 2013), Vol. 290.
[92]P. Schwerdtfeger, B. Assadollahzadeh, and A. Hermann, "Convergence of the Møller–Plesset perturbation series for the fcc lattices of neon and argon," Phys. Rev. B **82**, 205111 (2010).
[93]P. Bateman and E. Grosswald, "On Epstein's zeta function," Acta Arithmetica **9**, 365–373 (1964).
[94]A. A. Terras, "Bessel series expansions of the Epstein zeta function and the functional equation," Trans. Am. Math. Soc. **183**, 477–486 (1973).
[95]A. Selberg and S. Chowla, "On Epstein's zeta-function," J. Reine Angew. Math. **227**, 87–110 (1967).
[96]N. Levinson and R. M. Redheffer, *Complex Variables* (Holden Day, 1970).
[97]A. Burrows, S. Cooper, and P. Schwerdtfeger, "The Madelung constant in N dimensions," Proc. R. Soc. A **478**, 20220334 (2022).